12-14-2020 2:30 PM

Reliability-Based Calibration of Design Wind Load, Snow Load and Companion Load Factors Considering Climate Change Effect

Qian Tang, *The University of Western Ontario*

Supervisor: Hong,Hanping, *The University of Western Ontario*

A thesis submitted in partial fulfillment of the requirements for the Doctor of Philosophy degree in Civil and Environmental Engineering

Abstract

Wind load and snow load are two of the environmental loads that need to be considered for structural design. This study compared the statistical characteristics of the annual maximum thunderstorm and non-thunderstorm winds based on the updated wind speed dataset and carried out the extreme value analysis for wind load by treating the synoptic and thunderstorm winds separately. The results indicated that for southern Ontario and the southern part of the Prairies, the extreme winds could be dominated by the thunderstorm winds. The consideration of both thunderstorm winds and synoptic winds separately to recommend the reference wind velocity pressure for the codified structural design was made.

Extreme value analysis for snow depth and snow load was also carried out. The statistics of and probabilistic models for the annual maximum ground snow depth and ground snow load (as well as snowpack bulk density) were assessed. The rain component of the roof snow load was evaluated, and the correlation between snow component and rain component of the annual maximum roof snow load was investigated. It turns out that the correlation between snow component and rain component of the annual maximum roof snow load was negligible. This suggested that the use of the sum of the ground snow load and rain load to evaluate the roof snow load could be conservative and the use of the well-known square-root-of-the-sum-of-squares (SRSS) rule to evaluate the roof snow load based on the snow component and rain component was recommended.

By using the newly developed statistics of the wind and snow, a reliability-based design code calibration for the National Building Code of Canada was carried out. The analysis considered the stationary extremes derived from observed meteorological data and included the nonstationary climate change effects. New design load factors and companion load factors for the ultimate limit state and serviceability limit state by considering wind load and snow load were recommended. Scaling factors that account for climate change effects were also suggested.

Keywords

Annual maximum wind speed, Climate change, Code calibration, Design code, Extreme value analysis, Load factor, Reliability analysis, Snow depth, Snow hazard mapping, Snow load, Target reliability index, Wind hazard mapping, Wind load

Summary for Lay Audience

Wind load and snow load are two of the environmental loads that need to be considered for structural design. This study investigates the largest wind and snow loads that could affect the performance of structures. It also evaluates the effect of the structures in a notional sense. Moreover, it evaluates the potential climate change effects of the largest wind and snow loads, and on the structural safety.

The largest wind loads are assessed in terms of extreme wind speed by considering the thunderstorm and non-thunderstorm winds separately. Such an assessment was not available in the literature for Canada. The assessment allowed us to map the wind hazard and to identify regions that are prone to thunderstorm winds. Maps are developed and recommended for practical use.

The evaluation of the snow loads considers both the snow component and rain component as indicated in the National Building Code. The statistics of and probabilistic models for the annual maximum ground snow depth and ground snow load (as well as snowpack bulk density) were assessed and presented. An evaluation for rain and snow components of the roof snow load indicates that extreme rain and snow events are less likely to happen concurrently. This result indicated a modification for the current snow load evaluation method that leads to a relatively conservative estimation.

With the newly developed statistics of the wind and snow, new wind and snow load factors were suggested for the National Building Code of Canada to ensure the structural reliability achieves the required safety level. In addition, new practical approach in defining the design wind and snow loads by considering climate change effects is recommended.

Co-Authorship Statement

The materials presented in this thesis are based on three joint-authored manuscripts.

A version of Chapter 2, co-authored with H.P. Hong, will be submitted to a peer-reviewed journal for possible publication.

A version of Chapter 3, co-authored with H.P. Hong and others, will be submitted to a peer-reviewed journal for possible publication.

A version of Chapter 4, co-authored with H.P. Hong and others, will be submitted to a peer-reviewed journal for possible publication.

Acknowledgments

First and foremost, I would like to express my deep and sincere gratitude to my supervisor, Dr. Hanping Hong, for the continuous support and guidance throughout my Ph.D. study and research. His patience, motivation, enthusiasm, and immense knowledge have always been helping and inspiring me to pursue my academic goal.

Many thanks go to my thesis committee members for their careful reading and constructive comments that help to improve this thesis.

I also want to thank my colleagues at Western University for providing me the essential help and support when I need it most.

Last but not least, I am deeply and forever indebted to my parents and my wife for their love, support, and encouragement.

Table of Contents

List of Tables

List of Figures

Nomenclature

Chapter 2

$P_{N/A\text{-}TH}$	The probability of no thunderstorm occurrence in a year
V_{AH}	The annual maximum wind speed
$v_{AH\text{-}T}$	The *T*-year return period values of the annual maximum (hourly-mean) wind speed
μ_X	The mean of *X*
v_x	The COV of *X*
σ_X	The standard deviation of X

Chapter 3

R_A	The annual maximum 1-day rain amount
$r_{A\text{-}T}$	The *T*-year return period value of R_A
S_A	The annual maximum ground snow depth
S_{AL}	The annual maximum ground snow load data
$s_{A\text{-}T}$	The T-year return period values of the annual maximum snow depth
$s_{\mathrm{Gmax},i}$	The ground snow load for the *i*-th year
$s_{\mathrm{Gmax}\xi,i}$	The days within the *i*-th year where the ground snow load is greater than $\xi s_{\mathrm{Gmax},i}$
S_L	The ground snow load
$s_{L\text{-}T}$	The *T*-year return period value of the annual maximum ground snow load

$s_L(T)$	The T-year return period value of S_L
$s_{\text{max-}i}$	The ground snow depth for the i-th year
S_R	The rain component of the snow load
$s_{\text{Rmax-}i}$	The 1-day winter rain load for the i-th year
$s_{R\text{-}T}$	The T-year return period value of S_R
ρ_b	The snowpack bulk density

Chapter 4

C_{gr}	The transformation factor that converts the ground snow load at a given site to an appropriate roof snow load
D	The dead load
I_S	The importance factor for the snow load
I_W	The importance factor for the wind load
P_f	The failure probability
p_{NT}	The probability of no thunderstorm occurrence per year
p_0	The probability of zero annual maximum S_A
R	The resistance
$R_{L/D}$	The ratio of factored live load to factored dead load
$R_{S/D}$	The ratio of the factored design snow load to the factored design dead load
$R_{W/D}$	The ratio of the factored design wind load to the factored design dead load
S_A	The annual maximum ground snow depth

$s_{A\text{-}T}$	The *T*-year return period values of the annual maximum snow depth
S_n	The nominal snow load
S_R	The rain component of roof snow load
T_{Short}	A relatively short return period
T_{long}	A relatively long return period
V_{AH}	The annual maximum wind speed
W	The wind load
W_n	The nominal wind load
Z_S	The normalized transformation factor for snow load
α_{CL}	The companion live load factor
α_{CS}	The companion snow load factor
α_{CW}	The companion wind load factor
α_L	The live load factor
α_S	The snow load factor
α_W	The wind load factor
β_{50}	The reliability index for a design working life of 50 years
β_{minA}	The minimum annual reliability index
β_{T50}	The target reliability index for a design working life of 50 years
β_{TminA}	The target reliability index for β_{minA}

η_{CS}	The scaling factor due to climate change for snow load
η_{CW}	The wind load scaling factor accounting for climate change
v_{VAH}	COV of V_{AH}
$v_{AH\text{-}T}$	The T-year return period values of the annual maximum (hourly-mean) wind speed

Chapter 1

1. Introduction

1.1. Literature review

Wind loads recommended in the structural design codes in the National Building Code of Canada (NBCC) are developed based on extreme value analysis by mixing both the extreme thunderstorm and non-thunderstorm (i.e., commingled) winds. The reference wind velocity pressure implemented in the NBCC prior to, and including 1990, can be found in NRC (1990). Estimates of the 10-, 30- and 100-year return period values of the annual maximum wind velocity pressures were provided in the code. These return period values were calculated based on the return period values of the annual maximum wind speed. It was indicated that the Gumbel probability distribution was used to fit the annual maximum wind speed by using the least-squares method. Yip and Auld (1993) and Yip et al. (1995) described the update of the reference wind velocity pressures implemented in the 1995 edition of the NBCC (NRC 1995). Again, the Gumbel distribution was used to fit the annual maximum wind speed but using the method of moments (MOM). The companion-action load combinations were implemented in NBCC-2005, and the 50-year return period value of the (annual maximum) wind velocity pressure coupled with a wind load factor of 1.4 is recommended (Bartlett et al. 2003a,b). The factored design wind load corresponds to approximately the 500-year return period value of the annual maximum wind speed. The 50-year return period values of the wind velocity pressure were calculated based on their corresponding 30-year values recommended in the 1995 edition of the NBCC and by considering that the annual maximum wind speed is a Gumbel variate. An updated wind velocity pressure for the 2010 edition of the NBCC was carried out by fitting the Gumbel distribution to the annual extreme wind speed using the MOM.

Snow load on the roof is another environmental load specified in design codes. The roof snow load in the NBCC (NRC 2015) consists of two components: the snow component and the rain component. Variations exist in the definition of each component between different versions of the code (Boyd 1961; Newark 1984; Newark et al. 1989; Hong and Ye 2014).

The snow component is calculated based on the ground snow load (Taylor and Allen 2000; Bartlett et al. 2003a,b). The issues that need to be addressed to estimate the ground snow load include (Newark et al. 1989) the average annual snowpack bulk density and the return period value of the annual maximum ground snow depth. The spatial variation of the snowpack bulk density for Canada was presented in Newark (1984) and Newark et al. (1989) for the update of the 1990 edition of NBCC. No new data on the annual snowpack bulk density covering Canada were found in the literature for the development of newer editions of NBCC since 1990. The estimation of the return period value of the annual maximum ground snow load and spatial interpolation is affected by the data availability, adopted probabilistic models, and probability distribution fitting methods.

The NBCC (NRC 2015) prescribes the design loads for design buildings in Canada. Similar to other structural design codes in the world, the load factors in the NBCC were calibrated based on the limit state design format. A key issue for the reliability-based design code calibration is the selection and assignment of the probabilistic models of the random variables involved in the limit state functions. The probabilistic models of extreme wind velocity and ground snow load can be developed based on their historical records alone if the effects of climate change can be neglected. In such a case, the extreme of the climatological elements could be assumed to be stationary. An influential study focused on the calibration of structural design codes in the U.S. was presented in Ellingwood et al. (1980). Some of the earlier studies of reliability-based design code calibration focused on Canadian structural design practice were presented in Allen (1975), Nowak and Lind (1979), Kennedy (1984), MacGregor et al. (1983), and Foschi et al. (1993). An update to the probabilistic models used to calibrate load and companion factors for the wind and snow loads in the current NBCC was given in Bartlett et al. (2003a,b).

Besides the stationary extremes, the climate is changing, and the temporal temperature increasing trend affects the extreme environmental parameters, which need to be considered for structural design. The design wind and snow loads in the past and current editions of the NBCC were calibrated using the probabilistic models of the extreme wind and snow loads that were developed based on the historical meteorological data. The possible effect of climate change on structural code making was not considered. Climate change may have implications in

structural design code making since climate change leads to nonstationary statistics of the extreme wind speed, ground snow depth, and precipitation (Cannon et al. 2019).

1.2. Objectives and organization of the thesis

The objectives of the thesis were:

1) to compare and characterize the wind hazards based on the extreme thunderstorm and non-thunderstorm winds as well as commingled winds and to investigate the impact of considering the mixed wind climate on the wind hazard mapping

2) to provide statistics and probabilistic models for the annual maximum ground snow depth, ground snow load, and snowpack bulk density using up to date routinely reported meteorological variable, and to map snow hazard in terms of annual maximum ground snow depth and ground snow load.

3) To carry out reliability-based design code calibration by considering the mixed wind climates, the spatially-varying snow hazard, to potentially modify the format for the loads used in the National building code of Canada to improve reliability consistency (i.e., by changing load factors and specification of the nominal loads).

4) To carry out reliability-based design code calibration by considering nonstationary effect due to climate change, and to suggest a practical and simple to implement load format which could cope with climate change effect.

The remainder of this study was organized as follows. In Chapter 2, two digital archives containing historical wind records were considered for wind hazard mapping for Canada. For the probabilistic analysis, the use of different probabilistic models for thunderstorm and non-thunderstorm winds was investigated; such an investigation is unavailable in the literature. The return period values of the annual maximum wind speed were estimated by treating the non-thunderstorm and thunderstorm winds separately. In addition, the effect of spatial smoothing methods was discussed.

In Chapter 3, the probabilistic modeling of the annual maximum ground snow depth was developed based on the historical snow depth dataset. The ground snow loads were estimated based on the ground snow depth and the corresponding snowpack bulk density. The statistical analysis of the rain load, which is one of the roof snow load components, was also carried out. The adequacy of the format used to evaluate the roof snow load based on the snow load component and rain load component implemented in the NBCC was discussed.

In Chapter 4, a design code calibration was carried out for NBCC. The calibration adopted a target reliability index that was used to calibrate the wind load and snow load in the current NBCC. The calibration for the wind load considers the mixed wind climates, which were never discussed in previous versions of NBCC. The calibration was focused on the improvement of the reliability consistency considering the fact that the statistics of wind and snow load are spatially-varying across Canada. Most importantly, the calibration considered the effects of nonstationary extreme wind and snow loads due to climate change. The calibration analysis was aimed at suggesting a set of design wind load, snow load, and companion load factors that could be potentially adopted in a future edition of NBCC.

Finally, Chapter 5 summarized the main conclusions drawn from the previous chapters. Recommendations were given for future work.

1.3. References

Allen, D.E. (1975). Limit states design—a probabilistic study. Canadian Journal of Civil Engineering, 2(1), 36-49.

Bartlett, F.M., Hong, H.P. and Zhou, W. (2003a). Load factor calibration for the proposed 2005 edition of the National Building Code of Canada: Statistics of loads and load effects, Canadian Journal of Civil Engineering, 30 (2) 429-439.

Bartlett, F.M., Hong, H.P. and Zhou, W. (2003b). Load factor calibration for the proposed 2005 edition of the National Building Code of Canada: Companion-action load combinations, Canadian Journal of Civil Engineering, 30 (2) 440-448.

Boyd, D.W. (1961) Maximum snow depths and snow loads on roofs in Canada. Division of Building Research, Research Paper No. 142, National Research Council, Ottawa, Ont. In:

Proceedings of the Western Snow Conference, pp. 6–16, April

Cannon A. (2019). Climate-Resilient Buildings & Core Public Infrastructure Guidance on Updating Climate Design Values for Enhanced Resilience to Future Climate Conditions, ECCC, Draft report.

Ellingwood, B., Galambos T.V., MacGregor J.G. and Cornell C.A. (1980). Development of a probability based load criterion for American national standard A58. Nat. Bureau of Standards Special Pub. No. 577.

Foschi, R.O., Folz, B. and Yao, F. (1993). Reliability-based design of wood structures: background to CSA-086.1-M89. Canadian Journal of Civil Engineering, 20(3), 349-357.

Hong, H.P. and Ye, W. (2014). Analysis of extreme ground snow loads for Canada using snow depth records. Natural hazards, 73(2), 355-371.

Kennedy, D.L. (1984). Limit states design of steel structures in Canada. Journal of Structural Engineering, 110(2), 275-290.

MacGregor, J.G., Mirza, S.A. and Ellingwood, B. (1983). Statistical analysis of resistance of reinforced and prestressed concrete members. In Journal Proceedings (Vol. 80, No. 3, pp. 167-176).

Newark, M.J. (1984). A new look at ground snow loads in Canada. Proceedings, Eastern Snow Conference, Vol. 29, 41st Annual Meeting, Washington, DC, pp. 37-48.

Newark, M.J., Welsh, L.E., Morris, R.J. and Dnes, W.V. (1989). Revised ground snow loads for the 1990 National Building Code of Canada. Canadian Journal of Civil Engineering, 16(3): 267-278.

Nowak, A.S. and Lind, N.C. (1979). Practical code calibration procedures. Canadian Journal of Civil Engineering, 6: 112–119

NRC (1990) National Building Code of Canada. Institute for Research in Construction, National Research Council of Canada, Ottawa

NRC (1995) National Building Code of Canada. Institute for Research in Construction, National Research Council of Canada, Ottawa

NRC (2015) National Building Code of Canada. Institute for Research in Construction, National Research Council of Canada, Ottawa

Taylor, D.A. and Allen, D.E. (2000). Statistical variation and duration of snow load on flat roofs

in Canada. Institute for Research in Construction, National Research Council of Canada, Ottawa, Ont. Unpublished study.

Yip, T. and Auld, H. (1993). Updating the 1995 National building code of Canada wind pressures. In Proceedings of the Electricity ’93 Engineering and Operating Division Conference. Canadian Electrical Association, Montréal, Canada.

Yip, T., Auld, H. and Dnes, W. (1995). Recommendations for updating the 1995 National building code of Canada wind pressures. In *Proceedings of the 9th International Conference on Wind Engineering*. International Association for Wind Engineering, New Delhi, India.

Chapter 2

2. Extreme value analysis of thunderstorm and non-thunderstorm winds for Canada

2.1. Introduction

Wind loads recommended in the structural design codes in the National Building Code of Canada (NBCC) were developed based on the extreme value analysis of mixed thunderstorm and non-thunderstorm winds (i.e., commingled winds). The reference wind velocity pressure implemented in the NBCC prior to, and including 1990, can be found in NRC (1990). Estimates of the 10-, 30- and 100-year return period values of the annual maximum wind velocity pressures were provided in the code. These return period values were calculated based on the return period values of the annual maximum wind speed. It was indicated that the Gumbel probability distribution was used to fit the annual maximum wind speed by using the least-squares method.

Yip and Auld (1993) and Yip et al. (1995) described the update of the reference wind velocity pressures implemented in the 1995 edition of the NBCC (NRC 1995). Again, the Gumbel distribution was used to fit the annual maximum wind speed but using the method of moments (MOM). More specifically, they used wind records from 233 stations, each with at least ten years of data to estimate the 30-year return period value of the annual maximum wind speed by adopting the Gumbel distribution fitted using MOM. A 30-year return period of the annual maximum wind speed map was plotted and used to extract the tabulated values in NBCC; the estimation of the return period value was based on the at-site analysis. By assuming that the ratio of the standard deviation of the annual maximum wind speed to the 30-year return period value of the annual maximum wind speed is a constant, the estimation of the return period values for a return period other than 30 years were carried out (Yip et al. 1995). The error caused by using such a simplifying assumption was discussed and quantified in Hong et al. (2014).

The companion-action load combinations were implemented in NBCC-2005, and the 50-year return period value of the (annual maximum) wind velocity pressure coupled with a wind load

factor of 1.4 was recommended (Bartlett et al. 2003a,b). The factored design wind load corresponds to approximately the 500-year return period value of the annual maximum wind speed. The 50-year return period values of the wind velocity pressure were calculated based on their corresponding 30-year return period values recommended in the 1995 edition of the NBCC and by considering that the annual maximum wind speed is Gumbel distributed. An updated wind velocity pressure for the 2010 edition of the NBCC was carried out by fitting the Gumbel distribution to the annual extreme wind speed using the MOM. For the update, a constant coefficient of variation (COV) of the annual maximum wind speed, V_{AH}, equal to 0.124 was adopted for all of the meteorological stations considered (Morris 2009). A comparison of the 50-year return period values of the annual maximum (hourly-mean) wind speed, $v_{AH\text{-}T}$, (for T = 50 years) inferred from the 2005 edition, and 2010 edition of the NBCC indicated that there are significant changes in $v_{AH\text{-}50}$ for some locations common in these two editions of the code (Hong et al. 2014). The largest decrease in $v_{AH\text{-}50}$ in the 2010 edition of the NBCC as compared to that in the 2005 edition of the NBCC is about 30%; the largest increase is less than 10%, and the majority of the changes are within 10%. Two relatively high wind regions in the Northwest Territories and Nunavut in the 2005 edition of the NBCC were eliminated in the 2010 edition of NBCC. A series of continuous "consistent" wind speed regions from east to west shown in the wind map inferred from the 2010 edition of the NBCC is not present in that inferred from the 2005 edition of the NBCC. This observed difference is likely due to the use of a constant COV to develop $v_{AH\text{-}50}$ for the 2010 edition of the NBCC.

For the extreme wind hazard assessment, the Gumbel distribution, the generalized extreme value distribution (GEVD) and the generalized Pareto distribution (GPD) are the most widely used probabilistic models (Frank 2001; Sacre 2002; Holmes and Moriarty 1999; Kasperski 2002; Miller 2003; Hong et al. 2014; Mo et al. 2015). For the Gumbel distribution, the most often used distribution fitting methods include MOM, the method of the maximum likelihood (MML), the method of L-moments (MLM) (Hosking 1990), the least-squares method, and the generalized least-squares method (GLM) (Lloyd 1952; Lieblein 1974; Hong et al. 2013). The results from Lowery and Nash (1970) indicate that MOM is less biased than MML. Hong et al. (2013) showed that in general, GLM outperforms MLM, MML, and MOM, and MLM outperforms MML and MOM. Based on these studies, it is recommended that the use of GLM

and MLM for fitting the Gumbel distribution is to be used. MOM, MLM, and MML are also often used methods if GEVD and GPD are considered. The Gumbel distribution and GEVD are frequently adopted to fit the annual maximum wind speed data, while GPD is applied to the wind speeds over a threshold.

A wind hazard mapping for Canada was carried out based on the annual maximum wind speed from more than 230 stations, where at least 20 years of useable data are available from each site or station (Hong et al. 2014). For the at-site analysis, the wind speed records from up to the year-end 2010 in Environment and Climate Change Canada (ECCC) HLY01 digital archive (see http://www.climate.weatheroffice.gc.ca/prods_servs/documentation_index_e.html#hly01) was used. They concluded that the Gumbel distribution is preferable to GEVD for more than 70% of the considered stations. The consideration of at least 20 years of useable data was aimed at reducing the statistical uncertainty in the estimated wind hazard due to the small sample size (Cook 1985; Hong et al. 2016); this attitude differed from that considered in evaluating wind hazard for previous versions of the code.

The use of the regional frequency analysis (Hosking and Wallis 1997) for wind hazard mapping was presented in Hong and Ye (2014) to investigate further the wind hazard and to reduce the effect of small sample size on the estimated $v_{AH\text{-}T}$. For their study, the same data set used in Hong et al. (2014) was considered. The k-means, hierarchical and self-organizing map clustering (Kohonen 2001; Hastie et al. 2001; Lin and Chen 2006) and statistical tests were used to identify clusters or "superstations" for regional frequency analysis. A comparison of the $v_{AH\text{-}50}$ values estimated based on the regional frequency analysis to those obtained from the at-site analysis indicated that they are in good agreement, especially if the Gumbel model is adopted. It is noteworthy that the use of cluster analysis to identify the climatic zones was also attempted for other countries (Fovell and Fovell 1993; Kruger et al. 2012).

The above shows that none of the studies focused on Canadian wind hazard maps and structural design code development considered the thunderstorm and non-thunderstorm winds separately. The adequacy of using the commingled extreme wind speed data in estimating the return period values of annual maximum wind speed for Canadian design codes was never scrutinized. The

estimation of the wind hazard by separating winds in thunderstorm winds and non-thunderstorm winds were presented in Lombardo et al. (2009) and Lombardo (2012). Such a separation could be important since the probabilistic characteristics of the extreme thunderstorm winds can be different from those of the extreme non-thunderstorm winds. The differences affect the estimated $v_{AH\text{-}500}$, and the reliability of the designed structures subjected to the wind loading.

The main objectives of this chapter were to 1) compare the statistical characteristics of the annual maximum thunderstorm and non-thunderstorm winds, 2) estimate wind hazard based on the thunderstorm and non-thunderstorm winds as well as commingled winds, and 3) map the wind hazard for thunderstorm winds, non-thunderstorm winds and commingled winds. For the statistical analysis and probabilistic modelling of the wind hazards, both the daily records archived by ECCC in DLY04 digital archive and the hourly records archived by ECCC in HLY01 are used.

2.2. Wind records

The characteristics of the anemometer types operated in Canada and the types of wind data recorded at meteorological stations were presented in Yip and Auld (1993) and Yip et al. (1995). The wind speed records for the meteorological stations were stored in digital archives, including DLY04 and HYL01 (see http://www.climate.weatheroffice.gc.ca/prods_servs/documentation_index_e.html#hly01), which were considered in the following.

The HLY01 contains wind records representing one- or two- or 10-minute average wind speed recorded immediately before the hour but mostly 2-minute average wind speed. A wind hazard assessment was reported in Hong et al. (2014) by using the recorded wind speed up until the end of the year 2010. Since more up to date wind records in HLY01 (i.e., until December 2017) were available at the beginning of this study, the analysis that has been carried out in Hong et al. (2014) was repeated in the following section. By considering the data from this digital archive and only including the stations, where each has at least 20 years of useable data, a total of 469 stations was identified. This number is much greater than the 232 stations identified in Hong et al. (2014). The locations of 469 stations were identified in Figure 2.1, indicating

relatively good spatial coverage. The annual maximum wind speeds were adjusted for exposure and height. The exposure adjustment was carried out based on the method recommended in ESDU (2002) and by following the steps described in Mara et al. (2013). The adjusted wind speed represents the wind speed for the standard exposure condition referred to in NBCC (NRC 2015) and represented the annual maximum moving average of the hourly-mean wind speed, V_{AH}. For extracting values of V_{AH}, the data quality control and assessment procedure described in Hong et al. (2014) was followed. In processing the wind speed, no distinction was made for the thunderstorm winds or non-thunderstorm winds because an indicator of wind type was not provided in this digital archive. Therefore, the processed values of V_{AH} could be viewed as of commingled winds. However, the recorded wind speed represents time-averaged (usually 10-min or 2-min) wind speed before the hour. It may not necessarily capture the maximum of the 3-second gust wind speed from a thunderstorm event, and the wind speed that was processed and extracted from HLY01 could be used as a proxy for the synoptic winds. For this reason, this processed V_{AH} will be considered as synoptic winds in the following.

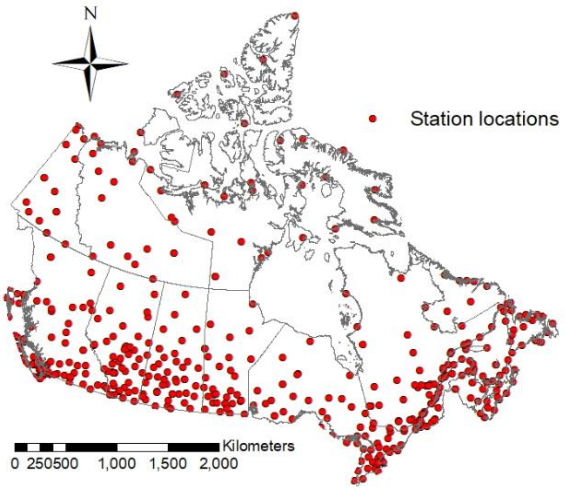

Figure 2.1. Locations of the stations from HLY01 (439 stations, each with at least 20 years of useable data).

The DLY04 digital archive available to this study contained meteorological information up until the end of the year 2017 from 361 meteorological stations. It was noted that the wind records were only available from 1954 to 2014. The database provided the daily maximum 3-second

gust mean wind speed and identified whether a thunderstorm event caused the recorded wind speed. A data processing carried out indicated that the thunderstorm winds were recorded in 297 stations out of 361 stations. A preliminary screening of the data from each station was carried out. To reduce the small sample size effects on the assessment of the statistics of the extreme wind speed and to have sufficient spatial coverage, it was decided that data from a station was to be included if it contains at least 10 years of useable data (thunderstorm or non-thunderstorm). This resulted in a dataset from a total of 222 stations, of which the locations were shown in Figure 2.2. In general, the spatial coverage for the northern region is relatively sparse. The distribution of the number of years of data in a station was shown in Figure 2.3. It indicated that there were only 156 stations, each with at least 20 years of useable data. The maximum length of data in a station was 61 years.

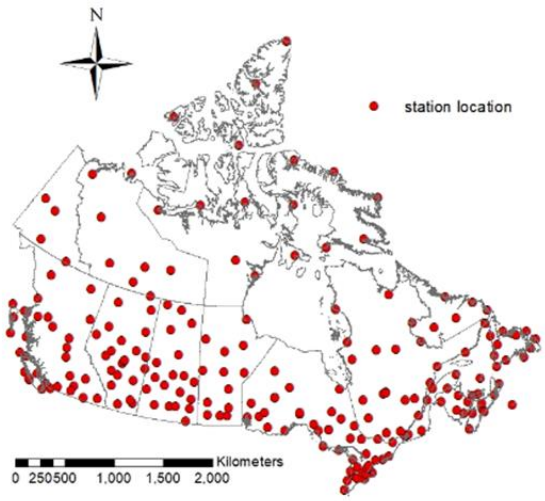

Figure 2.2. Locations of the meteorological stations where wind speed records in DYL04 are considered.

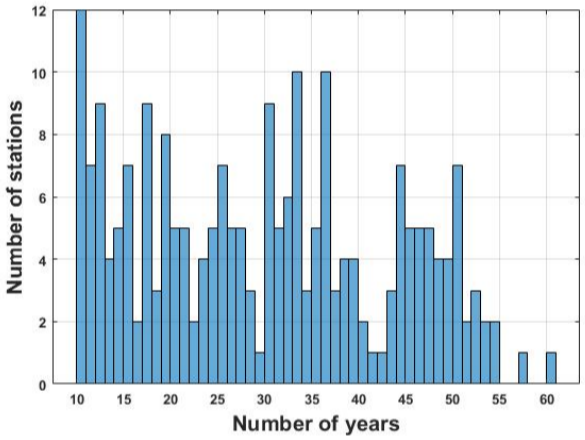

Figure 2.3. Distribution of the number of years of useable data at each station.

After data quality control, including the deletion of anomalous values, analysis of the data for the stations identified in Figure 2.2 indicated that thunderstorm activities were shown in 195 out of 222 stations, each with at least 10 years of useable thunderstorm wind speed data. These stations were identified in Figure 2.4a. The distribution of the number of years of useable data was shown in Figure 2.4b, indicating that there were only 147 stations, each with at least 20 years of useable data. The maximum length of data in a station was 58 years.

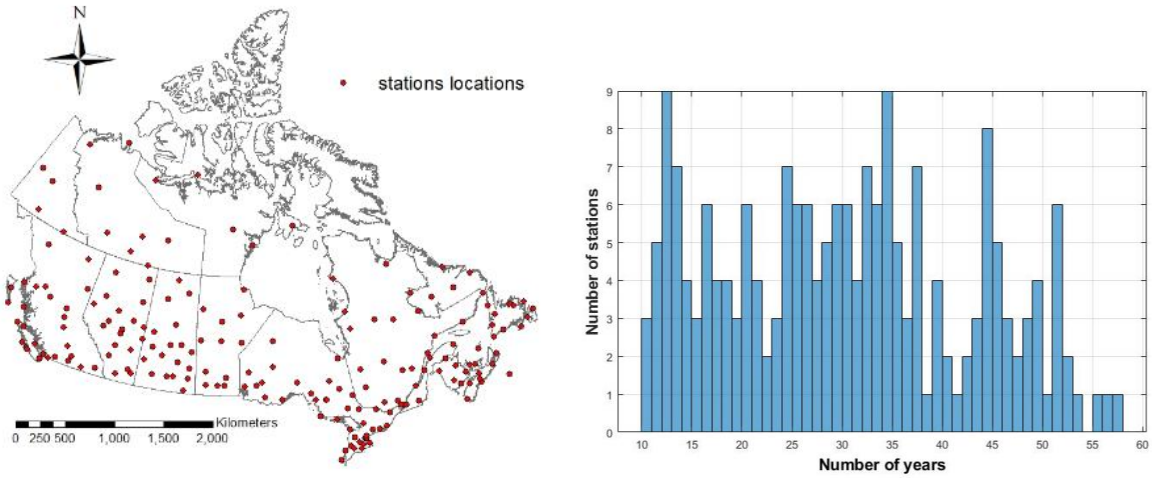

a) b)

Figure 2.4. Locations of the stations recorded thunderstorm winds (195 stations, each with at least 10 years of useable data) and distribution of the number of years of useable

data: a) Spatial distribution of the stations and, b) distribution of the number of years of useable data.

The reported daily maximum 3-second gust wind speed due to thunderstorm events for each station was extracted. An event-based maximum wind speed analysis procedure (Cook 1982) was used to process the extracted thunderstorm winds. This was to ensure that potential serial correlation was removed from the observed data. The wind speed data obtained in such a manner for each station, and after the exposure and height correction, were all converted to the hourly-mean wind speed by dividing the reported wind speed by a factor of 1.52 according to the well-known Durst curve (ASCE 7-17 2017). This conversion was considered to facilitate the comparison with current Canadian design practice. Unless otherwise indicated, the wind speed presented in the following was given in terms of hourly-mean wind speed at 10 m height above the ground surface and for open exposure condition as described in NBCC.

2.3. Statistics of annual maximum wind speed

By using the extracted V_{AH} from HLY01, the mean and coefficient of variation (COV) of V_{AH} at each station identified in Figure 2.1 were calculated. For 14 capital cities, the calculated mean and standard deviation were presented in Table 2.1. The calculated statistics from all the considered stations were used as the basis to develop their corresponding maps. For the mapping, the ordinary kriging (with nugget not equal to zero so to obtain a smoothed map) implemented in the ArcGIS (ESRI 2011; Johnston et al. 2003) was used, and the obtained results were presented in Figure 2.5. Unless otherwise indicated, the ordinary kriging with nugget not equal to zero was employed throughout this chapter so to obtain smoothed maps. The issue of using nugget equal to or not equal to zero in representing the wind hazard will be discussed in the following sections.

Table 2.1. Statistics of extreme winds (P_{NT} = probability of non-thunderstorm per year).

City	Annual maximum from HLY01	Annual maximum Non-thunderstorm winds from DLY04	Annual maximum Thunderstorm winds from DLY04

	Mean (km/hr)	COV	Mean (km/hr)	COV	Mean (km/hr)	COV	P_{NT}
Victoria	61.4	0.126	59.9	0.141	34.5	0.257	0.280
Whitehorse	56.8	0.134	53.2	0.158	33.5	0.250	0.043
Yellowknife	51.7	0.119	50.2	0.116	32.7	0.166	0.044
Iqaluit	78.4	0.167	66.8	0.168			1.000
Edmonton	72.7	0.083	62.0	0.118	57.0	0.176	0.025
Regina	75.5	0.107	69.3	0.135	63.1	0.178	0.024
Winnipeg	67.7	0.114	62.2	0.141	61.6	0.167	0.000
Ottawa	66.7	0.114	59.1	0.124	55.4	0.150	0.000
Toronto	64.3	0.119	58.7	0.083	53.3	0.203	0.000
Quebec	69.3	0.113	61.4	0.109	53.7	0.165	0.051
Fredericton	60.0	0.115	64.3	0.118	54.0	0.231	0.021
Halifax	66.0	0.144	63.2	0.133	44.6	0.227	0.000
Charlottetowm	71.2	0.117	70.8	0.129	42.8	0.223	0.017
St.John's	91.9	0.122	83.5	0.121	52.1	0.306	0.017

The table shows that the mean and COV of V_{AH} vary from city to city; the average COV value for the selected 14 cities is around 0.12. The statistics of V_{AH} by using data from DLY04 will be discussed shortly. The maps of the statistics of V_{AH} presented in Figure 2.5 were with greater granularity as compared to those shown in Hong et al. (2014), which is based on wind records up to 2010 with only 232 stations, as mentioned earlier. This was especially the case for the map of COV. The COV values of V_{AH} shown in Figure 2.5 ranges from about 0.05 to 0.3 with an average of 0.132, which differs slightly from 0.138 obtained in Hong et al. (2014), and from the 0.135 representing the average value inferred from an earlier version of the NBCC (Bartlett et al. 2003) and from the weighted average of 0.124 used in Morris (2009). The COV value for about 70% of the considered stations is within 0.1 to 0.2. This range of values is considered as the representative range of COV and is used for most reliability analysis to be carried out. As a slightly conservative assumption, 0.138 could be suggested as the typical representative reference value.

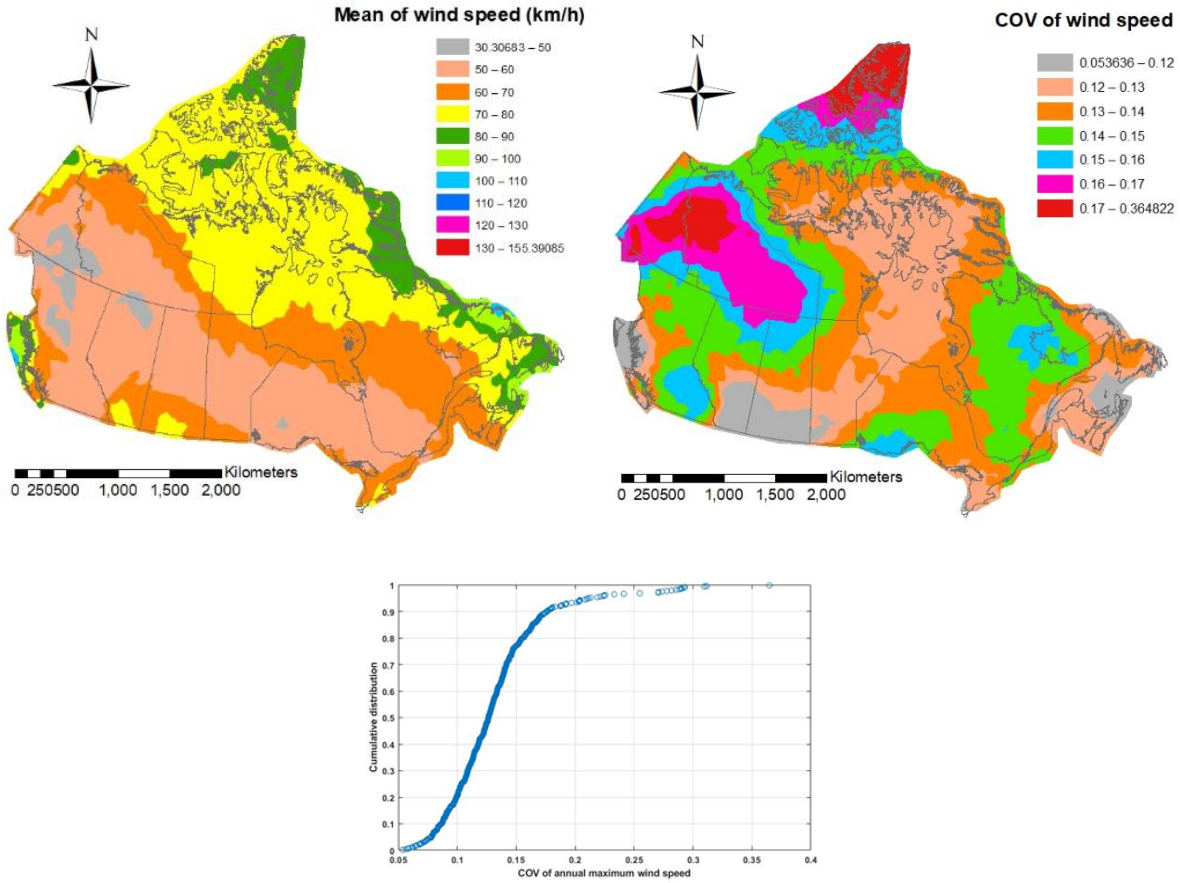

Figure 2.5. Spatial variation of the mean and coefficient of variation of V_{AH} considering the wind records from HLY01, and the distribution of COV (the mean of COV equals 0.132).

The processed wind records form DLY04 were used to establish three groups of wind records: commingled winds, thunderstorm winds, and non-thunderstorm winds. For each group of the wind records, the annual maximum wind speed V_{AH} recorded at each station was extracted. The mean and COV of non-zero samples of V_{AH} at each station for each group were calculated. For the 14 capital cities, the mean and COV of V_{AH} for the non-thunderstorm winds and the thunderstorm winds were presented in Table 2.1 for comparison purposes. The table indicated that the COV values of the thunderstorm winds are consistently greater than those obtained based on the synoptic winds (i.e., V_{AH} extracted from HLY01 digital archive). Also, the mean of the annual maximum thunderstorm wind speed is consistently lower than that obtained for

the synoptic winds. The calculated statistics from all the stations identified in Figure 2.2 were used as the basis to develop the maps of the mean and COV values. It is emphasized again that for the case of thunderstorm winds, only the non-zero V_{AH} values recorded were considered as in some stations, there were no thunderstorm winds recorded during a year. The maps were presented in Figures 2.6 to 2.8. Several observations could be drawn from Figures 2.5 to 2.8:

1) A comparison of the statistics shown in Figure 2.5 obtained for commingled winds based on the wind record from DLY04 to those presented in Figure 2.4 indicates that they exhibit similar spatial trends, especially for the mean. This suggests that, in general, the two datasets are consistent, at least qualitatively, and by considering commingled winds.

2) The mean of V_{AH} for the commingled winds is comparable to that for the non-thunderstorm winds based on data from DLY04. The mean of V_{AH} for thunderstorm winds is the lowest among the three groups of winds considered. This lower value for the annual maximum thunderstorm winds is due to that the annual maximum thunderstorm wind speed is not necessarily the greatest wind speed every year at a considered meteorological station.

3) The COV values of V_{AH} for the commingled winds are comparable to those for non-thunderstorm winds. Furthermore, the range of COV values shown in Figures 2.6 and 2.8 is comparable to that obtained based on hourly data from the HLY01 digital archive, as shown in Figure 2.5.

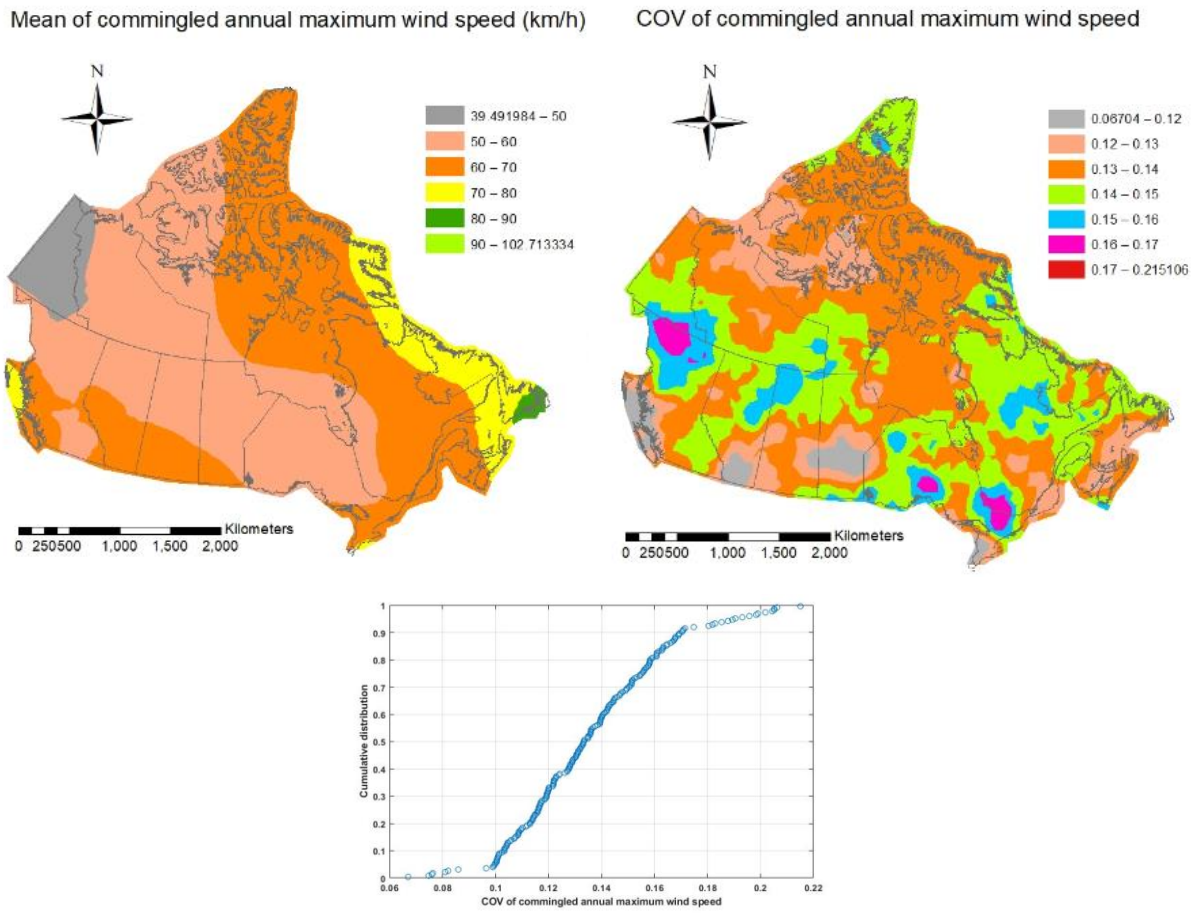

Figure 2.6. Spatial variation of the mean and coefficient of variation of V_{AH} considering the commingled winds, and the distribution of COV (the mean of COV equals 0.136).

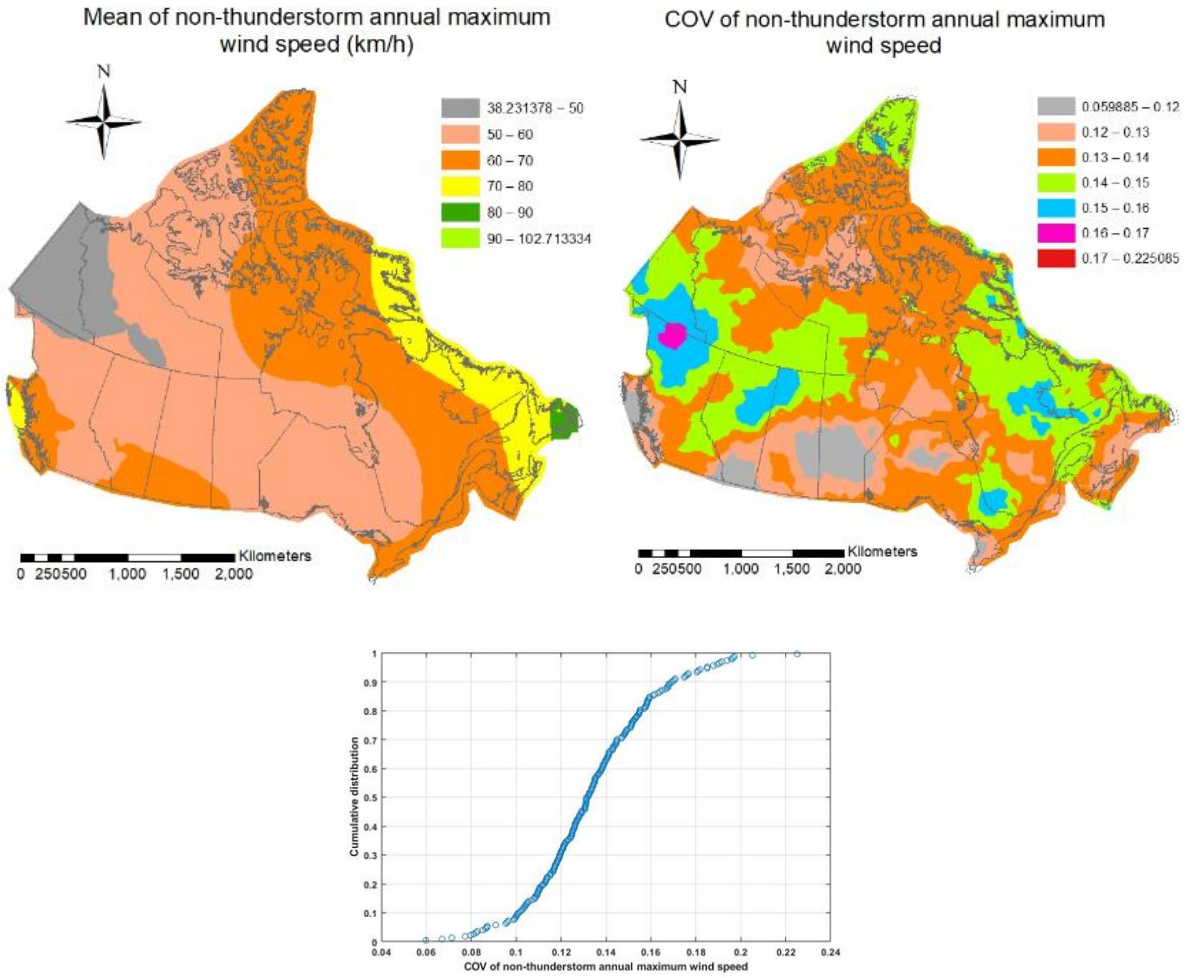

Figure 2.7. Spatial variation of the mean and coefficient of variation of V_{AH} considering the non-thunderstorm winds, and the distribution of COV (the mean of COV equals 0.134).

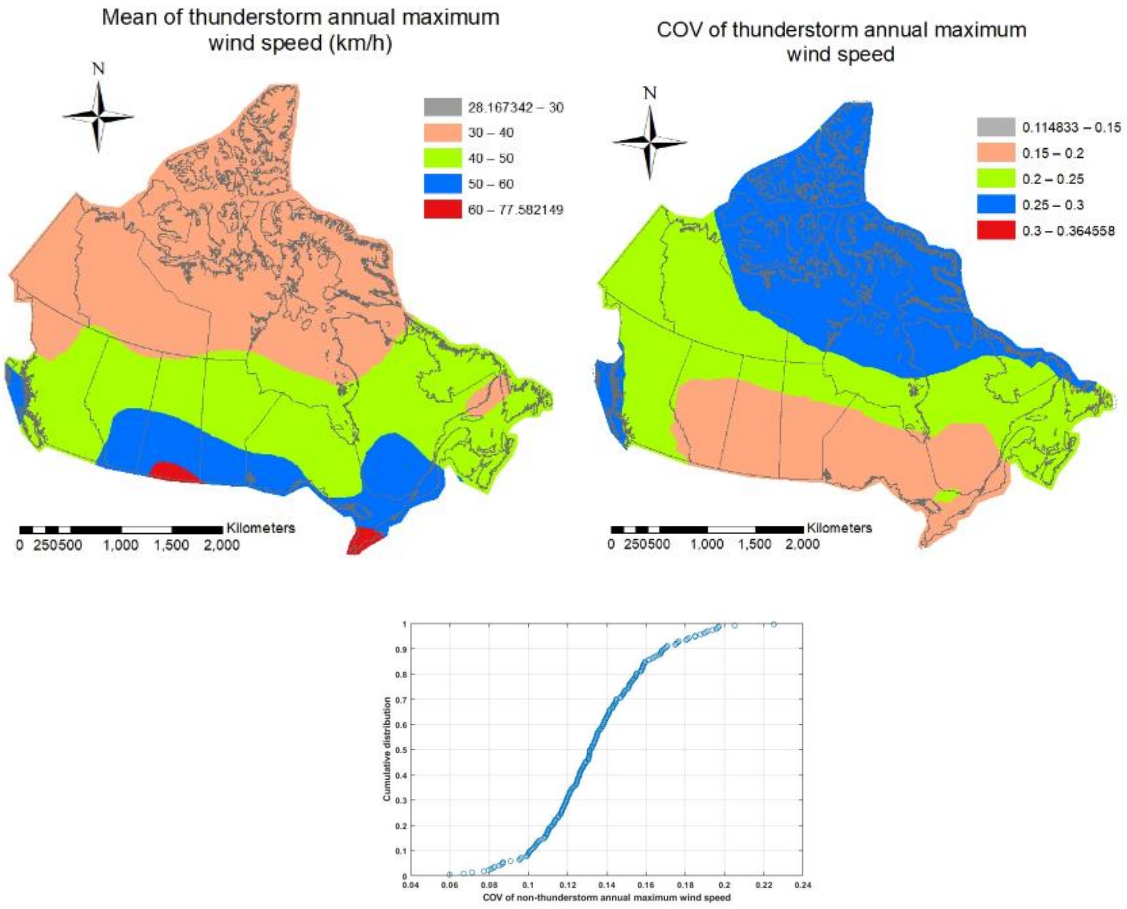

Figure 2.8. Spatial variation of the mean and coefficient of variation of V_{AH} considering the thunderstorm winds, and the distribution of COV (the mean of COV equals 0.21).

4) The spatial trends of the COV values for the commingled winds estimated by using the data from DLY04 are less apparent as compared to those observed based on HLY01 digital archive. This was partly attributed to that the results presented in Figure 2.6 contained statistics derived based on sample size between 10 to 20 (i.e., 10 to 20 annual maximum data points) for some stations. While an analysis by using data from DLY04 digital archive for stations, each with more than 20 years of useable data, was also carried out, the obtained map for COV again was similar to that shown in Figure 2.6 but not comparable to that presented in Figure 2.5 due to limited spatial coverage. For this reason, such a map was not included.

5) The COV values of V_{AH} for thunderstorm winds can be higher than those of the non-

thunderstorm winds. This simply indicates that the degree of uncertainty in annual maximum thunderstorm winds for a site is higher. An inspection of the results shown in Figures 2.6 to 2.8 indicates that the regions with larger COV values of the annual maximum thunderstorm winds are associated with the regions with lower mean values of the annual maximum thunderstorm winds.

6) The COV value of V_{AH} for thunderstorm winds increases from south to north. As will be seen, this increase is associated with decreased thunderstorm activities. For the southern region of Canada, the COV value is less than 0.2. This observation is important, and as will be seen, the wind hazard is dominated by thunderstorm winds only for the southern part of Canada.

To quantitatively evaluate the trends of thunderstorm activities, the probability of no thunderstorm occurrence in a year, $P_{N/A\text{-}TH}$, was calculated and shown in Figure 2.9a. The figure showed that the thunderstorm occurrence rate decreases from south to north. The most significant thunderstorm activities were found in southern Ontario and the southern part of the Prairies. Also, the calculated average number of thunderstorm events at a site per year was shown in Figure 2.9b. As expected, the spatial trends of the rate per year are similar to those of $P_{N/A\text{-}TH}$. The average number of thunderstorm events for a region that is prone to thunderstorm activities is about 15 per year.

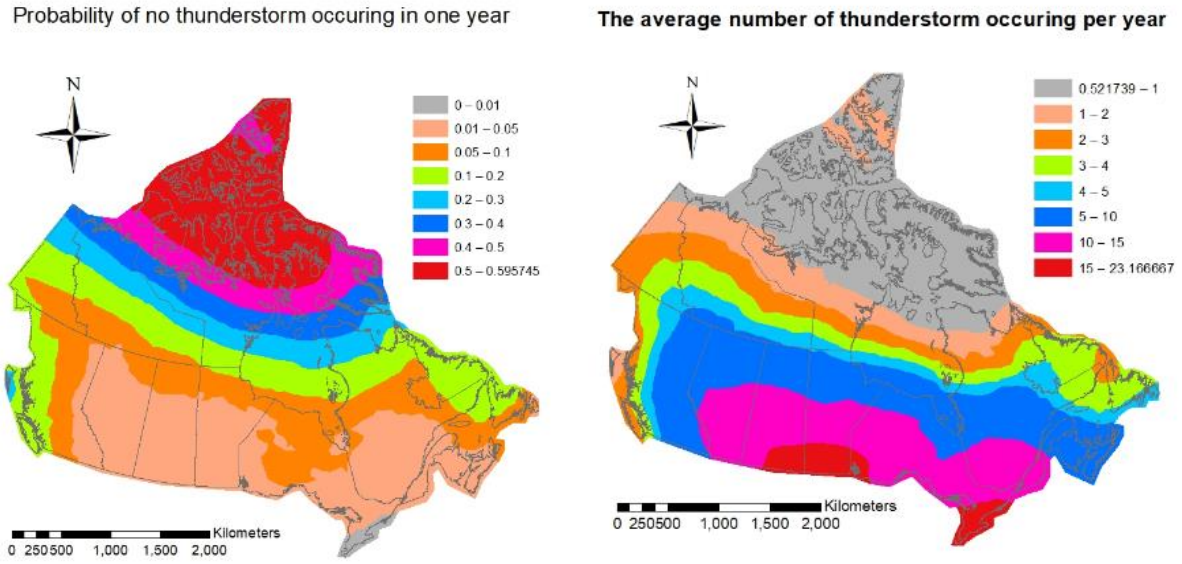

a) b)

Figure 2.9. The probability of no thunderstorm occurrence in a year, $P_{N/A\text{-}TH}$, and thunderstorm occurrence rate per year.

2.4. Preferred probabilistic model of annual maximum wind speed

2.4.1. Models for synoptic, commingled and non-thunderstorm winds

As mentioned in the introduction, two of the most commonly used probability distributions for V_{AH} are the Gumbel distribution and GEVD. The Gumbel distribution $F_{GU}(x)$ is expressed as (Castillo 1988; Coles 2001),

$$F_{GU}(x) = \exp\left(-\exp\left(-(x-u)/a\right)\right), \tag{2.1}$$

where x denotes the value of the random variable X (representing V_{AH}), and a and u are model parameters. The mean μ_X and the standard deviation σ_X are equal to $u + 0.5772a$ and $a\pi/\sqrt{6}$, respectively. The COV of X, v_x, by definition, equals σ_X/μ_X. For the distribution fitting, the MOM, MML, MLM, and GLM could be considered, but MLM and GLM are preferred (Castillo 1988; Hosking and Wallis 1997; Hong et al. 2013).

GEVD, $F_{GE}(x)$, is expressed as (Castillo 1988; Coles 2001),

$$F_{GE}(x) = \exp\left(-\left(1-k(x-u)/a\right)^{1/k}\right), \text{ for } k \neq 0 \tag{2.2}$$

where u, a and k are the model parameters. This distribution turns to the Gumbel distribution shown in Eq. (2.1) if k tends to 0.

A fitting exercise was carried out by using these two models for the samples of V_{AH} obtained from HLY01. Based on the Akaike information criterion, including the effect of sample size, (*AICc*) (Akaike 1974; Cavanaugh 1997), the Gumble model is preferred for wind data from about 70% of stations, which is consistent with the finding given in Hong et al. (2014). A plot of the fitted Gumbel distribution was presented in Figure 2.10 for 14 capital cities to illustrate the adequacy of the fit. The plots for the annual maximum wind speed extracted from DLY04 for the commingled winds and the non-thunderstorm winds were discussed in the following.

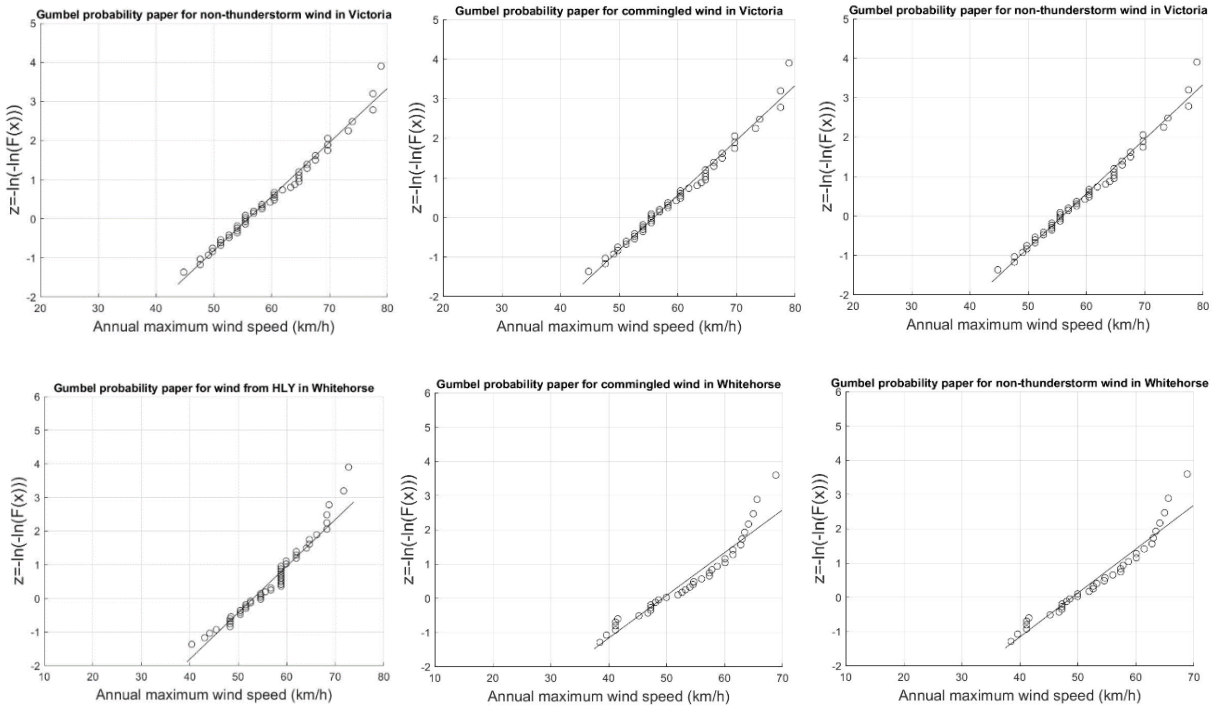

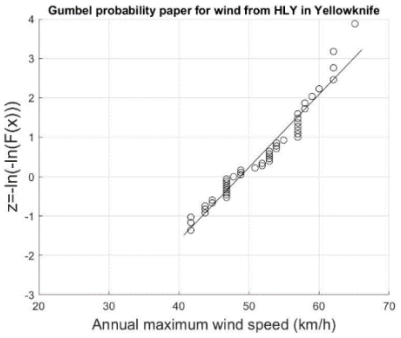
Gumbel probability paper for wind from HLY in Yellowknife
z=-ln(-ln(F(x)))
Annual maximum wind speed (km/h)

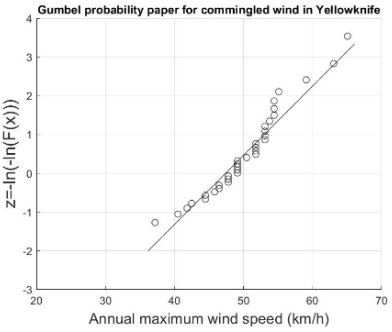
Gumbel probability paper for commingled wind in Yellowknife
z=-ln(-ln(F(x)))
Annual maximum wind speed (km/h)

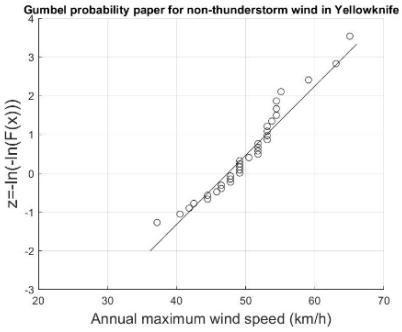
Gumbel probability paper for non-thunderstorm wind in Yellowknife
z=-ln(-ln(F(x)))
Annual maximum wind speed (km/h)

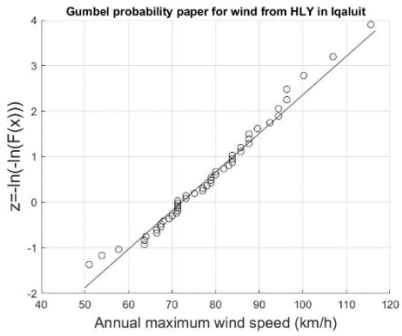
Gumbel probability paper for wind from HLY in Iqaluit
z=-ln(-ln(F(x)))
Annual maximum wind speed (km/h)

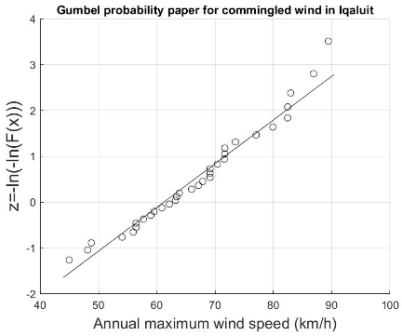
Gumbel probability paper for commingled wind in Iqaluit
z=-ln(-ln(F(x)))
Annual maximum wind speed (km/h)

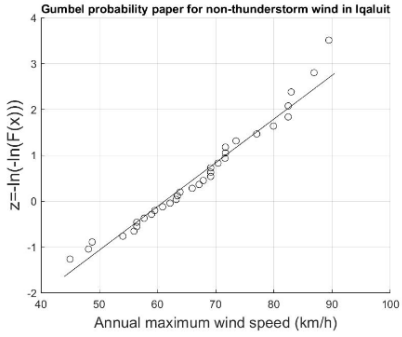
Gumbel probability paper for non-thunderstorm wind in Iqaluit
z=-ln(-ln(F(x)))
Annual maximum wind speed (km/h)

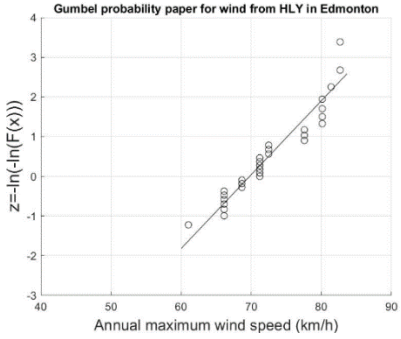
Gumbel probability paper for wind from HLY in Edmonton
z=-ln(-ln(F(x)))
Annual maximum wind speed (km/h)

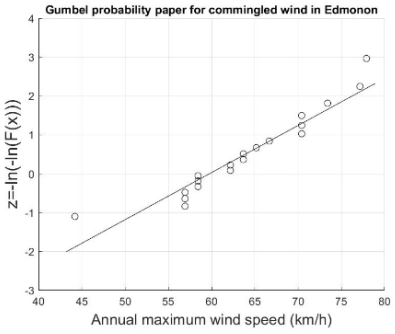
Gumbel probability paper for commingled wind in Edmonon
z=-ln(-ln(F(x)))
Annual maximum wind speed (km/h)

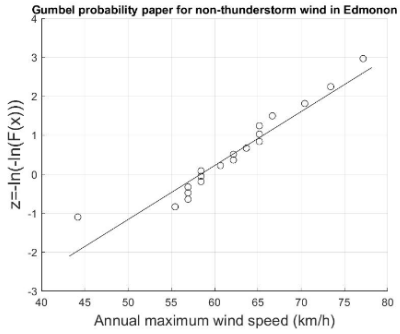
Gumbel probability paper for non-thunderstorm wind in Edmonon
z=-ln(-ln(F(x)))
Annual maximum wind speed (km/h)

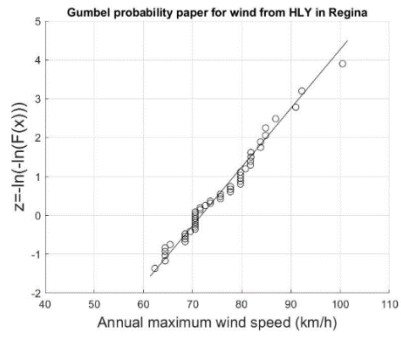
Gumbel probability paper for wind from HLY in Regina
z=-ln(-ln(F(x)))
Annual maximum wind speed (km/h)

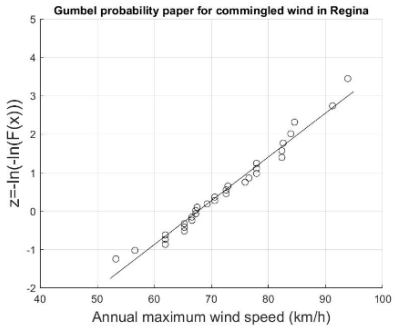
Gumbel probability paper for commingled wind in Regina
z=-ln(-ln(F(x)))
Annual maximum wind speed (km/h)

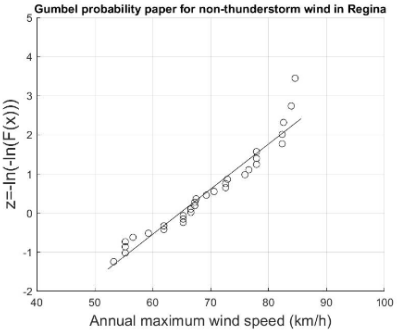
Gumbel probability paper for non-thunderstorm wind in Regina
z=-ln(-ln(F(x)))
Annual maximum wind speed (km/h)

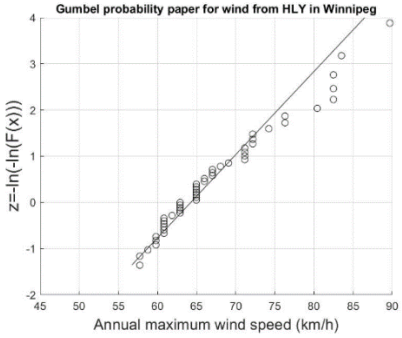
Gumbel probability paper for wind from HLY in Winnipeg
z=-ln(-ln(F(x)))
Annual maximum wind speed (km/h)

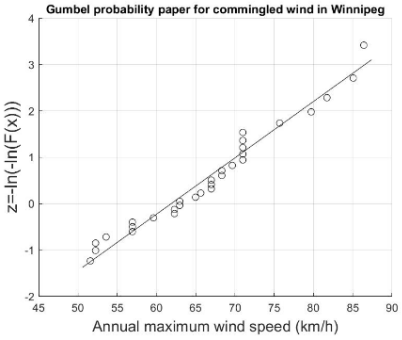
Gumbel probability paper for commingled wind in Winnipeg
z=-ln(-ln(F(x)))
Annual maximum wind speed (km/h)

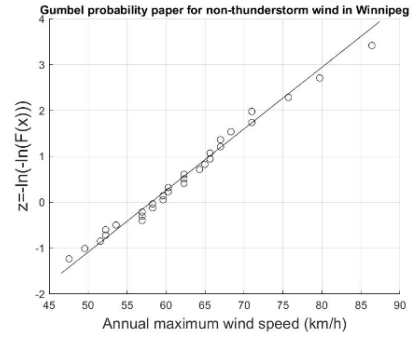
Gumbel probability paper for non-thunderstorm wind in Winnipeg
z=-ln(-ln(F(x)))
Annual maximum wind speed (km/h)

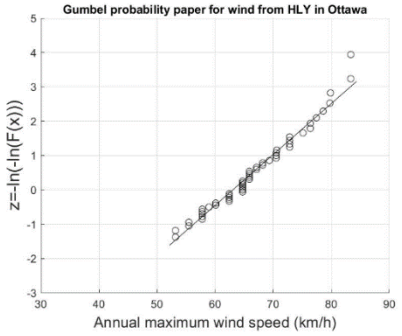
Gumbel probability paper for wind from HLY in Ottawa
z=-ln(-ln(F(x)))
Annual maximum wind speed (km/h)

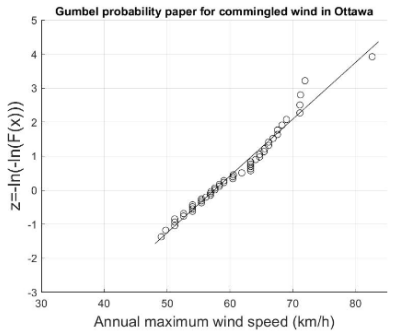
Gumbel probability paper for commingled wind in Ottawa
z=-ln(-ln(F(x)))
Annual maximum wind speed (km/h)

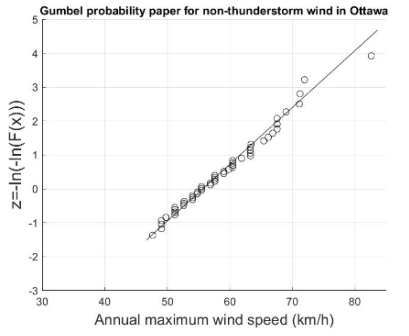
Gumbel probability paper for non-thunderstorm wind in Ottawa
z=-ln(-ln(F(x)))
Annual maximum wind speed (km/h)

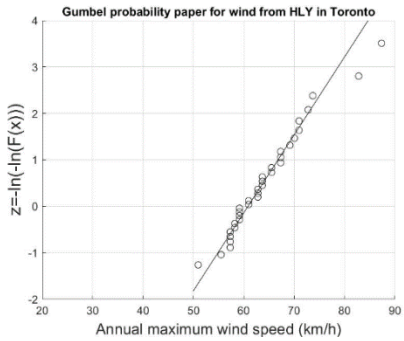
Gumbel probability paper for wind from HLY in Toronto
z=-ln(-ln(F(x)))
Annual maximum wind speed (km/h)

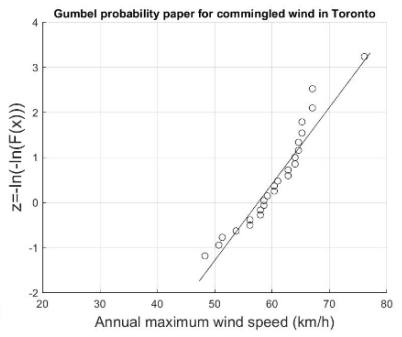
Gumbel probability paper for commingled wind in Toronto
z=-ln(-ln(F(x)))
Annual maximum wind speed (km/h)

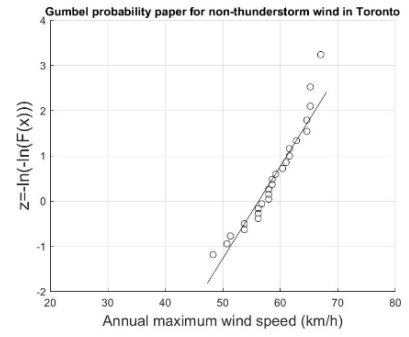
Gumbel probability paper for non-thunderstorm wind in Toronto
z=-ln(-ln(F(x)))
Annual maximum wind speed (km/h)

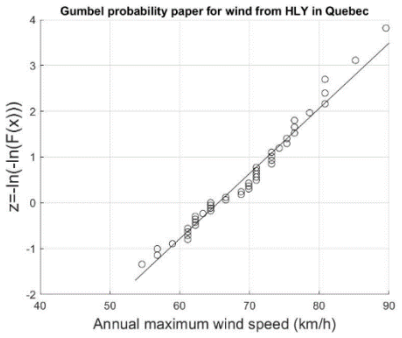
Gumbel probability paper for wind from HLY in Quebec
z=-ln(-ln(F(x)))
Annual maximum wind speed (km/h)

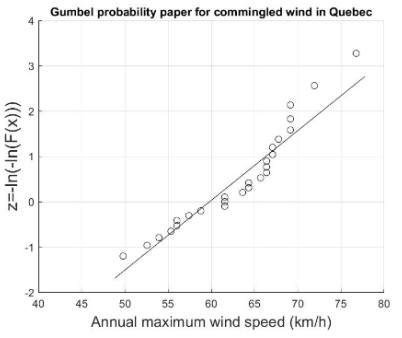
Gumbel probability paper for commingled wind in Quebec
z=-ln(-ln(F(x)))
Annual maximum wind speed (km/h)

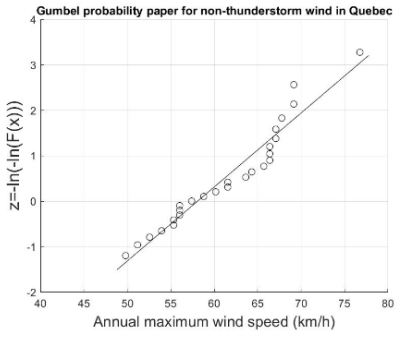
Gumbel probability paper for non-thunderstorm wind in Quebec
z=-ln(-ln(F(x)))
Annual maximum wind speed (km/h)

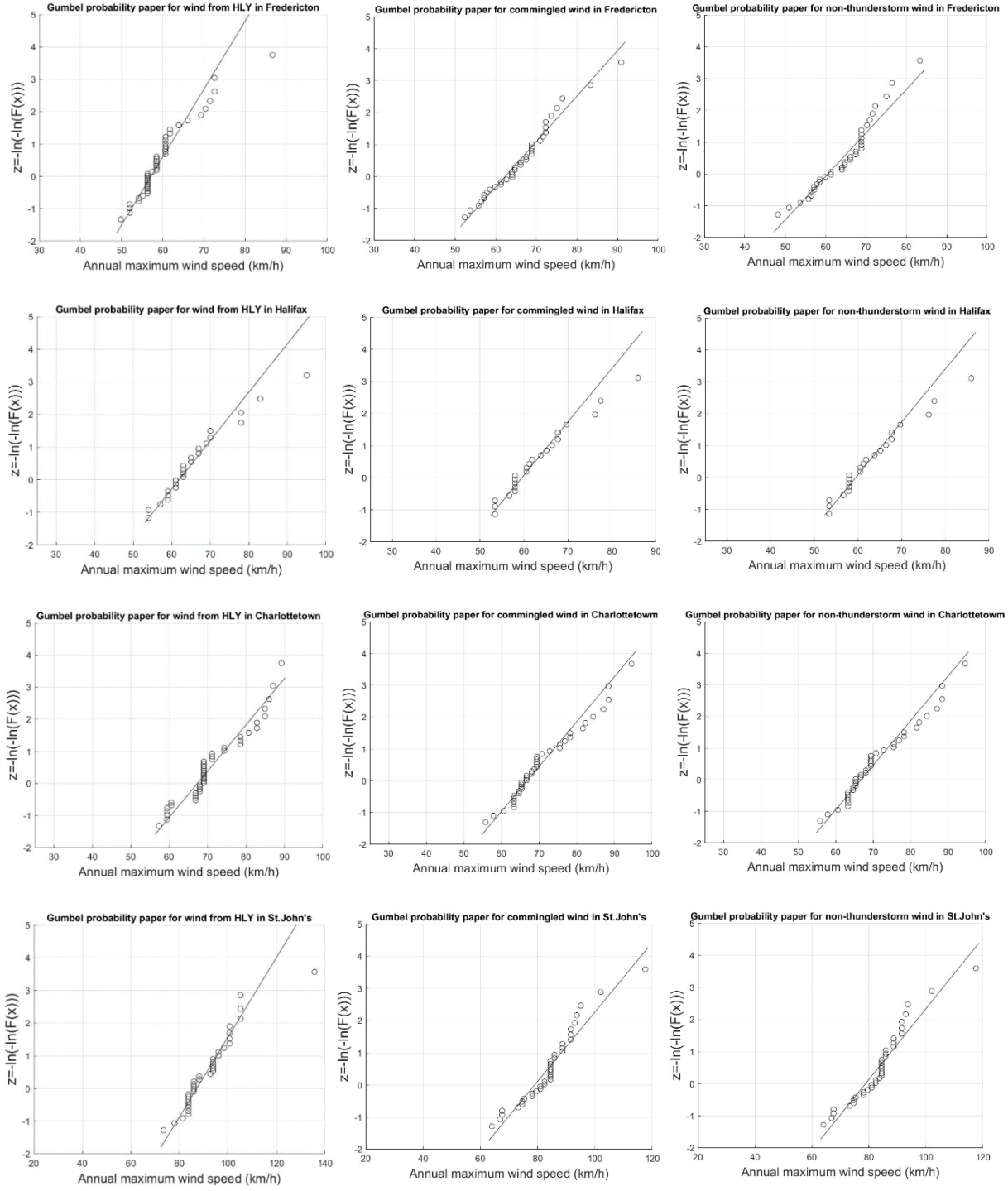

Figure 2.10. Samples and fitted distribution of V_{AH} shown in Gumbel probability paper for 14 capital cities. The first column showed the distribution of V_{AH} based on HLY01.

The second and third columns showed the distribution of V_{AH} for the commingled winds and the non-thunderstorm based on DLY04, respectively.

A fitting exercise was also carried out for the annual maximum wind speed for the commingled winds and the non-thunderstorm winds obtained from DLY04. Based on *AICc*, the preferred model between these two models for wind data from each station was identified and shown in Figure 2.11. The figure does not show clear spatial trends in the preferred probabilistic model. The ratio between the stations where GEVD distribution is preferred to the total number of stations is 36% for the commingled winds and 33% for the non-thunderstorm winds.

In other words, the use of GEVD for the annual maximum wind speed for around 30% stations is preferred, and the use of Gumbel distribution for the annual maximum wind speed for around 70% stations is preferred. The percentage is similar to that indicated earlier but considering the V_{AH} extracted from HLY01 digital archive.

To further illustrate the probability distribution of the annual maximum wind speed, the empirical distribution of V_{AH} for the commingled winds and for the non-thunderstorm winds was also shown in Figure 2.10 for 14 capital cities. A visual inspection of the plots indicates that the Gumbel distribution provides, in general, an acceptable fit. However, there are differences between the sampled values from the HLY01 and DLY04 digital archives. Since the data quality for HLY01 was considered to be better than that for DLY04 and the historical meteorological record for HLY01 is longer than that for DLY04, it is considered that the results obtained from HLY01 were more representative of the statistics of the wind climate, and could be used as a proxy for the synoptic winds.

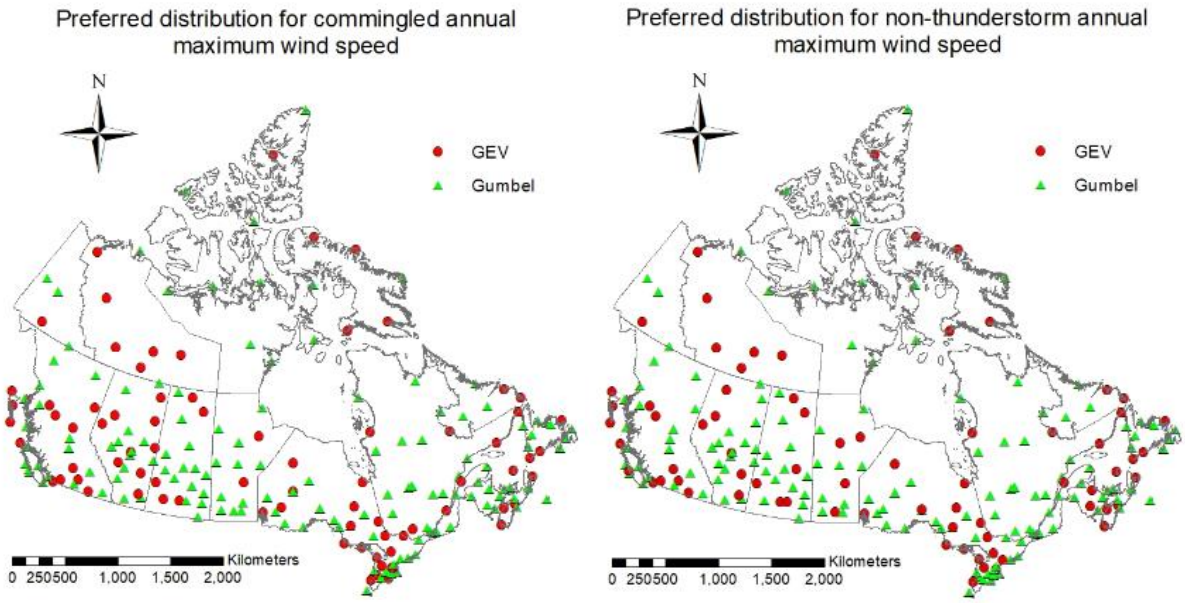

Figure 2.11. Preferred probability distribution model between the Gumbel distribution and GEVD considering the commingled winds, and non-thunderstorm winds.

2.4.2. Model for thunderstorm winds

Rather than carrying out the distribution fitting based on the annual maximum thunderstorm wind speed, a fitting exercise was carried out for the event-based maximum thunderstorm winds by using two commonly used probability distributions, namely, Gumbel distribution and GEVD. Based on *AICc*, the preferred model between these two models for wind data from each station was identified. The result shows that the use of GEVD for more than 70% of the stations is preferred, although the differences are not very large. MML and MLM are employed to estimate the parameters for GEVD. The square root of the sum of the squared error of the fitted model by considering MML is greater than that by using MLM in about 90% cases. For this reason, the model obtained based on MLM is adopted for the remaining part of this chapter. The fitted models for 14 capital cities were shown in Figure 2.12.

For completeness and comparison purposes, the fitted Gumbel distribution for the same considered 14 sites was presented in the figure. In addition, a distribution fitting was also carried out by using the Gumbel distribution and GEVD but for the annual maximum thunderstorm winds. The use of the *AICc* suggested that the Gumbel distribution is preferred for most cases.

The fitted distributions for the capital cities, as well as the empirical distribution based on the samples, were depicted in the last column in Figure 2.12. A visual inspection of the plots also suggested that, in general, the use of the Gumbel distribution fits the annual maximum thunderstorm winds well.

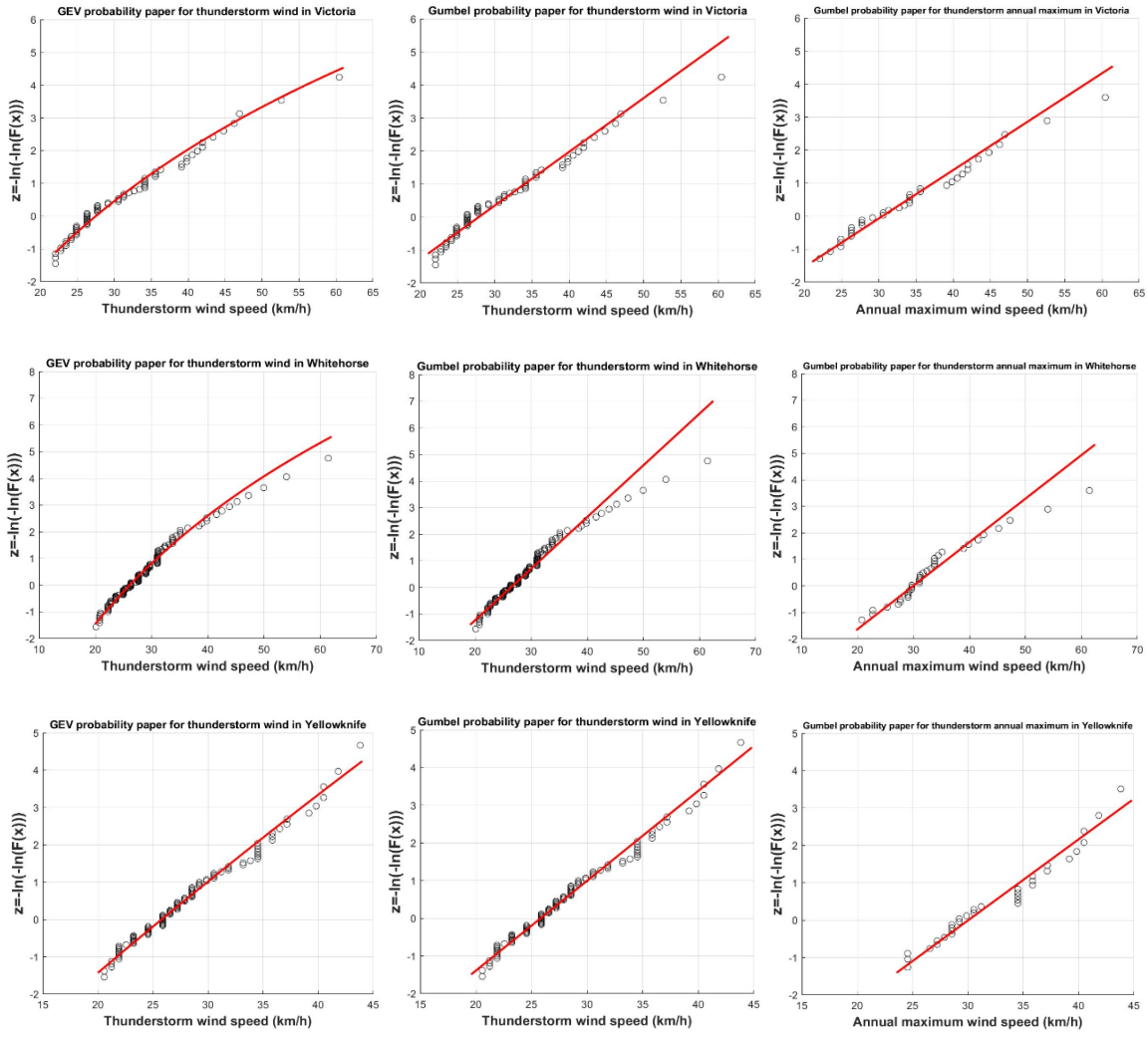

Thunderstorm winds were not recorded for Iqaluit.

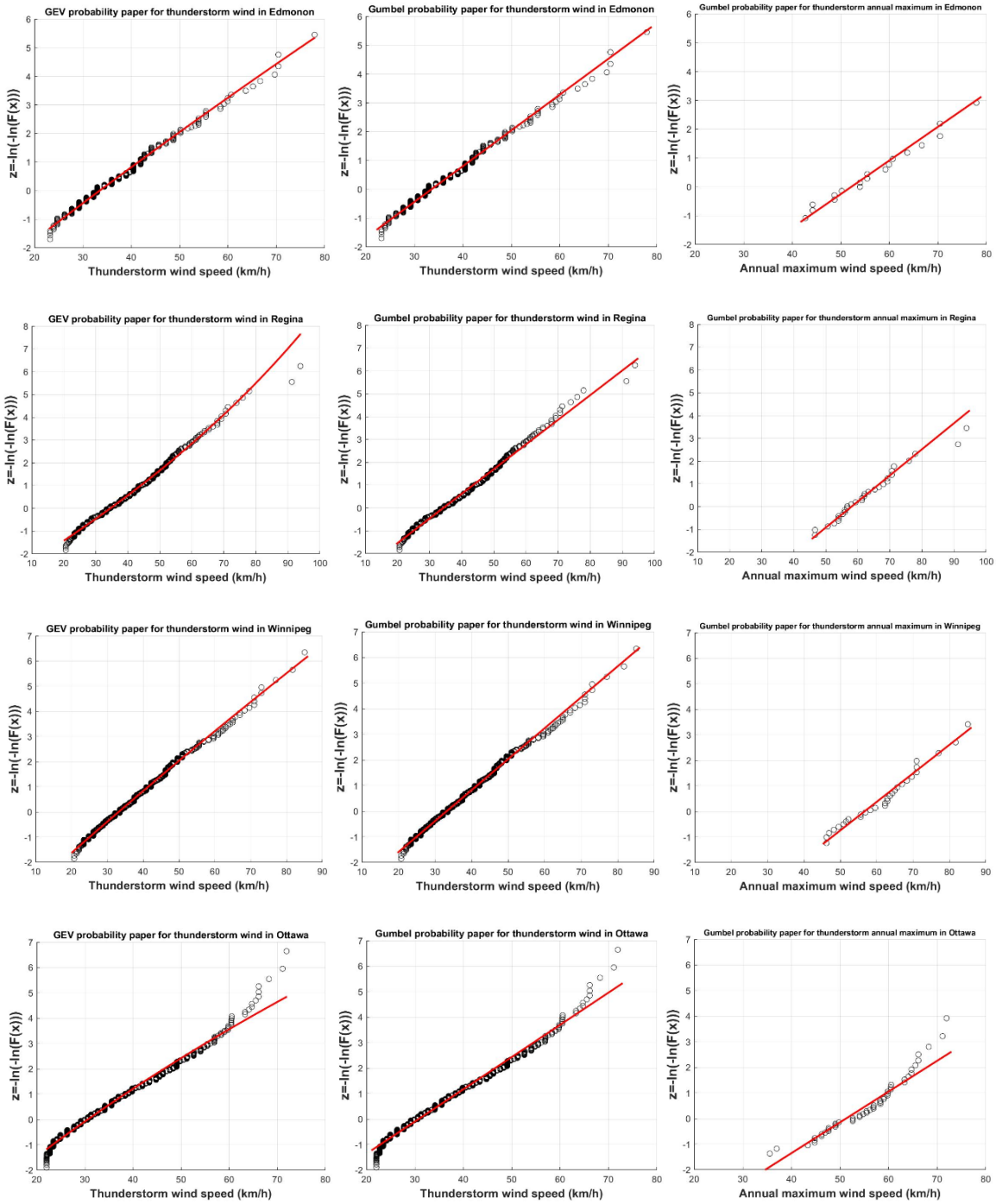
GEV probability paper for thunderstorm wind in Edmonon
Gumbel probability paper for thunderstorm wind in Edmonon
Gumbel probability paper for thunderstorm annual maximum in Edmonon
GEV probability paper for thunderstorm wind in Regina
Gumbel probability paper for thunderstorm wind in Regina
Gumbel probability paper for thunderstorm annual maximum in Regina
GEV probability paper for thunderstorm wind in Winnipeg
Gumbel probability paper for thunderstorm wind in Winnipeg
Gumbel probability paper for thunderstorm annual maximum in Winnipeg
GEV probability paper for thunderstorm wind in Ottawa
Gumbel probability paper for thunderstorm wind in Ottawa
Gumbel probability paper for thunderstorm annual maximum in Ottawa
z=-ln(-ln(F(x)))
Thunderstorm wind speed (km/h)
Annual maximum wind speed (km/h)

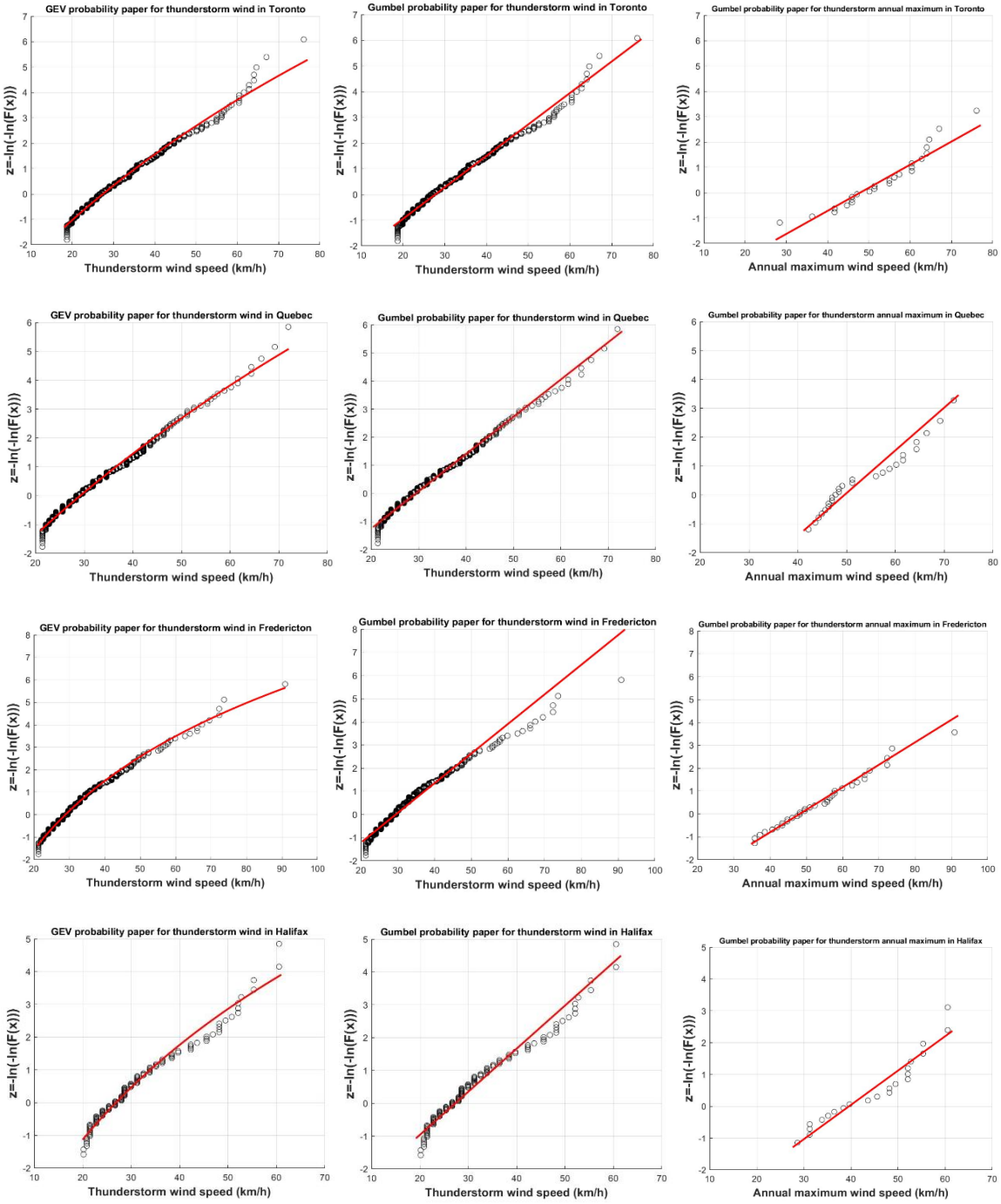
GEV probability paper for thunderstorm wind in Toronto
Gumbel probability paper for thunderstorm wind in Toronto
Gumbel probability paper for thunderstorm annual maximum in Toronto
GEV probability paper for thunderstorm wind in Quebec
Gumbel probability paper for thunderstorm wind in Quebec
Gumbel probability paper for thunderstorm annual maximum in Quebec
GEV probability paper for thunderstorm wind in Fredericton
Gumbel probability paper for thunderstorm wind in Fredericton
Gumbel probability paper for thunderstorm annual maximum in Fredericton
GEV probability paper for thunderstorm wind in Halifax
Gumbel probability paper for thunderstorm wind in Halifax
Gumbel probability paper for thunderstorm annual maximum in Halifax
z=-ln(-ln(F(x)))
Thunderstorm wind speed (km/h)
Annual maximum wind speed (km/h)

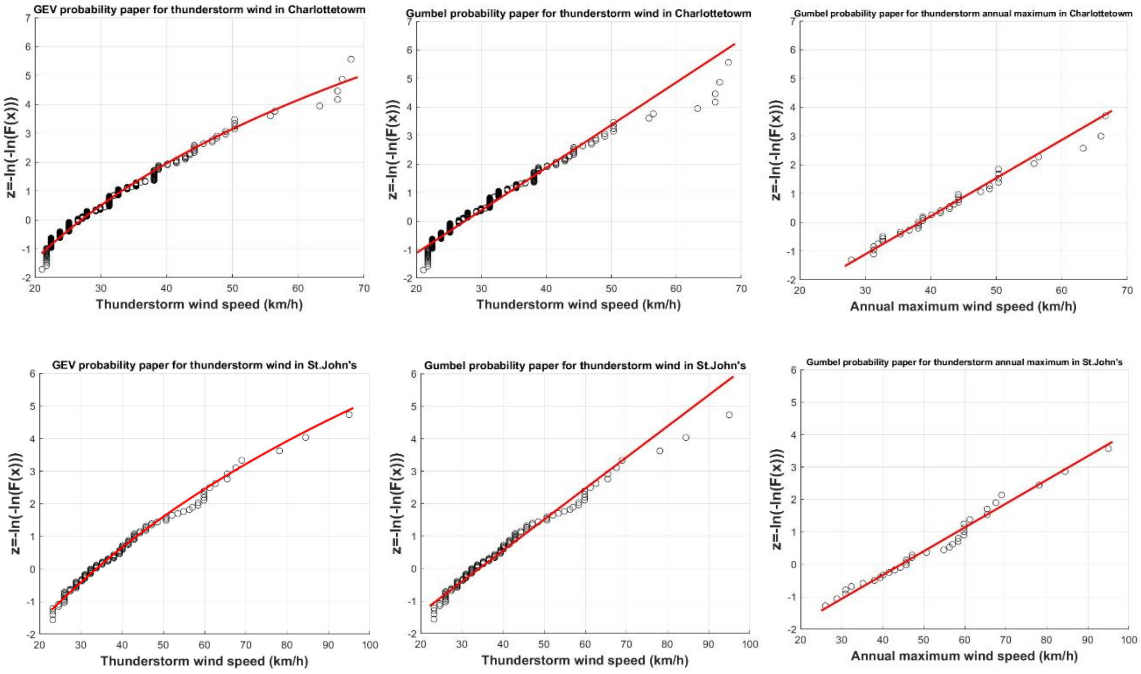

Figure 2.12. Samples and fitted distribution for the event-based and annual maximum based wind speed from thunderstorm winds.

2.5. Estimated return period values of annual maximum wind speed and wind hazard maps

2.5.1. Wind hazard for commingled and non-thunderstorm winds

Although one could estimate the return period values of V_{AH} based on the preferred distribution model at each site. This causes non-uniformity on the selected model, especially considering there were no clear spatial trends on the preferred distribution model. Therefore, following the practice in developing the previous version of the NBCC and considering that the Gumbel distribution for samples of V_{AH} is preferred for about 70% of all stations, the use of Gumbel distribution for the code making could be preferred. By adopting this model and carrying out the fitting using GLM, $v_{AH\text{-}50}$ and $v_{AH\text{-}500}$ based on V_{AH} obtained from HLY01 for each station were calculated. These values, which were considered as a proxy for the synoptic winds, were used as the basis to map the wind hazard, as shown in Figure 2.13. The results in the figure indicated that the spatial trends of $v_{AH\text{-}50}$ and $v_{AH\text{-}500}$ are similar for T = 50 and 500 years. As the number of stations considered to develop the maps depicted in Figure 2.13 was almost double

that considered in Hong et al. (2014), the resolution of the maps presented in Figure 2.13 is preferred.

The mapping of the wind hazard for the commingled winds and the non-thunderstorm winds based on the DLY04 digital archive was also carried out following the same procedure. The obtained results were presented in Figure 2.14. A comparison of the results presented in Figures 2.13 and 2.14 indicated that the return period values obtained based on HLY01 are greater than those for the commingled winds based on DLY04. One of the causes for the observed differences could be attributed to that the use of a single Gumbel distribution to fit extreme winds in mixed wind climate for estimating the return period value is inadequate (Gomes and Vickery 1978).

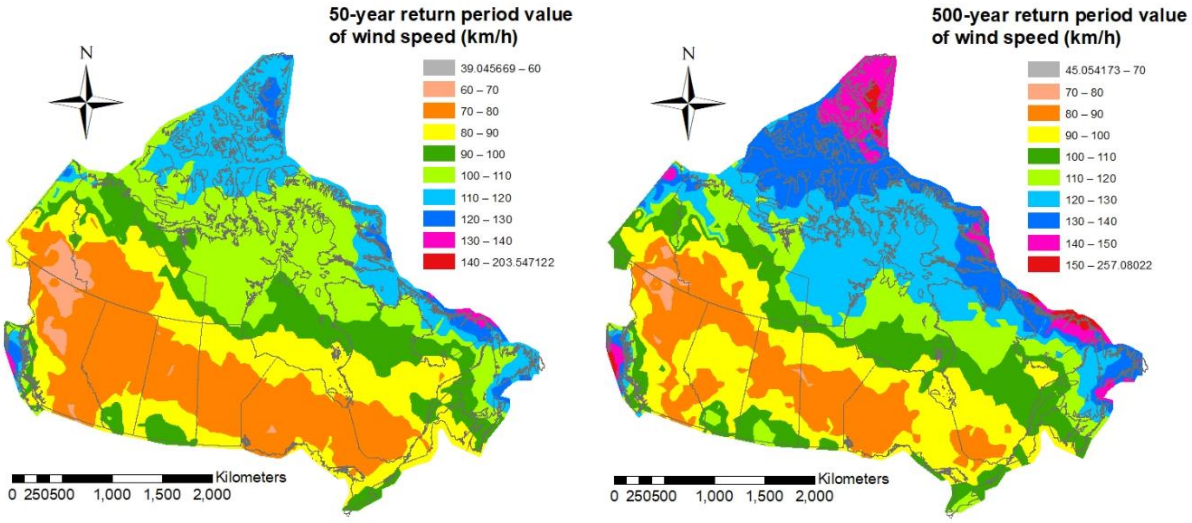

Figure 2.13. Contour map of statistics, $v_{AH\text{-}50}$ and $v_{AH\text{-}500}$ based on the wind records from HLY01 database.

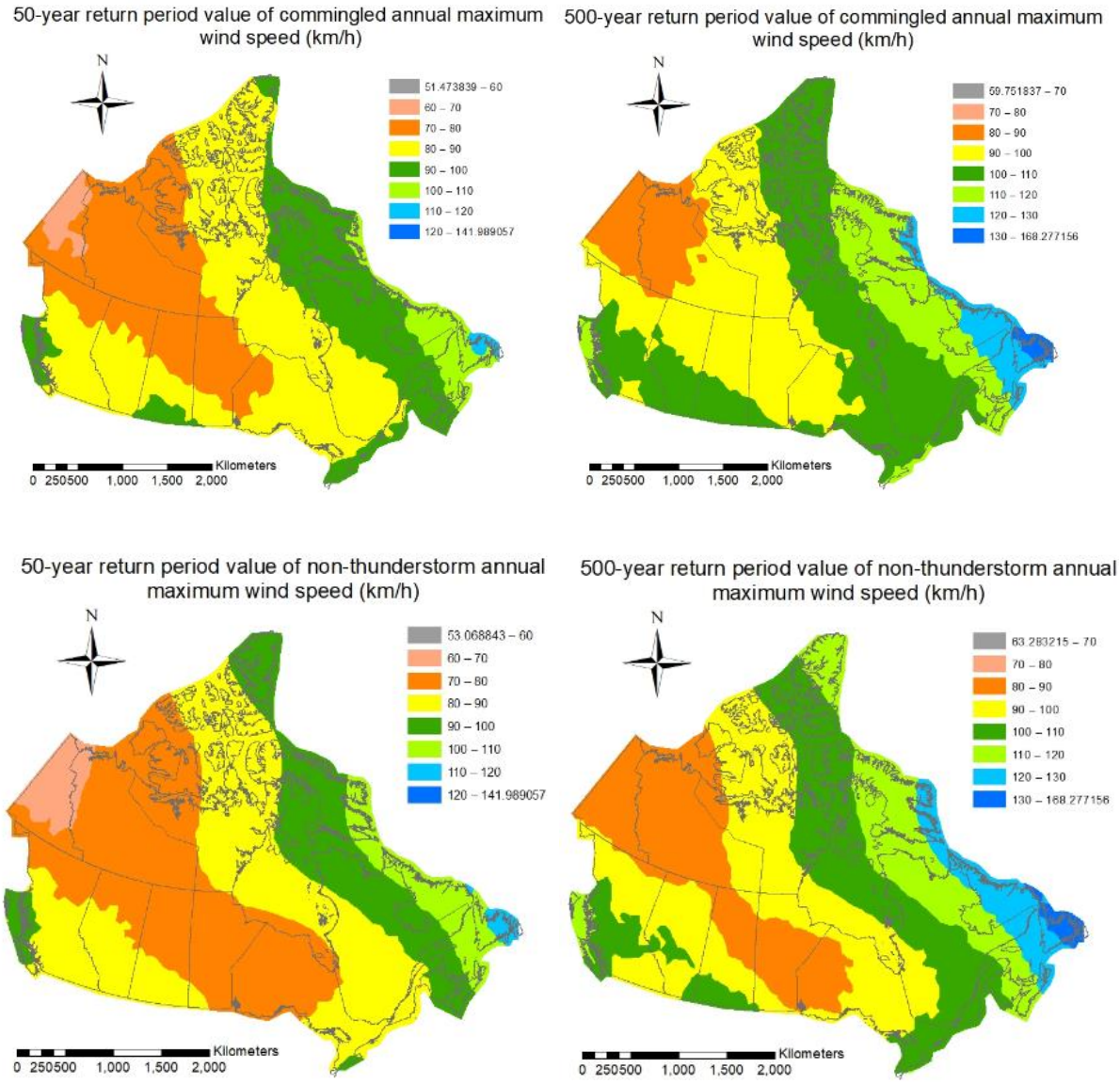

Figure 2.14. Estimated return period values of V_{AH} by considering commingled winds, and non-thunderstorm winds.

In general, $v_{AH\text{-}T}$ for the commingled winds is comparable to that for the non-thunderstorm winds. In some areas, however, $v_{AH\text{-}T}$ for the commingled winds is slightly greater than that for the non-thunderstorm winds. Moreover, the spatial trends and the values of $v_{AH\text{-}T}$ obtained based on HLY01 resemble better those for the non-thunderstorm winds than for the commingled winds presented in Figure 2.14. This could be used to support further treating $v_{AH\text{-}T}$, which is estimated based on HLY01, as a proxy for the synoptic winds.

2.5.2. Hazard for thunderstorm winds

For the estimation of the return period value of the annual maximum of the thunderstorm winds, first, the use of the distribution fitted to the event-based maximum wind is considered. In such a case, $v_{AH\text{-}T}$ could be estimated by assuming that the occurrence of the thunderstorm at a site follows a Poisson process with a rate of λ per year. Let $F_E(\ )$ denote the cumulative probability distribution of the event-based wind speed of thunderstorm winds. The cumulative probability distribution of the annual maximum wind speed, $F_A(V_{AH})$ is then given by,

$$F_A(v_{AH}) = \left(F_E(v_{AH})\right)^{\lambda} \approx \exp\left(-\lambda(1-F_E(v_{AH}))\right) \approx 1-\lambda(1-F_E(v_{AH})), \tag{2.3}$$

where the approximation holds for small values of $(1-F_E(v_{AH}))$. Based on Eq. (2.3), $v_{AH\text{-}T}$, can be obtained by using,

$$v_{AH-T} = F_E^{-1}\left(1-1/(\lambda T)\right), \tag{2.4}$$

in which $F_E^{-1}(\ )$ is the inverse cumulative probability distribution of $F_E(v_{AH})$. The occurrence rate per year, λ, was already given in Figure 2.9.

Based on the model described in Section 2.4.2, the occurrence rate presented in Figure 2.9 and Eq. (2.4), the estimated $v_{AH\text{-}T}$ for T = 50 and 500 years were shown in Figure 2.15. The results shown in the figure indicated that the spatial trends of $v_{AH\text{-}50}$ and $v_{AH\text{-}500}$ for the southern part of Canada are similar. However, the estimated $v_{AH\text{-}500}$ varies drastically from site to site. This was attributed partly to the effect of the small sample size for the thunderstorm winds in the northern part of Canada, and to the fact that the upper tail quantile values of the wind speed are very sensitive to the distribution parameters for GEVD.

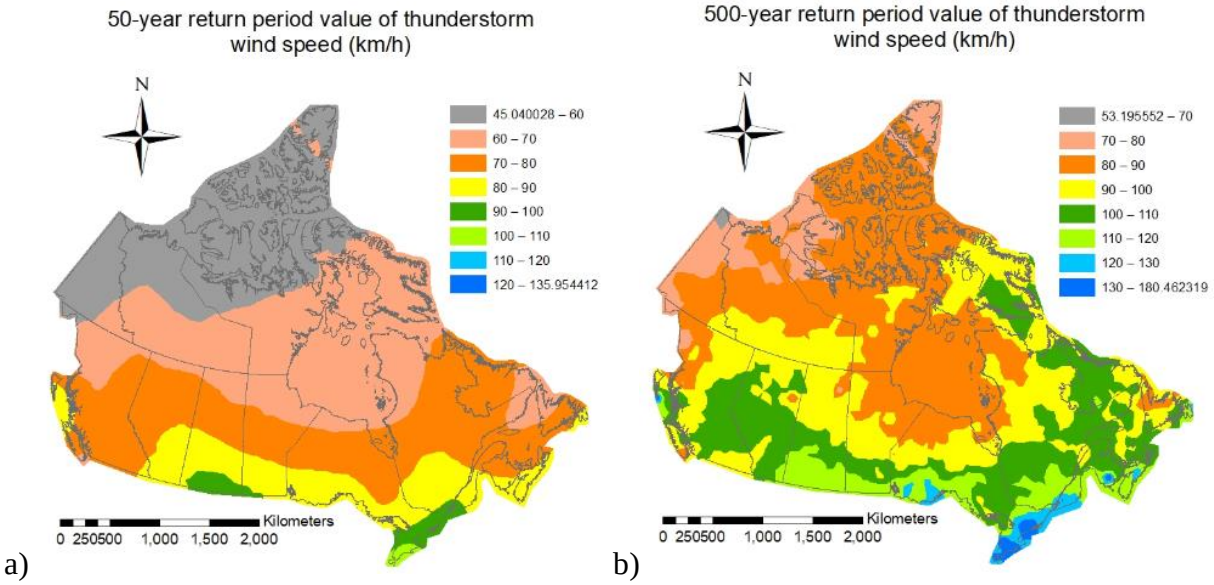

Figure 2.15. Estimated return period values for thunderstorm wind speed using event-based distribution: a) the 50-year return period value, and b) the 500-year return period value.

Furthermore, the estimation of $v_{AH\text{-}T}$ was carried out for T = 50 and 500 years based on the annual maximum distribution of thunderstorm winds, where the Gumbel distributed is adopted. The obtained values were mapped in Figure 2.16. A comparison of the estimated $v_{AH\text{-}T}$ for T = 50 years presented in Figures 2.15 and 2.16 indicated that the estimated $v_{AH\text{-}T}$ for such a return period is insensitive to whether the event-based approach or block maxima (i.e., the annual maximum) based approach was used. However, there are relatively large differences in the estimated $v_{AH\text{-}500}$ by using the former or the latter. The use of the fitted Gumbel distribution of the annual maximum thunderstorm winds resulted in smooth contour maps with spatial trends that mimic those of $v_{AH\text{-}50}$. It also resulted in the spatial trends that are more consistent with the thunderstorm activities or the annual occurrence rate shown in Figure 2.9. Based on the above observations and currently available data, it was suggested that the annual maximum thunderstorm wind speed could be adequately modelled using the Gumbel distribution fitted to their annual maximum values.

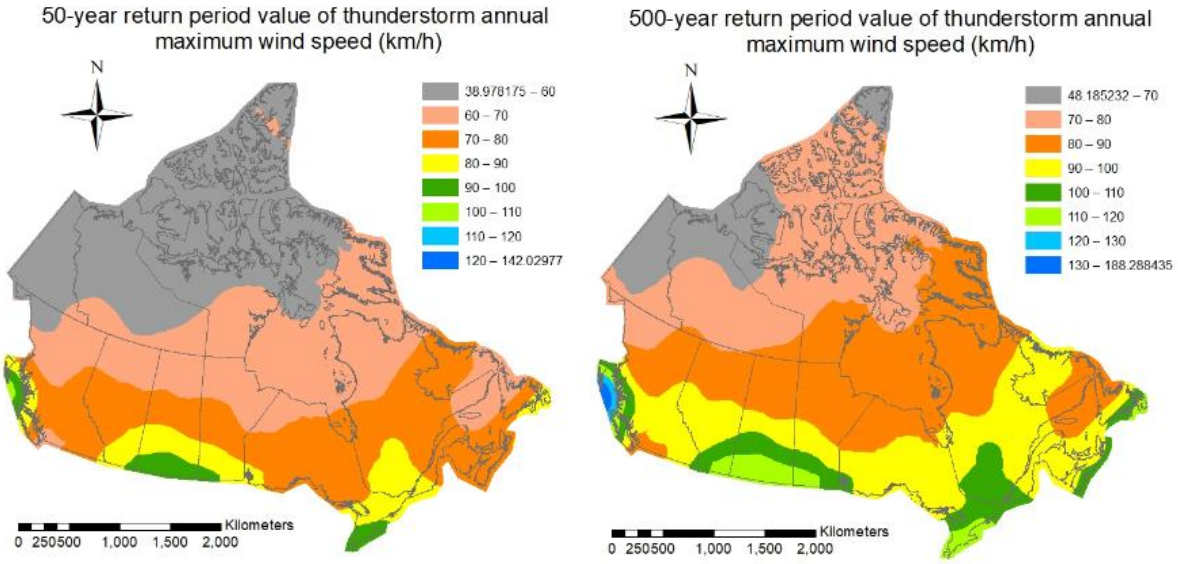

a) b)

Figure 2.16. Estimated return period values for thunderstorm wind speed using annual maximum distribution: a) the 50-year return period value; b) the 500-year return period value.

In general, the results presented in Figures 2.14 to 2.16 indicated that the return period values for the synoptic winds (see Figure 2.13) for sites away from the southern Ontario and the southern part of the Prairies are higher than those for the thunderstorm winds. For a site in southern Ontario or the southern part of the Prairies, qualitatively, $v_{AH\text{-}50}$ for thunderstorm winds is comparable to the synoptic winds, and $v_{AH\text{-}500}$ for thunderstorm winds are higher than those for the synoptic winds.

2.5.3. Comparison of return period values of annual maximum wind speed for different types of winds

To see whether the wind hazard was dominated by a thunderstorm or synoptic winds, $v_{AH\text{-}50}$ and $v_{AH\text{-}500}$ for non-thunderstorm and thunderstorm winds for the stations included in DLY04 were calculated and compared in Figure 2.17. The plots showed that the wind hazard is dominated by the thunderstorm winds for some sites in the south and near Canada and the U.S. border. The thunderstorm winds become more dominant as the return period increases. Also shown in

Figure 2.17 were the maps of the ratio of $v_{AH\text{-}T}$ for thunderstorm winds to $v_{AH\text{-}T}$ of commingled winds based on DLY04 for T = 50 and 500 years. From the result, it can be concluded that for T = 50 years, the wind hazard is dominated by the thunderstorm winds for southern Ontario and the southern part of the Prairies. Such a region extends slightly further towards the north as T increases from 50 to 500 years. However, the identified region, where the thunderstorm winds dominate the wind hazard, depends on the extreme value analysis method (i.e., event-based and block maxima approaches). In general, the region is larger if the event-based approach was used to evaluate $v_{AH\text{-}T}$ for thunderstorm winds.

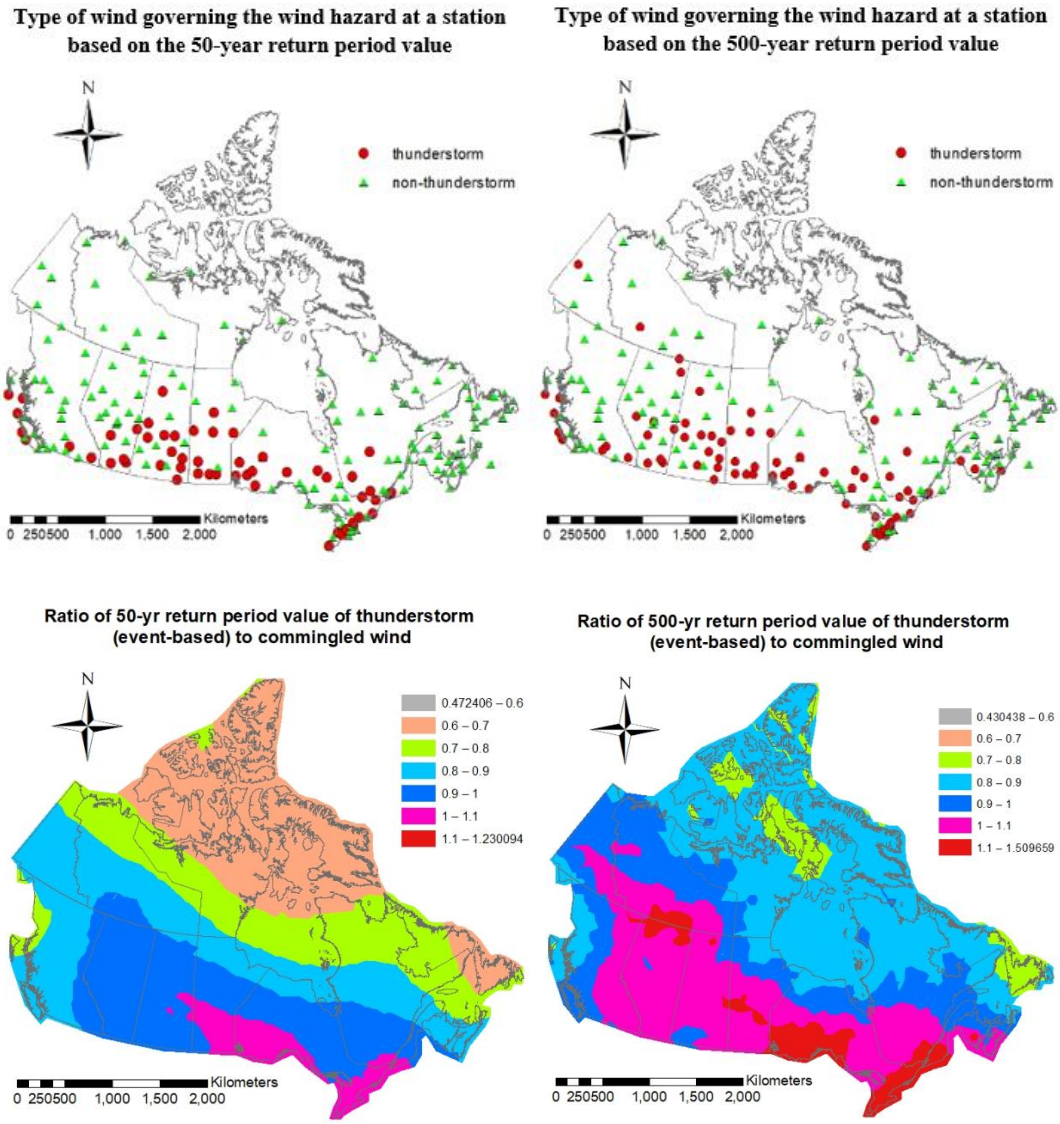

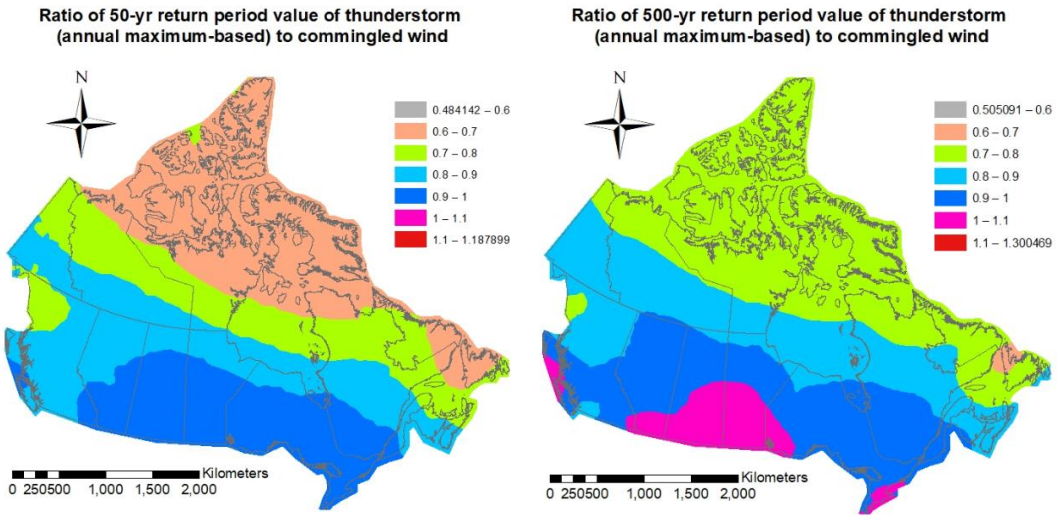

Figure 2.17. Predominant wind type (i.e., non-thunderstorm or thunderstorm) at different sites and the ratio of $v_{AH\text{-}T}$ for thunderstorm winds to commingled winds (left plots for T = 50 years and right plots T = 500 years). For the second row, the estimation of $v_{AH\text{-}T}$ for thunderstorm winds is carried out using the event-based approach. For the last row, the estimation of $v_{AH\text{-}T}$ for the thunderstorm winds is carried out using block maxima (i.e., annual maximum) approach.

Additionally, the ratio of $v_{AH\text{-}T}$ for the thunderstorm winds to that calculated based on HLY01, representing a proxy to the synoptic winds, was presented in Figure 2.18. The ratios indicated that the wind hazard is dominated by the thunderstorm winds only for a very small portion of the southern region of Canada if T = 50 years is considered. However, this identified region increases as T = 500 years was considered. This and the observations made to Figure 2.17 indicated the importance of separating the thunderstorm and non-thunderstorm winds to estimate the wind hazard, at least for part of the (central) southern region of Canada. In all cases, the ratio based on the annual maximum analysis approach is much more spatially consistent.

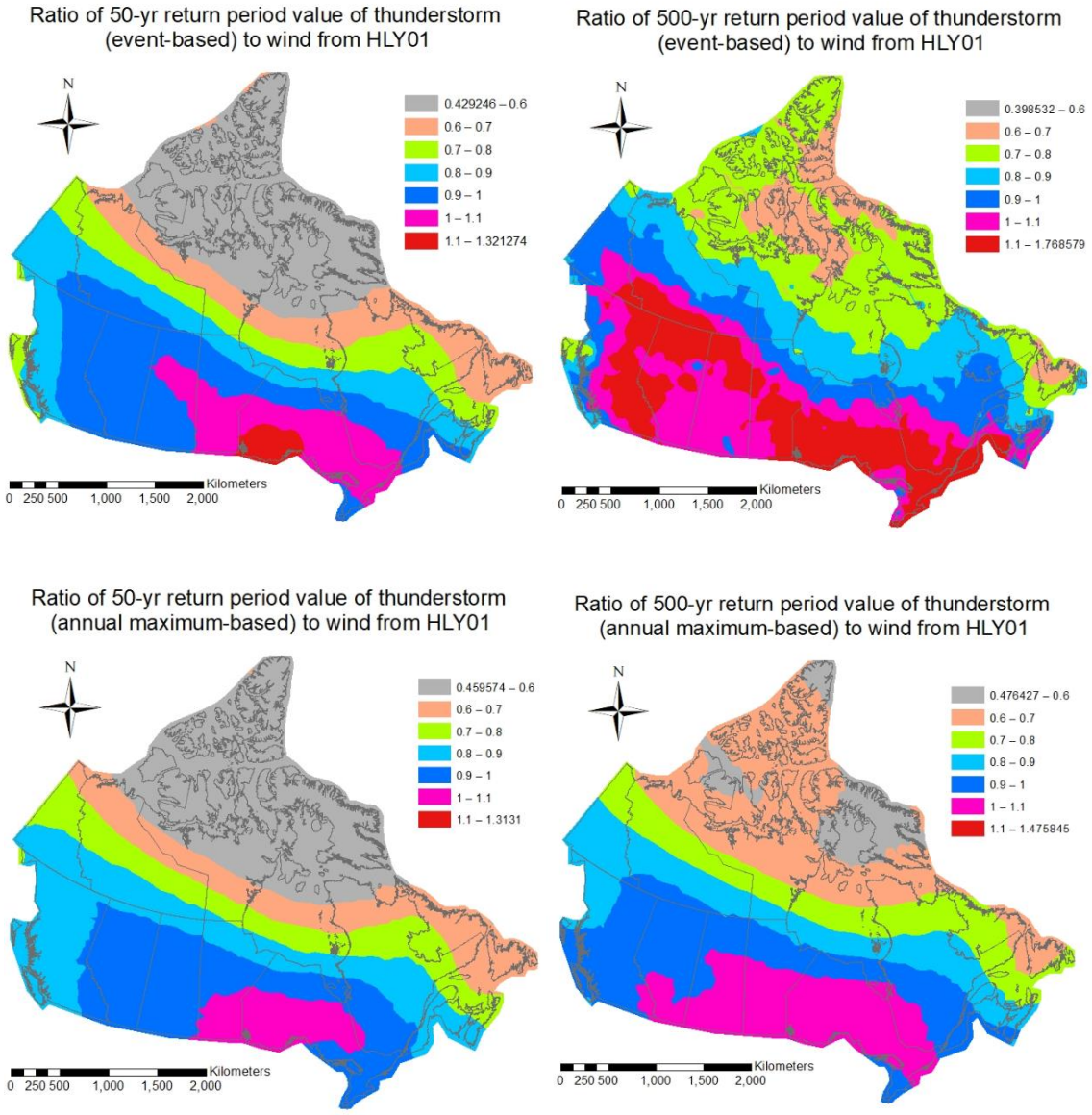

Figure 2.18. Ratio of $v_{AH\text{-}T}$ for thunderstorm winds estimated using the wind records in DLY04 to $v_{AH\text{-}T}$ for the commingled winds estimated using wind records in HLY01. (left plots for T = 50 years and right plots for T = 500 years). For the first rows, the estimation of $v_{AH\text{-}T}$ for thunderstorm winds is carried out using the event-based approach. For the second row, the estimation of $v_{AH\text{-}T}$ for thunderstorm winds is carried out using block maxima (i.e., annual maximum) approach.

By considering both the synoptic and thunderstorm winds (i.e., the mixed wind climates), the

cumulative probability distribution of the annual maximum wind speed, $F_{MC}(v_{AH})$, can be written as,

$$F_{MC}(v_{AH}) = P(\max(V_{TW}, V_{SW}) < v_{AH}) = P(V_{TW} < v_{AH})P(V_{SW} < v_{AH}), \quad (2.5)$$

where v_{AH} is the value of the annual maximum wind speed by considering both the synoptic and thunderstorm winds, V_{TW} and V_{SW} denote the annual maximum wind speed for the thunderstorm winds and for the synoptic winds, respectively, and $P(\cdot)$ denotes the probability of its argument. In particular, by adopting the Gumbel distributions for V_{TW} and V_{SW}, including the consideration of p_{NT}, Eq. (2.5) can be re-written as,

$$F_{MC}(v_{AH}) = \left[p_{NT} + (1 - p_{NT}) \exp\left(-e^{-\alpha_{TW}(v_{AH} - u_{TW})}\right)\right] \exp\left(-e^{-\alpha_{SW}(v_{AH} - u_{SW})}\right), \quad (2.6)$$

where α_{TW} and u_{TW} are model parameters for annual maximum wind speed for (non-zero) thunderstorm winds, and α_{SW} and u_{SW} are model parameters for annual maximum wind speed for synoptic winds. The estimated $v_{AH\text{-}T}$ for T= 50 and 500 years was presented in Figure 2.19 by considering the distribution models that were developed based on the previous sections for each of the considered meteorological stations depicted in Figures 2.1 and 2.4. For the estimation, if no thunderstorm winds were recorded at a station (i.e., p_{NT} = 1), only the synoptic winds were considered. As expected, the results presented in Figure 2.19 were greater than those presented in Figure 2.13 for synoptic winds and in Figure 2.16 for thunderstorm winds.

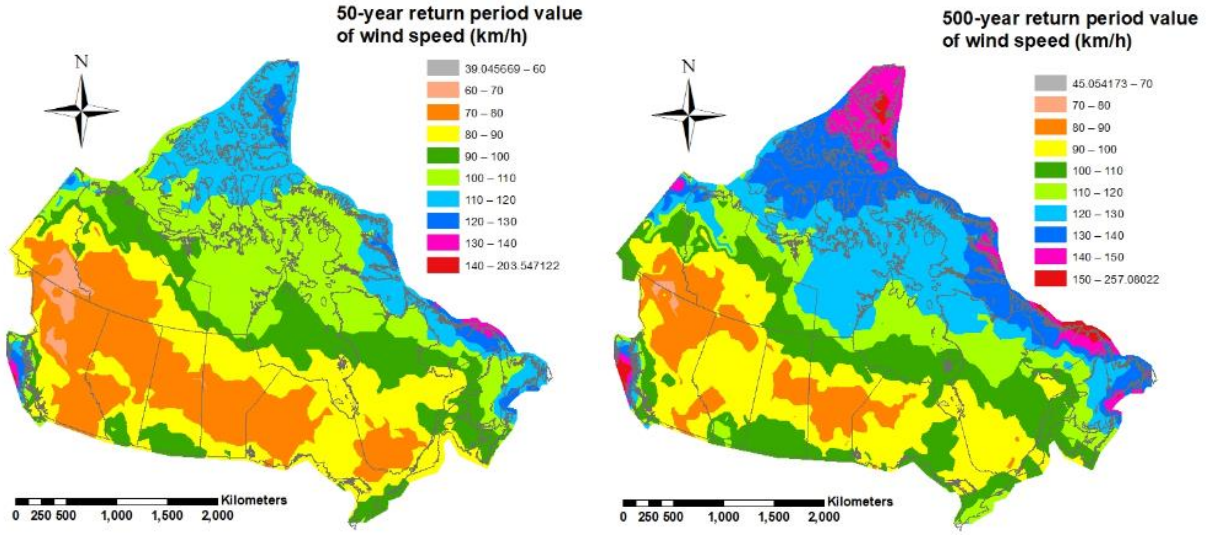

a) b)

Figure 2.19. Estimated return period values for annual maximum wind speed by considering mixed wind climates: a) the 50-year return period value; b) the 500-year return period value.

2.6. Effect of spatial smoothing using kriging with different nugget values

So far, the maps presented in the previous section were obtained based on the use of ordinary kriging with the nugget not equal to zero so to obtain smoother hazard maps. The use of nugget not equal to zero is not an exact interpolator in that the interpolated values at data points may not be equal to the given values. By setting the nugget equal to zero in the ordinary kriging, the interpolator becomes an exact interpolator. By using this option and the data used to map hazard maps for $v_{AH\text{-}50}$ and $v_{AH\text{-}500}$ depicted in Figures 2.13, 2.14, and 2.16, the hazard mapping was carried out again with the results presented in Figure 2.20.

A comparison of the plots shown in Figures 2.13, 2.14, and 2.16 to those corresponding ones in Figure 2.20 indicated that the contours presented in Figure 2.20 are much less smooth than those shown in Figures 2.13, 2.14 and 2.16. In fact, the use of different options for spatial smoothing could change the perception of the spatial trends of the wind hazard, especially for regions with sparsely distributed stations. Therefore, it was suggested that the ordinary kriging with nugget

not equal to zero is to be considered to obtain a more robust smoothed spatial trend of the wind hazard. This could be important for design code making, taking into account that the historical records in many places are non-existent or very short.

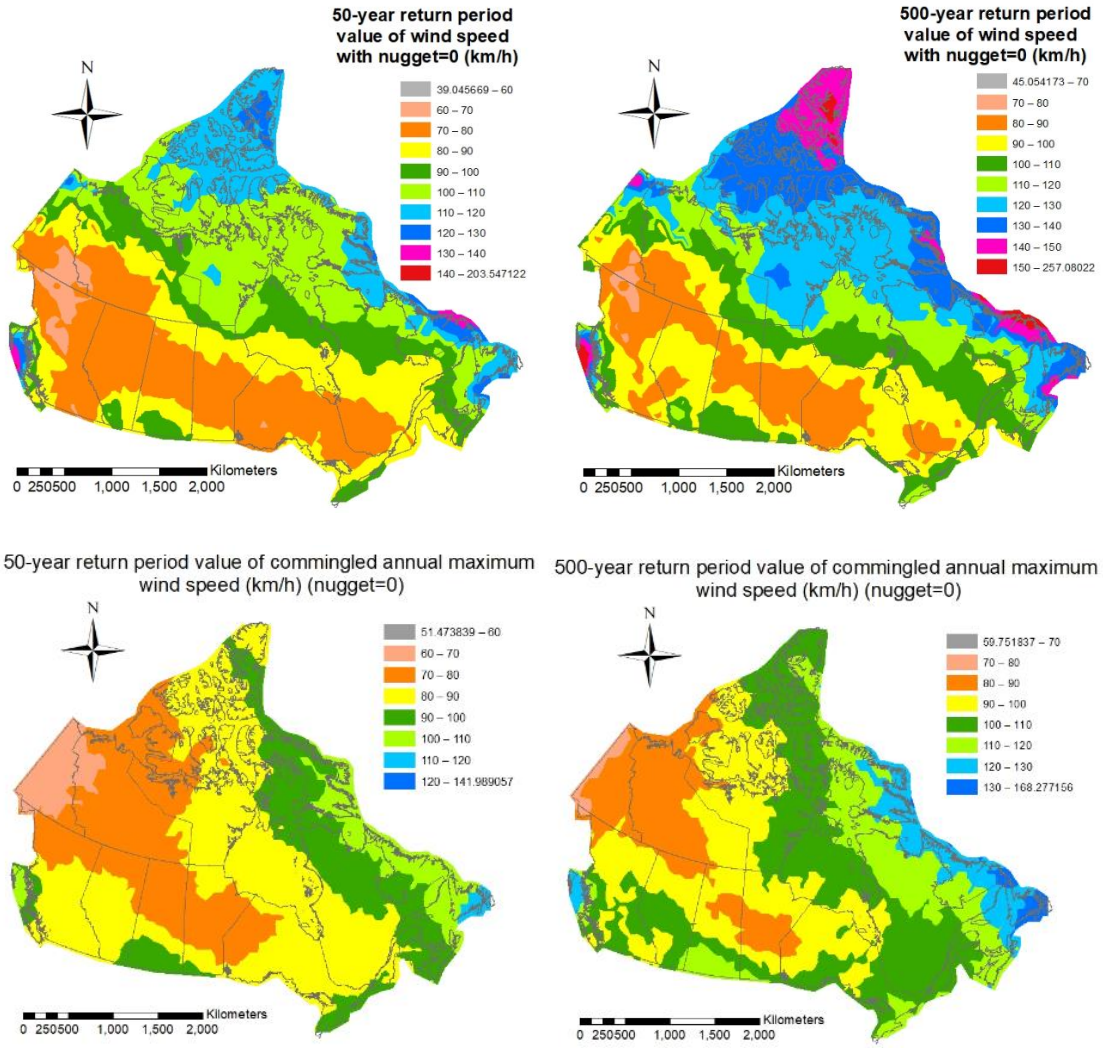

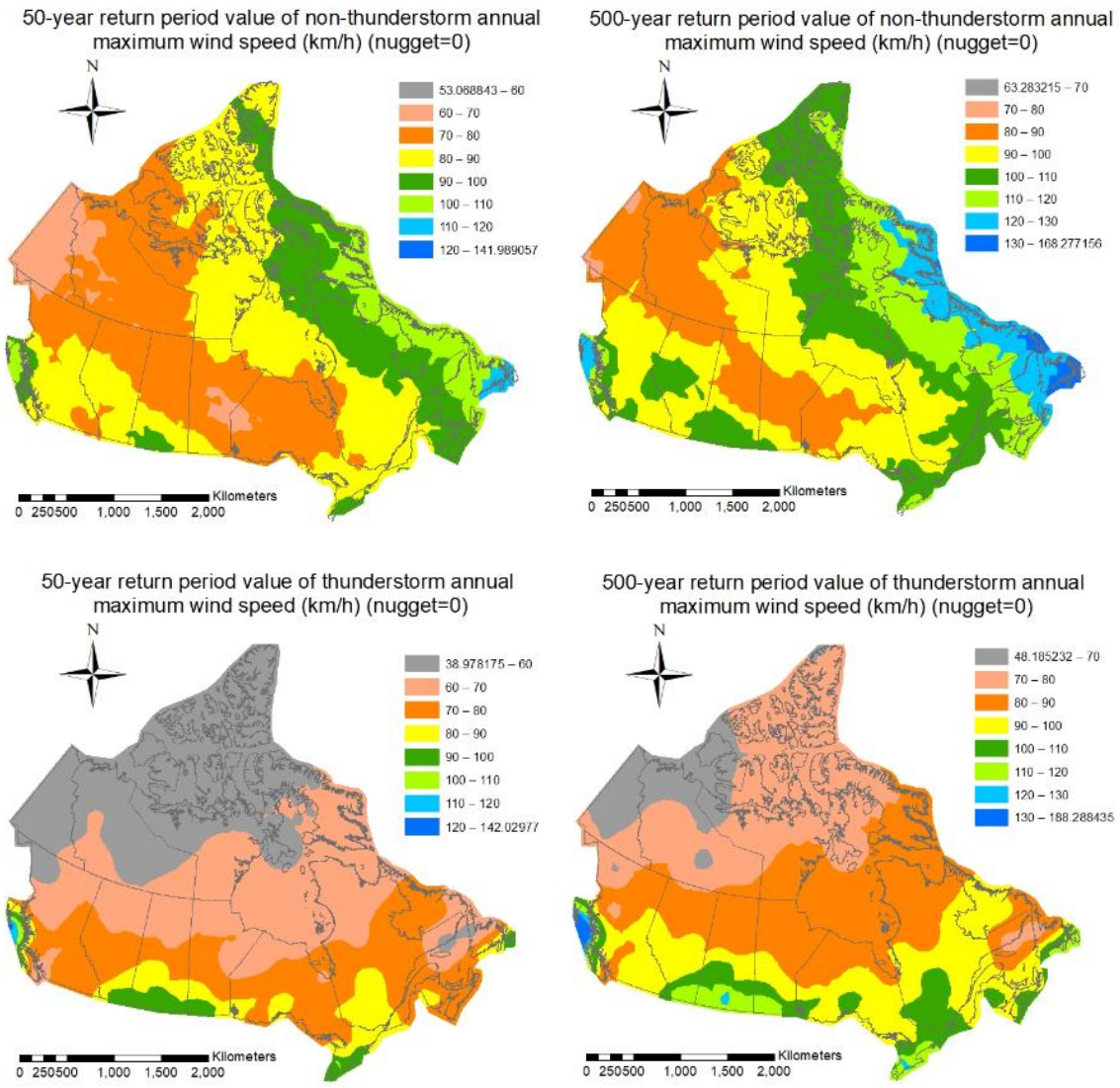

Figure 2. 20. Estimated return period values of V_{AH} mapped by using ordinary kriging with nugget equal to zero. The first row was for the estimated values based on HLY01. The second to the last rows were for the estimated values based on DLY04. The last raw was calculated based on the block maxima approach.

2.7. Conclusions

In this chapter, the statistical analysis and estimation of the spatially-varying wind hazard were carried out. The major observations were summarized as follows:

1. The Gumbel distribution could be adopted for the modelling of annual maximum wind speed

if only a single probabilistic model is to be adopted over Canada. This is justified since it is the preferred probability distribution for wind records from about 70% of the considered meteorological stations. This distribution is not only adequate for the synoptic winds but also for the thunderstorm winds.

2. The statistics of wind records from the HLY01 digital archive indicated that the COV ranges approximately from 0.05 to 0.2 with a typical value of 0.138.

3. The statistics of wind records from the DLY04 digital archive showed that for thunderstorm winds, the COV of V_{AH} ranges approximately from 0.1 to 0.35 with a mean value of 0.21. However, for sites with significant thunderstorm activities, and the wind hazard being dominated by the thunderstorm winds, the COV value is less than 0.2. It implies that if the return period values of the annual maximum wind speed for the synoptic winds and for the thunderstorm winds are properly estimated for a high return period (say 500 years), the distribution of the extreme winds in the upper tail could be approximated by using the Gumbel model with COV less than about 0.2 for most cases. The use of such a model could facilitate the reliability-based design code calibration for wind load.

4. The wind hazard at a site within southern Ontario and the southern part of the Prairies could be dominated by the thunderstorm winds, especially as the return period increases. This indicated that for these regions, the return period values of the annual maximum wind speed should be estimated by considering both thunderstorm winds and synoptic winds separately. Such estimated values should be used as the basis to recommend the reference wind velocity pressure for codified design. This is especially the case if a high return period, such as T = 500 years, is considered to assign the design wind load.

5. For practical consideration, outside of the regions mentioned in item 4), the return period values of the annual maximum wind speed estimated based on synoptic winds are suggested.

6. The use of kriging with nugget not equal to zero for hazard mapping is preferred if a relatively smooth hazard map is preferred, especially if the historical samples are scarce, and the spatial coverage by the meteorological stations is sparse.

2.8. References

Akaike, H. (1974). A new look at the statistical model identification. IEEE Transactions on Automatic Control, 19 (6), 716–723.

ASCE (2017). Minimum design loads for buildings and other structures. ASCE 7-17. Reston, VA: ASCE.

Bartlett, F.M., Hong, H.P. and Zhou, W. (2003a). Load factor calibration for the proposed 2005 edition of the National Building Code of Canada: Statistics of loads and load effects, Canadian Journal of Civil Engineering, 30 (2) 429-439.

Bartlett, F.M., Hong, H.P. and Zhou, W. (2003b). Load factor calibration for the proposed 2005 edition of the National Building Code of Canada: Companion-action load combinations, Canadian Journal of Civil Engineering, 30 (2) 440-448.

Castillo, E. (1988). Extreme Value Theory in Engineering. Academic Press, New York.

Cavanaugh, J.E. (1997). Unifying the derivations for the Akaike and corrected Akaike information criteria. Statistics & Probability Letters, 33(2), 201-208.

Coles, S. (2001). An introduction to statistical modeling of extreme values. Springer, London

Cook, N. (1985) The designers guide to wind loading of building structures part 1. Building Research Establishment, Dept. of the Environment.

Cook, N.J. (1982). Towards better estimation of extreme winds. Journal of Wind Engineering and Industrial Aerodynamics, 9(3), 295-323.

ESDU (2002). Computer program for wind speeds and turbulence properties: flat or hilly sites in terrain with roughness changes. Engineering Science Data Unit (ESDU) Data Item No. 01008.

ESRI (2011). ArcGIS Desktop: Release 10. Redlands, CA: Environmental Systems Research Institute.

Fovell, R.G. and Fovell, M.Y.C. 1993. Climate zones of the conterminous United States defined using cluster analysis. Journal of Climate 6, 2103–2135.

Frank, H. (2001). Extreme winds over Denmark from the NCEP/NCAR reanalysis. Technical Report Risø-R-1238(EN), Risø National Laboratory.

Gomes, L., & Vickery, B. J. (1978). Extreme wind speeds in mixed wind climates. Journal of Wind Engineering and Industrial Aerodynamics, 2(4), 331-344.

Hastie, T., Tibshirani, R. and Friedman, J.H. (2001). The elements of statistical learning: data mining, inference, and prediction. Springer New York.

Holmes, J.D. and Moriarty, W.W. (1999). Application of the generalized Pareto distribution to extreme value analysis in wind engineering. Journal of Wind Engineering and Industrial Aerodynamics, 83: 1-10.

Hong, H.P. and Ye, W. (2014). Estimating extreme wind speed based on regional frequency analysis. Structural Safety, 47, 67-77.

Hong, H.P., Mara, T.G., Morris, R., Li, S.H. and Ye, W. (2014). Basis for recommending an update of wind velocity pressures in Canadian design codes. Canadian Journal of Civil Engineering, 41(3), 206-221.

Hong, H.P., Ye, W. and Li, S.H. (2016). Sample size effect on the reliability and calibration of design wind load. Structure and Infrastructure Engineering,12(6), 752-764.

Hong, H.P., Li, S.H. and Mara, T. (2013) Performance of the generalized least-squares method for the extreme value distribution in estimating quantiles of wind speeds, Journal of Wind Engineering & Industrial Aerodynamics, 119: 121–132.

Hosking, J. (1990). L-moments: Analysis and estimation of distributions using linear combinations of order statistics. Journal of the Royal Statistical Society B, 52: 105–124.

Hosking, J.R.M. and Wallis, J.R. (1997). Regional frequency analysis: an approach based on L-moments. Cambridge University Press, Cambridge, UK.

Johnston, K., Ver Hoef, J.M., Krivoruchko, K., and Lucas, N. (2003). ArcGIS9, Using ArcGIS geostatistical analyst, Redlands, CA: Environmental Systems Research Institute.

Kasperski, M. (2002). A new wind zone map of Germany. Journal of Wind Engineering and Industrial Aerodynamics, 90: 1271–1287.

Kohonen, T. (2001). Self-Organizing Maps. Berlin-Heidelberg, Springer.

Kruger, A.C., Goliger, A.M., Retief, J.V. and Sekele, S.S. 2012. Clustering of extreme winds in the mixed climate of South Africa. Wind and Structures, Vol. 15: 87-109.

Lieblein, J. (1974). Efficient methods of extreme-value methodology. report NBSIR 74-602, National Bureau of Standards, Washington.

Lin, G.-F. and Chen, L.-H. (2006). Identification of homogeneous regions for regional frequency analysis using the self-organizing map. Journal of Hydrology, 324(1): 1–9.

Lloyd, E.H. (1952). Least–squares estimation of location and scale parameters using order statistics. Biometrika 39, 88–95.

Lombardo, F.T. (2012). Improved extreme wind speed estimation for wind engineering applications. Journal of Wind Engineering and Industrial Aerodynamics, 104, 278-284.

Lombardo, F.T., Main, J.A. and Simiu, E. (2009). Automated extraction and classification of thunderstorm and non-thunderstorm wind data for extreme-value analysis. Journal of Wind Engineering and Industrial Aerodynamics, 97(3-4), 120-131.

Lowery, M.D. and Nash, J.E. (1970). A comparison of methods of fitting the double exponential distribution. J Hydrol 10(3):259–275

Mara, T.G., Hong, H.P. and Morris, R.J. (2013). Effect of corrections to historical wind records on estimated extreme wind speeds. CSCE-2013 conference, Montreal, Canada.

Miller, C.A. (2003). A once in 50-year wind speed map for Europe derived from mean sea level pressure measurements. Journal of Wind Engineering and Industrial Aerodynamics, 91, 1813-1826.

Mo, H.M., Hong, H.P. and Fan, F. (2015). Estimating the extreme wind speed for regions in China using surface wind observations and reanalysis data. Journal of Wind Engineering and Industrial Aerodynamics, 143, 19-33.

Morris, R. (2009). Wind interim report on the updating of the design winds speeds in the National Building Code of Canada for the task Group on climatic loads. National Research Council of Canada, Ottawa, Canada.

NRC (1990) National Building Code of Canada. Institute for Research in Construction, National Research Council of Canada, Ottawa

NRC (1995) National Building Code of Canada. Institute for Research in Construction, National Research Council of Canada, Ottawa

NRC (2015) National Building Code of Canada. Institute for Research in Construction, National Research Council of Canada, Ottawa

Sacré, C. (2002). Extreme wind speed in France: the ’99 storms and their consequences. Journal of Wind Engineering and Industrial Aerodynamics, 90: 1163–1171.

Yip, T. and Auld, H. (1993). Updating the 1995 National building code of Canada wind pressures. In Proceedings of the Electricity ’93 Engineering and Operating Division

Conference. Canadian Electrical Association, Montréal, Canada.

Yip, T., Auld, H. and Dnes, W. (1995). Recommendations for updating the 1995 National building code of Canada wind pressures. In *Proceedings of the 9th International Conference on Wind Engineering*. International Association for Wind Engineering, New Delhi, India.

Chapter 3

3. Extreme ground snow depth and ground snow load for Canada

3.1. Introduction

Snow load on the roof is one of the environmental loads specified in design codes. It is important for designing structures in regions experiencing long winter seasons and heavy snowfalls. The roof snow load in the National Building Code of Canada (NBCC) (NRC 2015) consists of two components: the snow component and the rain component. Variations exist in the definition of each component between different versions of NBCC (Boyd 1961; Newark 1984; Newark et al. 1989; Hong and Ye 2014).

According to Newark (1984), the maximum 24-hour rainfall in months, which receives significant snow (generally December to March), was used as the basis to define the rain component from 1961 to 1980. Newark et al. (1989) suggested that, on average, this rain component, which was limited in magnitude to the value of the snow component of the load at a location, was roughly equivalent to 21- to 35-year return period value of the annual maximum 24-hour rainfall. They also estimated the rain component based on the extreme value analysis of 1-day "*winter*" rain amount, defined as the observed rain amount but limited to be equal to or less than the modelled snowpack water equivalent amount on each day for each considered location. This calculated return period value was considered to occur "concurrently with near-maximum snowpack water equivalent amounts." The use of a 30-year return period value of the annual maximum 1-day winter rain amount was considered in the 1990 edition of the NBCC. The use of a 50-year return period value of the annual maximum 1-day winter rain amount was considered for the rain component of the roof snow load since 2005 in NBCC. Similarly, in the same code, the 50-year return period value of the snow component of the roof snow load was implemented since 2005 in NBCC.

The snow component was calculated based on the ground snow load (Taylor and Allen 2000; Bartlett et al. 2003a,b). The issues that need to be addressed to estimate the ground snow load

include (Newark et al. 1989) the average annual snowpack bulk density and the return period value of the annual maximum ground snow depth. The spatial variation of the snowpack bulk density for Canada was presented in Newark (1984) and Newark et al. (1989) for the updating of the 1990 edition of NBCC. No new data on the annual snowpack bulk density covering Canada were found in the literature for the development of newer editions of NBCC since 1990. The estimation of the return period value of the annual maximum ground snow load and spatial interpolation is affected by the data availability, adopted probabilistic models, and probability distribution fitting methods.

The estimation of the return period value of the annual maximum ground snow depth was usually carried out using the at-site analysis approach, where the measured snow depth at a meteorological site is available (Hong and Ye 2014). In such a case, the annual maximum snow depth was extracted from the daily ground snow depth measurements. The extreme value analysis of the annual maximum ground snow depth could be carried out by adopting the Gumbel distribution and generalized extreme value distribution (GEVD) (Coles 2001). The lognormal distribution was also considered because it fits the U.S. data well (Ellingwood and Redfield 1983). The Gumbel distribution was employed for the annual maximum ground snow depth in Canada for structural design code making (Newark et al. 1989); GEVD was adopted to estimate the annual maximum snow depth in Switzerland (Blanchet et al. 2011). Hong and Ye (2014) processed the ground snow depth records from daily measurements for 1940 stations provided by Environment and Climate Change Canada (ECCC). They only used data from 549 climatological stations (each with at least 20 years of useable annual maximum snow depth data) for the extreme value analysis. Their results indicated that between the Gumbel distribution and GEVD, according to Akaike information criterion (Akaike 1974), the Gumbel distribution is preferable to GEVD for 72% of the considered stations. The consideration of at least 20 years of useable data was aimed at reducing statistical uncertainty due to a small sample size, although it may potentially exclude useful information from stations with shorter meteorological records.

One of the approaches to take advantage of the short ground snow depth records and to reduce the sample size effect is to apply the regional frequency analysis (Hosking and Wallis 1997). The regional frequency analysis was initially developed for the flood frequency analysis; it

requires to identify potential clusters or regions, to test homogeneity of the regions, and to carry out extreme value analysis using data within each homogenous region. The analysis considers that each station belongs to only a single region. A similar analysis was carried out by Ye et al. (2016) for annual maximum snow depth. It was observed that the estimated return period value of the annual maximum snow depth based on such an approach is consistent with that obtained based on the at-site analysis, especially for regions with significant historical snow depth records. Therefore, the use of regional analysis was not discussed further.

The main objectives of this chapter were to assess the statistics of and probabilistic models for the annual maximum ground snow depth and ground snow load (as well as snowpack bulk density), to evaluate the rain component of the roof snow load, and to assess the correlation between snow component and rain component of the annual maximum roof snow load. The assessment was carried out by considering the data available from ECCC DLY04 digital archive up to 2017 and from the Canadian Snow Data CD-ROM (CSD-CD-ROM)(MSC, 2000).

The remainder of this chapter was organized as follows. Section 3.2 was focused on the description of the ground snow data, the statistical analysis, and probabilistic modeling of the annual maximum ground snow depth. Section 3.3 was concentrated on the assessment of the snowpack bulk density and the annual maximum ground snow load based on data given in MSC (2000). A comparison of the return period value of the annual maximum ground snow load inferred from DLY04 and from MSC (2000) was given. This was followed by the analysis and discussion of the rain component of the roof snow load.

3.2. Snow depth records, and probabilistic modeling of annual maximum ground snow depth

The snow depth data are stored in the DLY04 digital archive and maintained by ECCC (see http://climate.weatheroffice.gc.ca/prods_servs/documentation_index_e.html#dly). A statistical analysis by using the snow depth records in this digital archive was reported in Hong and Ye (2014) by using the data up to June 2012 from 549 stations. Following the same analysis procedure, but considering more up to date information (i.e., up to 2017), an analysis was carried out and described below.

By screening the snow records in the database, it was found that there are 555 stations, each containing at least 20 years of useable data. The locations of the stations were shown in Figure 3.1. The empirical distribution of the length of the useable data was shown in Figure 3.2.

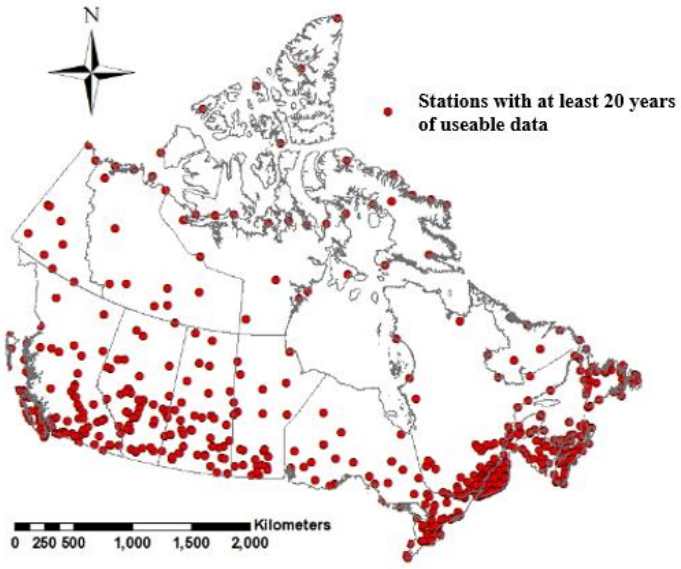

Figure 3.1. Location of the stations with at least 20 years of useable (non-zero) annual maximum snow depth.

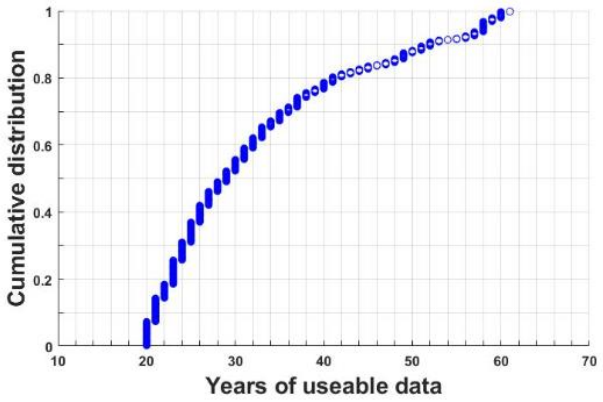

Figure 3.2. Empirical distribution of the length of useable data.

From these figures, it can be observed that the spatial coverage by the stations is much denser for regions near urban centers. The spatial coverage for the south is better than that for the north. The longest available record is 61 years. The mean and coefficient of variation (COV)

of the annual maximum ground snow depth, S_A, for each of the considered stations were calculated. When calculating the statistics, only the non-zero values of S_A were considered. The calculated mean and COV of S_A for each considered stations were used as the basis for spatial interpolation by using the ordinary kriging with nugget not equal to zero (ESRI 2011; Johnston et al. 2003). Unless otherwise stated, the use of nugget not equal to zero for spatial interpolation was considered throughout this chapter. The interpolated values were presented in Figure 3.3.

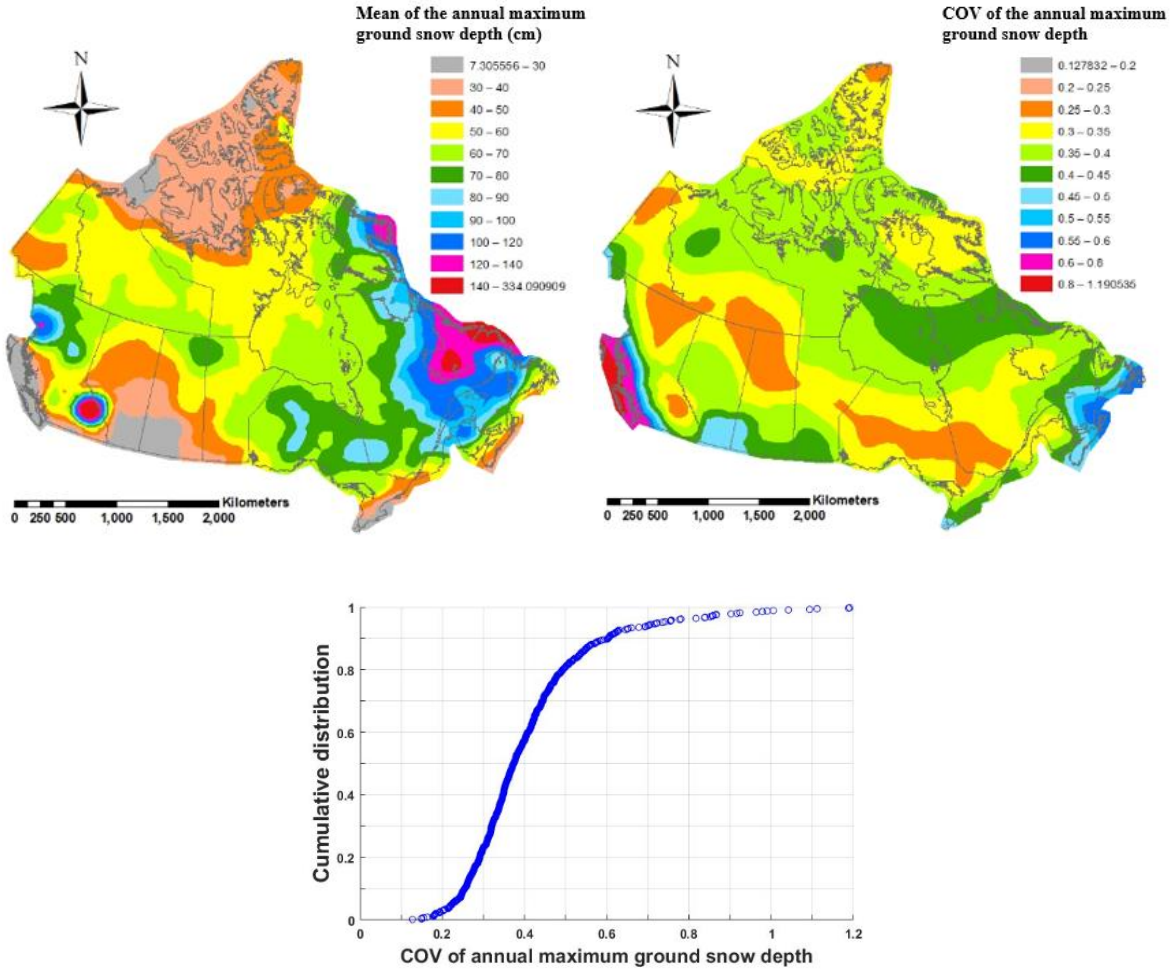

Figure 3.3. Contour maps of the mean and coefficient of variation, as well as the empirical distribution of COV of annual maximum snow depth.

As can be observed from the figure, both the mean and COV of the annual maximum snow depth vary from region to region. In general, the mean of S_A is greater in eastern Canada, and

there is an area in the Rocky Mountain with a large mean of S_A. The COV of S_A is very large for the eastern and western coastal regions. For the majority of locations away from these coastal regions, especially for populated regions near Canada and the U.S. border, the COV of S_A is less than 0.55.

The mean value of COV equals 0.408. It is noteworthy that if the annual maximum ground snow depth is considered to be Gumbel distributed, the 50-year maximum snow depth distribution is Gumbel distributed as well. In such a case, it can be shown that the use of this mean COV of S_A equal to 0.408 implies a COV of the 50-year maximum snow depth equals 0.181, which is slightly less than 0.2 that was used in Bartlett et al. (2003a,b) for the design code calibration. The use of COV of the 50-year maximum snow depth equal to 0.2 is equivalent to use a COV of S_A equal to 0.51. Based on these observations, it is suggested that a range of COV of S_A equal to 0.2 to 0.8 with a typical value of 0.5 could be considered for Canadian sites.

A distribution fitting was carried out for the extracted S_A values at each station by using commonly adopted distribution types for the annual maximum snow depth (i.e., Gumbel distribution, GEVD, and lognormal distribution). The Gumbel distribution for a random variable S, $F_{GU}(s)$, is given by (Coles 2001),

$$F_{GU}(s) = \exp\left(-\exp\left(-(s-u)/a\right)\right), \tag{3.1}$$

where s denotes the value of S, a and u are the scale and location parameters. GEVD, $F_{GE}(s)$, is given by (Coles 2001),

$$F_{GE}(s) = \exp\left(-\left(1-k(s-u)/a\right)^{1/k}\right), \text{ for } k \neq 0 \tag{3.2}$$

where u, a and k are the model parameters. GEVD reduces to the Gumbel distribution if k tends to 0. The lognormal distribution, $F_{LN}(x)$, is given by,

$$F_{LN}(x) = \Phi\left(\left(\ln x - m_{\ln x}\right)/\sigma_{\ln x}\right), \tag{3.3}$$

where $m_{\ln x}$ and $\sigma_{\ln x}$ are the distribution parameters and $\Phi(\ )$ denotes the standard normal distribution function.

The method of moments (MOM), the method of maximum likelihood (MML), the method of L-moments (MLM), and the generalized least-squares method (GLM) could be adopted for fitting the Gumbel distribution. In such a case, GLM outperforms MML and MLM (Hong et al. 2013). For many probability distribution models, MLM outperforms MOM (Hosking et al. 1985).

The selection of the preferred distribution could be carried out based on the Akaike information criterion (*AICc*), which takes into account the sample size effect (Akaike 1974; Cavanaugh 1997). *AICc* for a considered model is defined by,

$$AICc = \left(2m - 2\ln \hat{\mathcal{L}}\right) + \frac{2m^2 + 2m}{n - m - 1}, \tag{3.4}$$

where n is the sample size, m is the number of model parameters to be estimated and $\hat{\mathcal{L}}$ is the maximum value of the likelihood function of the model. Among a set of considered models, the model with the lowest *AICc* is preferred.

By considering the three distribution models shown in Eqs. (3.1) to (3.3), the calculation of *AICc* was carried out for the samples of S_A from each of the stations identified in Figure 3.1. Based on the calculated *AICc* values, it was concluded that the use of lognormal, Gumbel, and GEV distributions is preferred for 57%, 31%, and 12% of the considered stations, respectively. However, since the Gumbel distribution was traditionally used in mapping ground snow load and developing the NBCC, as mentioned in the introduction, the Gumbel distribution may be considered for future NBCC development. The preferred probability distribution identified by using *AICc* for each site was shown in Figure 3.4. As can be observed from the plot, there are no clear spatial trends for each of the distribution models.

By adopting the Gumbel distribution for S_A and carrying out the distribution fitting based on GLM, the obtained $s_{A\text{-}T}$ were mapped in Figure 3.5 for T = 50, 500, and 1000 years. For the

estimation of $s_{A\text{-}T}$, the possible occurrence of the annual maximum snow depth equal to zero was taking into account. The figures showed a more drastic spatial variation of the annual maximum snow depth as T increases. This was expected; it represents the compound effect of spatial variation of both the mean and COV of S_A. For comparison purposes, by adopting the lognormal distribution fitted using the MML, the obtained $s_{A\text{-}T}$ were mapped in Figure 3.6 for T = 50, 500, and 1000 years. A comparison of the plots shown in Figures 3.5 and 3.6 indicated that the use of the lognormal model resulted in slightly greater $s_{A\text{-}T}$, especially as T increases. In general, the use of the Gumbel and lognormal models resulted in very similar spatial trends of the estimated $s_{A\text{-}T}$.

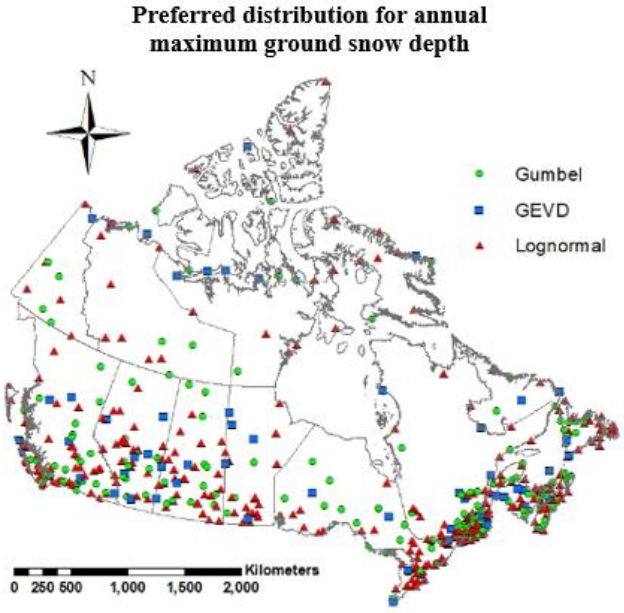

Figure 3.4. The preferred probability distribution for each meteorological station (for the non-zero annual maximum snow depth).

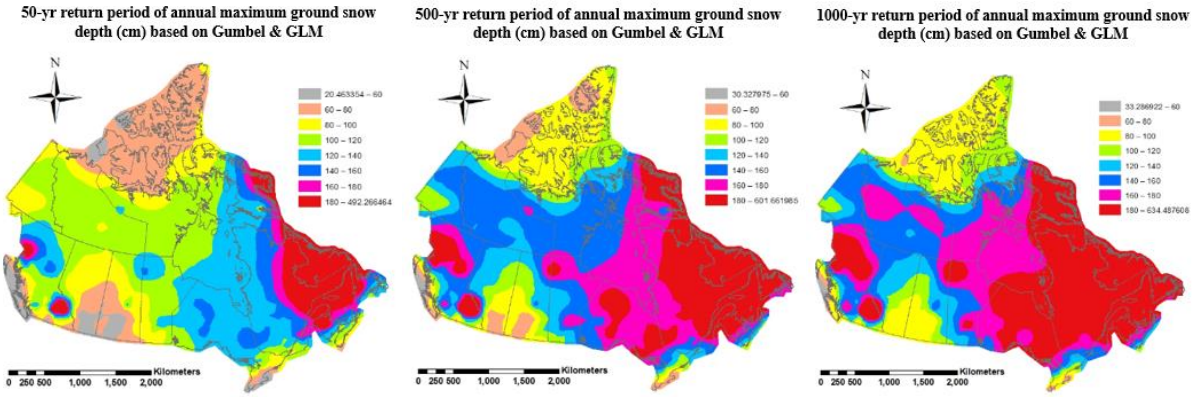

Figure 3.5. Contour maps of $s_{A\text{-}T}$, for T = 50, 500, and 1000 years by adopting the Gumbel distribution.

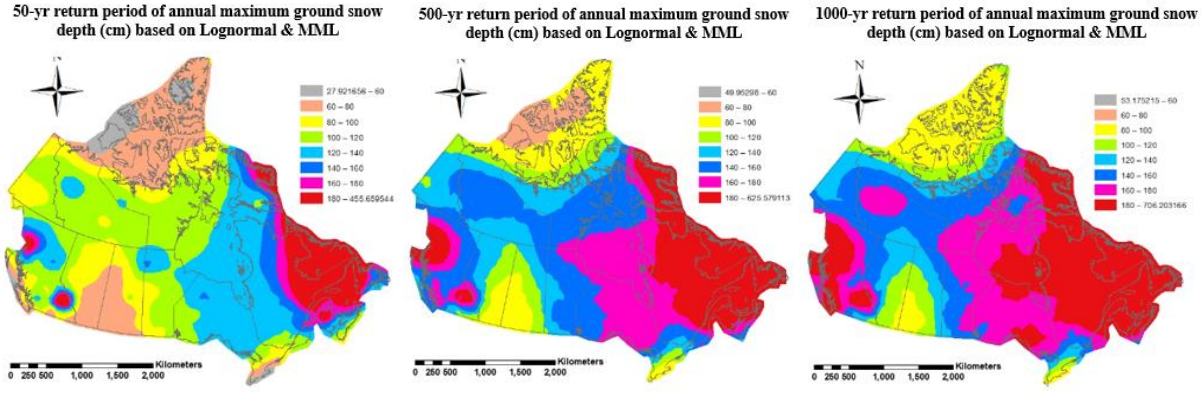

Figure 3.6. Contour maps of $s_{A\text{-}T}$, for T = 50, 500, and 1000 years by adopting the lognormal distribution.

3.3. Snowpack bulk density and ground snow load

According to the NBCC and the reliability-based design code calibration studies (Taylor and Allen 2000; Bartlett et al. 2003a,b), the roof snow load S could be expressed as,

$$S = C_{gr} S_L + S_R \tag{3.5}$$

where S_L is the ground snow load; S_R is the rain component of the snow load, and C_{gr} represents the transformation factor that converts the ground snow load at a given site to the snow component of the roof snow load.

The statistical analysis of the ground snow load can be carried out based on the reported snow water equivalent (SWE) values. SWE was not always available for a station. In such a case, the ground snow load, S_L, could be calculated based on snow depth and snowpack bulk density resulting in,

$$S_L = 0.01\gamma S_A, \tag{3.6}$$

where the ground snow load S_L is in Pa, S_A is in cm and γ (Pa/m) is the unity pressure of snow, which equals $\rho_b g$, g = 9.81 (m/s^2) is gravitational acceleration, and ρ_b is the snowpack bulk density (kg/m^3). The suggested snowpack bulk density by Newark (1984) (see also Newark et al. 1989) was presented in Figure 3.7. The results depicted in the figure indicated that the average ρ_b varies from region to region and ranges between 190 to 430 (kg/m^3). By neglecting the uncertainty in ρ_b, and using its average value, $\mu_{\rho b}$, the approximate T-year return period value of S_L, denoted by $s_L(T)$, could be calculated using,

$$s_L(T) = 0.01\mu_{\rho b} g s_{A-T}, \tag{3.7}$$

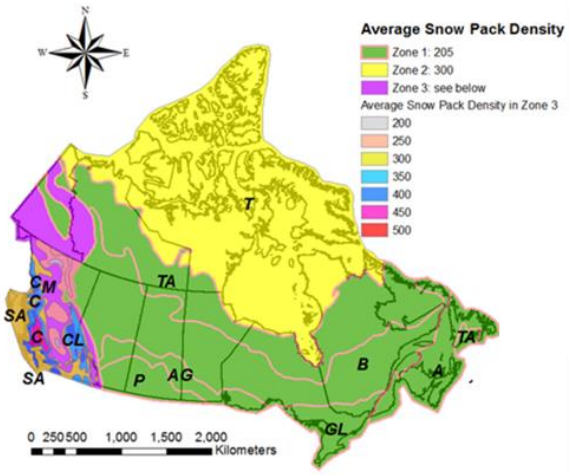

Region	Abbreviation	Snowpack bulk density (kg/m^3)	
		Mean	St.D.
Acadian	A	220	50
Aspen Grove	AG	220	40
Boreal	B	190	60
Coast	C	430	25
Columbia	CL	360	35
Great Lakes	GL	220	60
Montane	M	260	25
Prairie	P	210	40
Subalpine	SA	360	30
Tundra	T	300	80
Taiga	TA	200	80

Figure 3.7. Snowpack bulk density modified from (Newark 1984; Newark et al. 1989).

By using this equation and neglecting the uncertainty in ρ_b, taking ρ_b equal to its mean value, using the results shown in Figures 3.5 and 3.7, and applying Eq. (3.7), the obtained $s_L(T)$ was shown in Figure 3.8. The snow loads near the eastern coastal and western coastal regions are greater than those for the central region. For most sites, $s_L(T)$ is less than 5 kPa for T = 50 years.

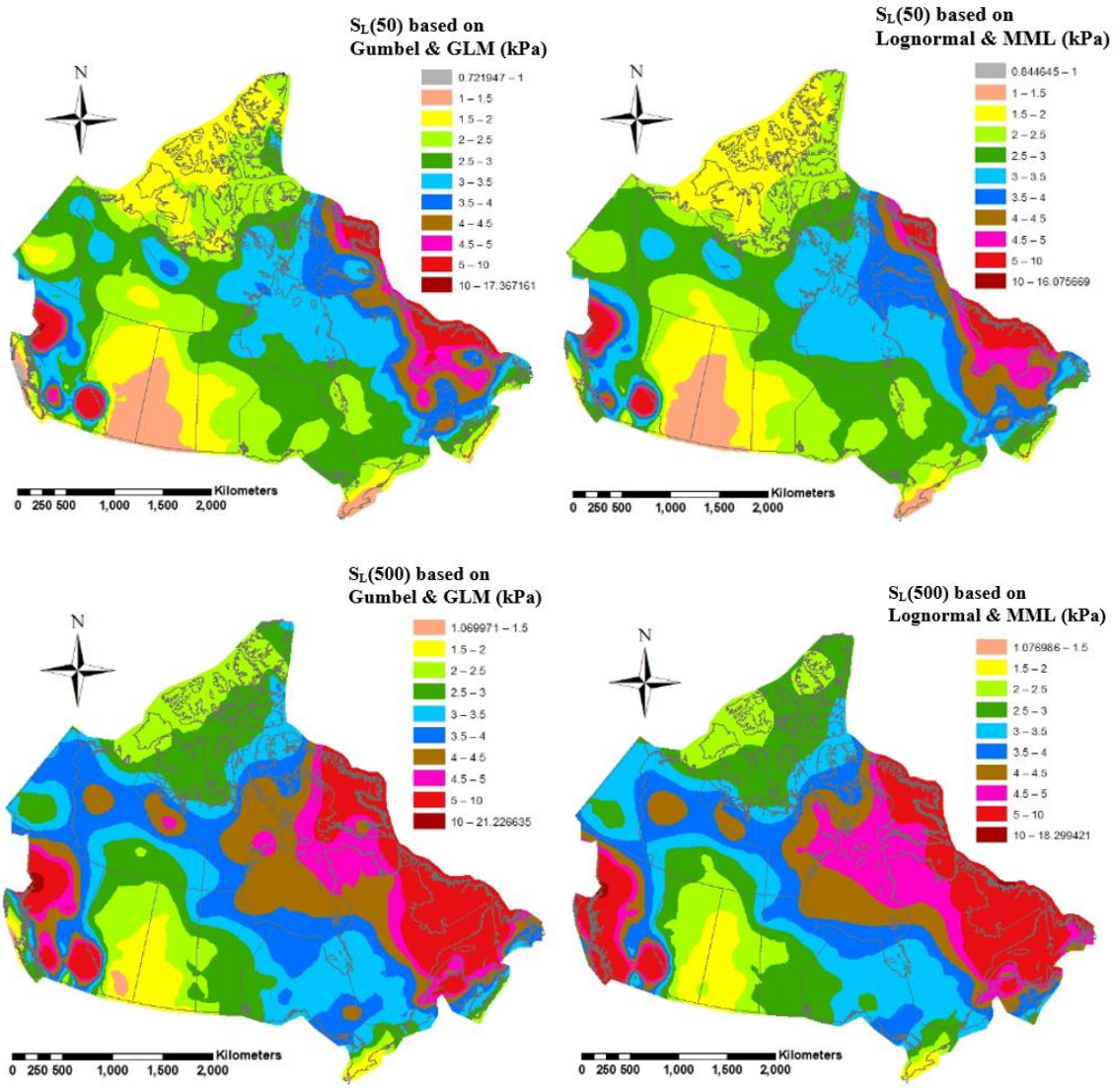

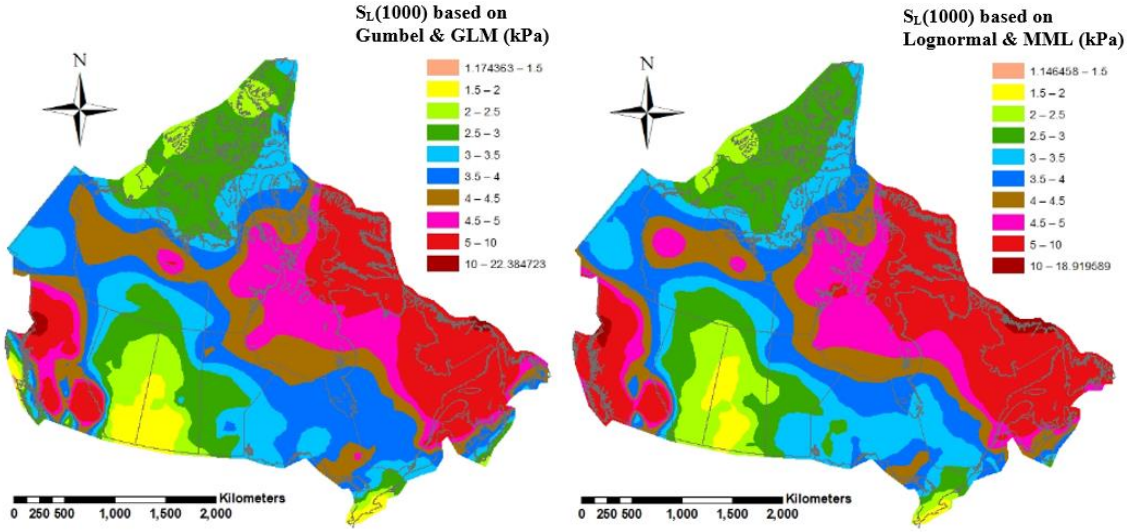

Figure 3.8. Contour maps of the return period values of the annual maximum ground snow load $s_L(T)$ for T = 50, 500, and 1000 years.

An attempt to update the snow density models presented in Figures 3.7 was made by using the reported snow information from CSD-CD-ROM (MSC, 2000). Some of the data quality control measures used to develop this database were unknown. The database provided the records of the snow depth and snow water equivalent. The snow water equivalent was converted to the snowpack bulk density. For the statistical analysis to be carried out below, the information recorded at a site was considered if the data was available at least for three months in a year, and the useable data should be at least for 20 years. The identified stations, each containing more than 20 years of useable data, were shown in Figure 3.9. It was observed that the longest available record is 75 years. The stations were mostly located in British Columbia, Ontario, and Quebec.

For each of the identified stations, the annual maximum snow depth and the ground snow load, which was calculated from the snow water equivalent and snow depth, were obtained. A plot of the mean and COV of S_A and of the ground snow load S_{AL} was shown in Figure 3.10. A comparison of the mean and COV of S_A shown in Figures 3.3 and 3.10 indicated that they are significantly different, although their overall trends are similar. Some of the statistics derived from CSD-CD-ROM may not be reliable. For example, the mean value of S_A for British Columbia in Figure 3.10 is very high as compared to that shown in Figure 3.3. The COV value

of S_A shown in Figure 3.10 tends to be smaller than that shown in Figure 3.3. A simple analysis indicated that the average of the COV value of S_A for Figure 3.10 is about 0.15 less than that for Figure 3.3. It was unclear what caused such a large discrepancy. Since the data in DLY04 was well documented and maintained, it was considered that the use of the statistics and models derived by using data in DLY04 for S_A was preferred.

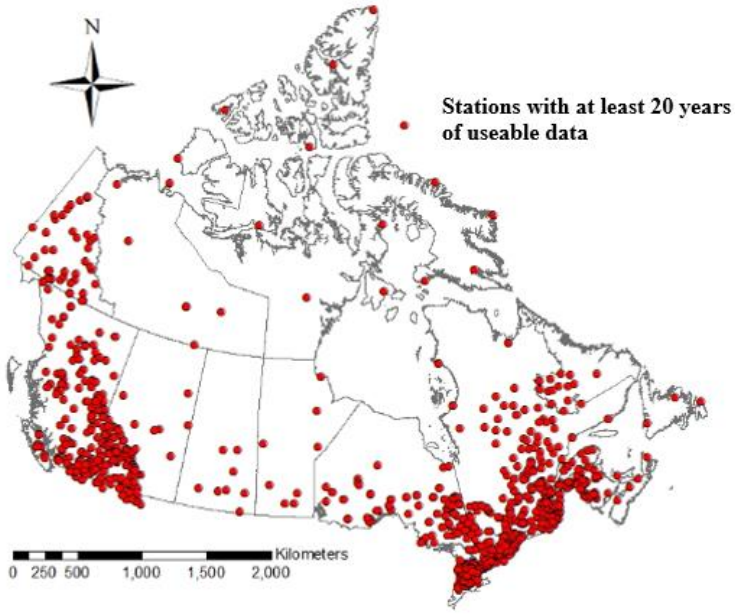

Figure 3.9. Location of the stations with at least 20 years of useable data based on data from CSD-CD-ROM.

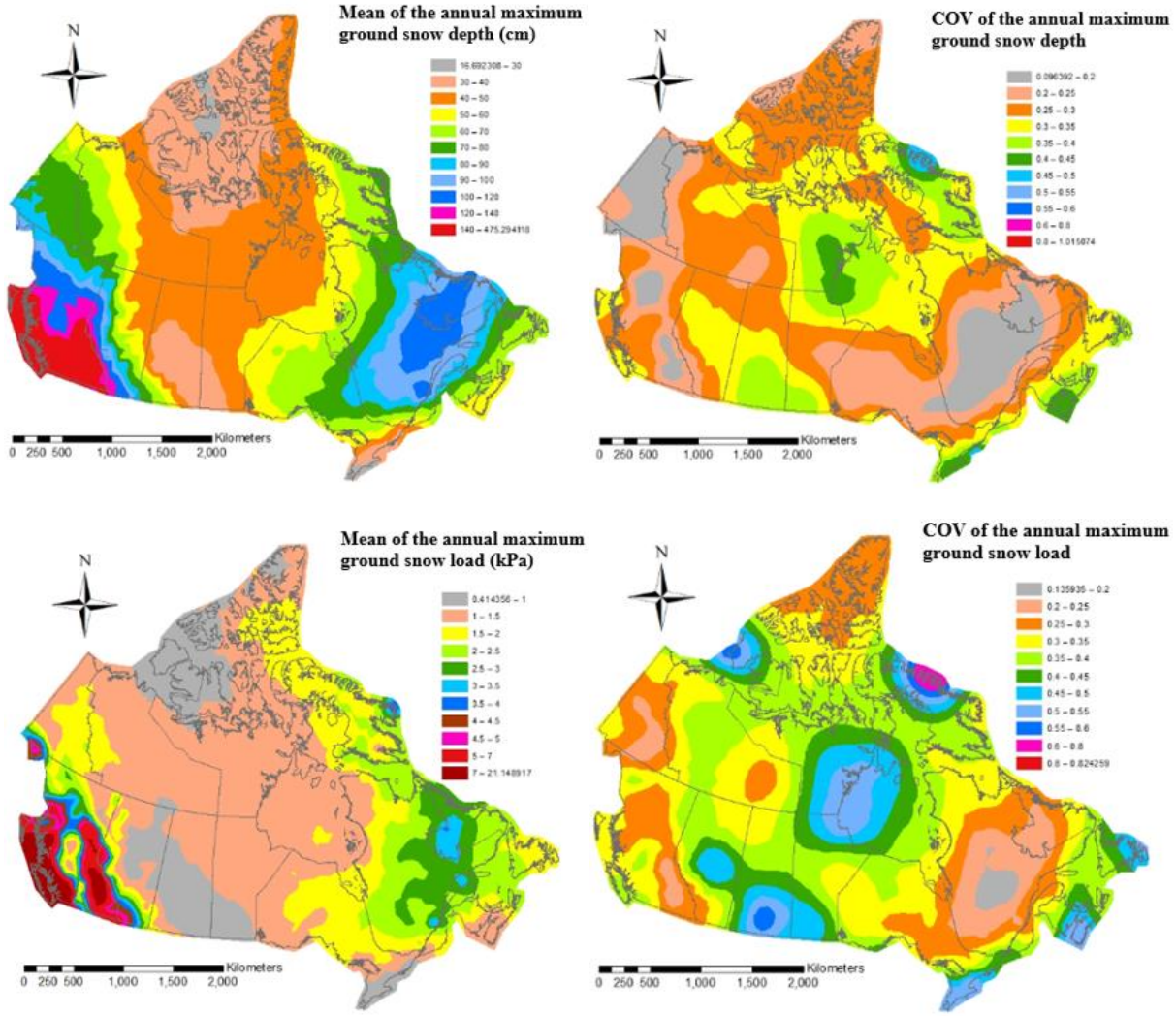

Figure 3.10. Statistics of the annual maxim snow depth and ground snow load by using the data from CSD-CD-ROM.

A distribution fitting was carried out by using the Gumbel distribution, lognormal distribution, and GEVD for the annual maximum ground snow load data, S_{AL}, that were extracted from CSD-CD-ROM. The use of *AICc* indicated that the lognormal, Gumbel, and GEV distributions are preferred for 46%, 30%, and 24% of all considered stations. Although the percentages were consistent with those observed when analyzing the annual maximum snow depth data, S_A, from DLY04, it must be emphasized that the analysis based on CSD-CD-ROM was for S_{AL}. This might imply that ρ_b is lognormally distributed since the annual maximum ground snow load (see Eq. (3.6)) is lognormally distributed if both ρ_b and S_A are independent and lognormal

distributed. The preferred probability distribution model identified by using *AICc* for each site was shown in Figure 3.11 to possibly identifying spatial trends of the preferred distribution type. Unfortunately, the identified preferred distribution types are intermingled spatially. Also, the locations for each of the preferred distribution types shown in Figure 3.11 do not follow the same pattern as those shown in Figure 3.4.

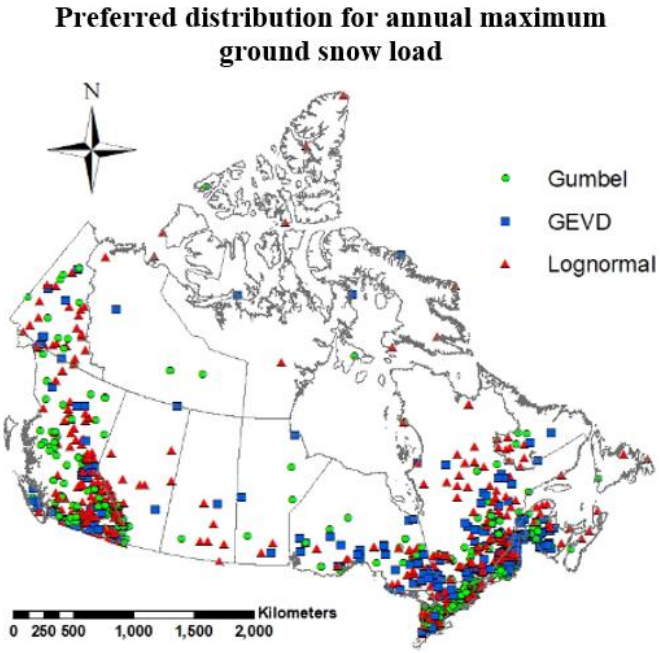

Figure 3.11. The preferred probability distribution for each meteorological station (for the annual maximum ground snow load).

By using the Gumbel model and lognormal model, the *T*-year return period value of the annual maximum ground snow load S_L, $s_{L\text{-}T}$, was calculated for $T = 50$, 500, and 1000 years. The hazard maps based on the estimated values were shown in Figure 3.12. The result presented in Figure 3.12 indicated that the spatial trends are consistent whether the lognormal model or Gumbel model was employed. However, a detailed quantitative assessment indicated that the estimated $s_{L\text{-}T}$ by using the lognormal model could be larger, in general, than that by using the Gumbel distribution, especially as T increases. This is because the lognormal distribution has an extended long upper tail as compared to that of Gumbel distribution.

A comparison of $s_L(T)$ presented in Figures 3.8 to $s_{L\text{-}T}$ depicted in Figure 3.12 indicated that

$s_L(T)$ presented in Figures 3.8 differ from those obtained by using the data in CSD-CD-ROM. Part of the differences may be attributed to the fact that the uncertainty in the snowpack bulk density was neglected in estimating the ground snow load shown in Figures 3.8. However, these figures showed that there are some similarities in the spatial trends of the estimated annual maximum ground snow load. This included a larger snow load hazard for the eastern coastal region, lower snow load hazard for the central region.

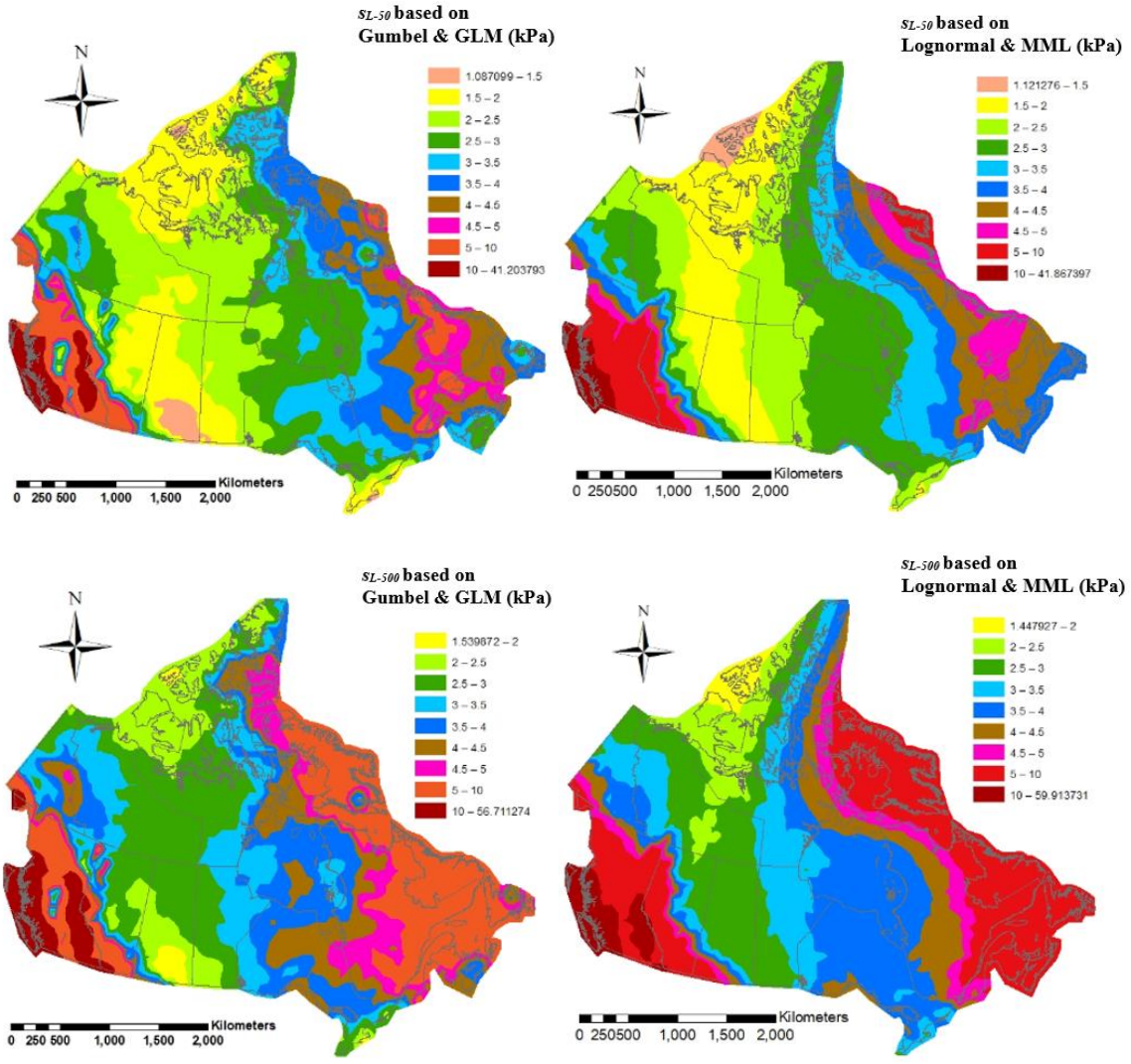

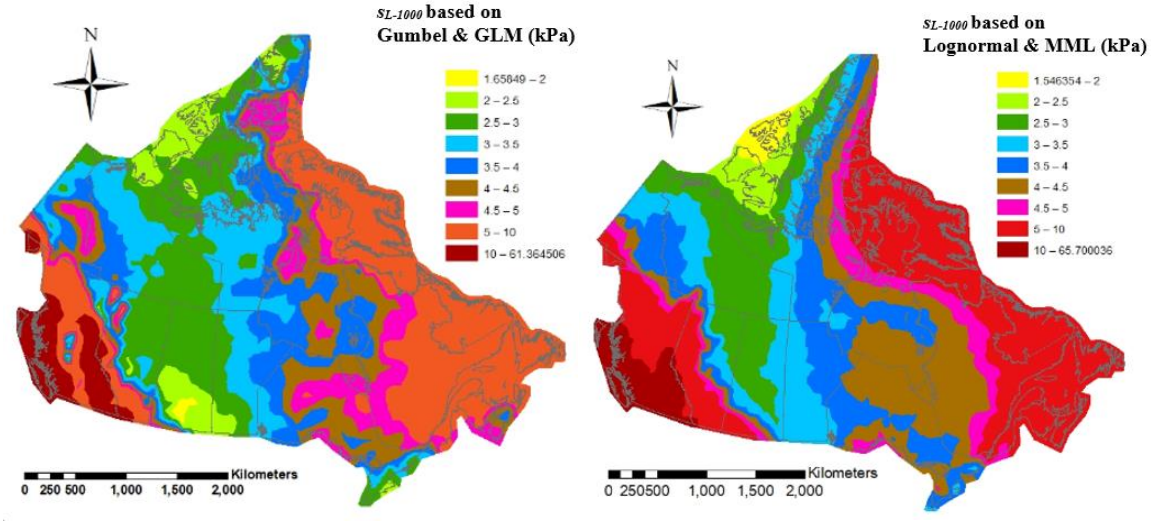

Figure 3.12. Contour maps of $s_{L\text{-}T}$ for T = 50, 500, and 1000 years based on the records in CSD-CD-ROM.

In an attempt to identify the source that caused the above-mentioned differences, the snowpack bulk density (calculated based on the SWE and snow depth) from 14 capital cities were extracted and analyzed. The obtained values versus their corresponding snow depths were shown in Figure 3.13. Also shown in the figure were the fitted linear relations. Since the *R*-squared values shown in the plots are less than 0.15 in all cases, it could be concluded that the data in CSD-CD-ROM indicated that the snowpack bulk density ρ_b could be assumed to be uncorrelated with the snow depth. Furthermore, there is no clear identifiable relation between ρ_b and snow depth. Therefore, one could assume that ρ_b is independent of the snow depth.

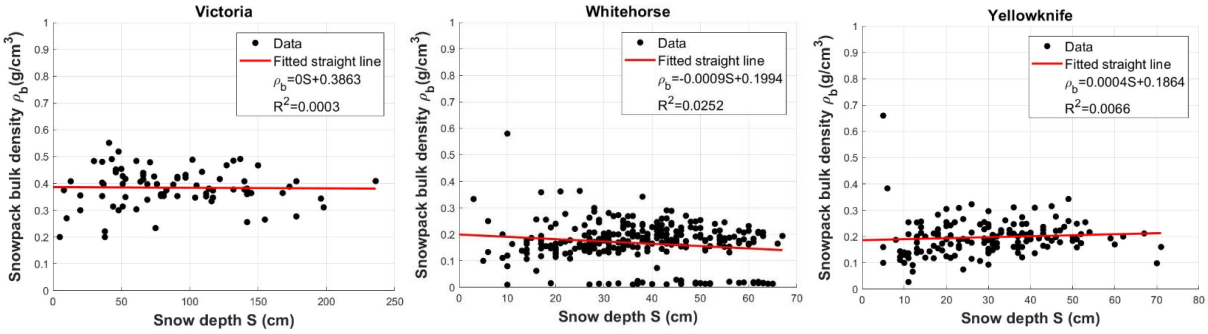

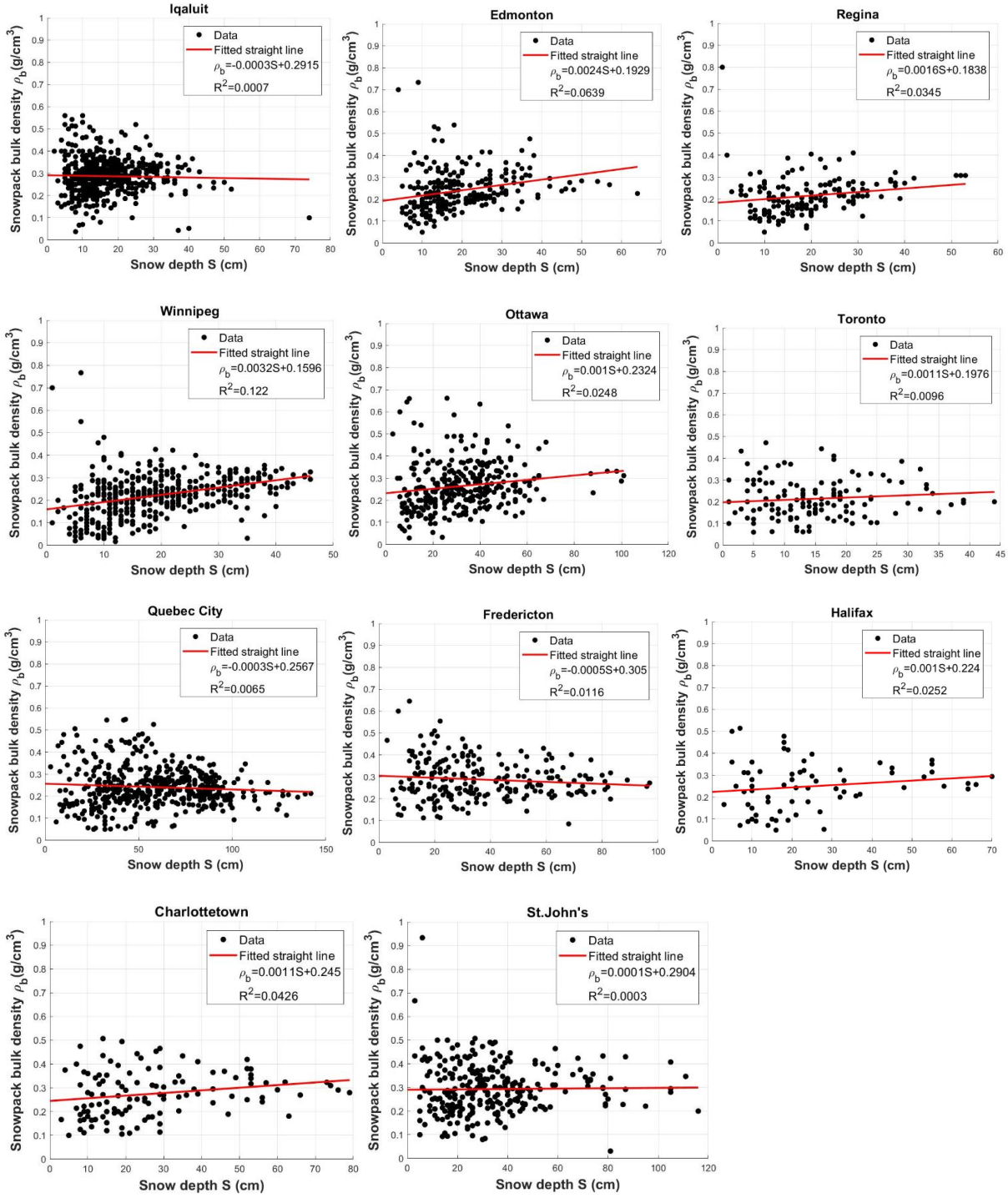

Figure 3.13. Snowpack bulk density versus snow depth for 14 capital cities.

Three sets of the mean and COV values of ρ_b were calculated for the 14 capital cities by considering each of the three conditions: all snow depth, snow depth ≥ mean snow depth, and

snow depth < snow depth. The obtained statistics were shown in Table 3.1. In most cases, the COV values shown in the table are greater than those that can be calculated based on the mean and standard deviation shown in Figure 3.7 given by Newark (1984) (see also Newark et al. 1989). The calculated means for many sites are close to those suggested by Newark (1984), especially if the data associated with snow depth greater than the mean snow depth is considered. For Whitehorse and Yellowknife, the mean value of ρ_b is much less than that suggested in Newark (1984).

Table 3.1. Estimated mean and COV of the snowpack bulk density for 14 capital cities.

Capital city	All snow depth data		For snow depth ≥ average snow depth		For snow depth < average snow depth	
	Mean(g/cm^3)	COV	Mean(g/cm^3)	COV	Mean(g/cm^3)	COV
Victoria	0.384	0.187	0.385	0.151	0.384	0.213
Whitehorse	0.167	0.469	0.160	0.507	0.174	0.433
Yellowknife	0.198	0.344	0.203	0.236	0.192	0.437
Iqaluit	0.287	0.280	0.292	0.218	0.284	0.317
Edmonton	0.238	0.403	0.265	0.310	0.220	0.455
Regina	0.215	0.401	0.237	0.268	0.198	0.490
Winnipeg	0.221	0.421	0.253	0.250	0.195	0.535
Ottawa	0.265	0.415	0.279	0.331	0.252	0.483
Toronto	0.214	0.465	0.233	0.461	0.200	0.457
Quebec City	0.241	0.368	0.236	0.257	0.247	0.443
Fredericton	0.288	0.317	0.275	0.231	0.296	0.353
Halifax	0.249	0.449	0.268	0.280	0.239	0.534
Charlottetown	0.275	0.349	0.302	0.256	0.256	0.403
St.John's	0.293	0.357	0.297	0.272	0.290	0.410

The mean and COV of ρ_b for each station identified in Figure 3.9 were calculated to investigate the spatial variability of the statistics of ρ_b. These values were depicted in Figure 3.14. A comparison of the results presented in this figure to those shown in Figure 3.7 indicated that the results in these figures differ significantly. The most striking difference was that the newly estimated average snowpack bulk density for part of Quebec and Atlantic provinces is greater than that suggested by Newark (1984), as shown in Figure 3.7. The values of the COV maps depicted in Figure 3.14 differ from the values that can be calculated by using the values shown in Figure 3.7. As the detailed documentation on the data quality control to the records in CSD-CD-ROM was unknown to this study, based on the observations, it was considered that the mean

of ρ_b suggested in Newark (1984) could be adopted as the reference values. Moreover, the range of COV values of ρ_b shown in the middle plot for COV in Figure 3.14 could be considered; with a typical value equal to 0.17 that was used in Bartlett et al. (2003a, b) for reliability-based calibration of snow load factors implemented in the 2005 edition of the NBCC. Furthermore, it was suggested that a long-term full-scale experimental investigation on the snowpack bulk density and ground snow load is very valuable to validate their statistical characteristics.

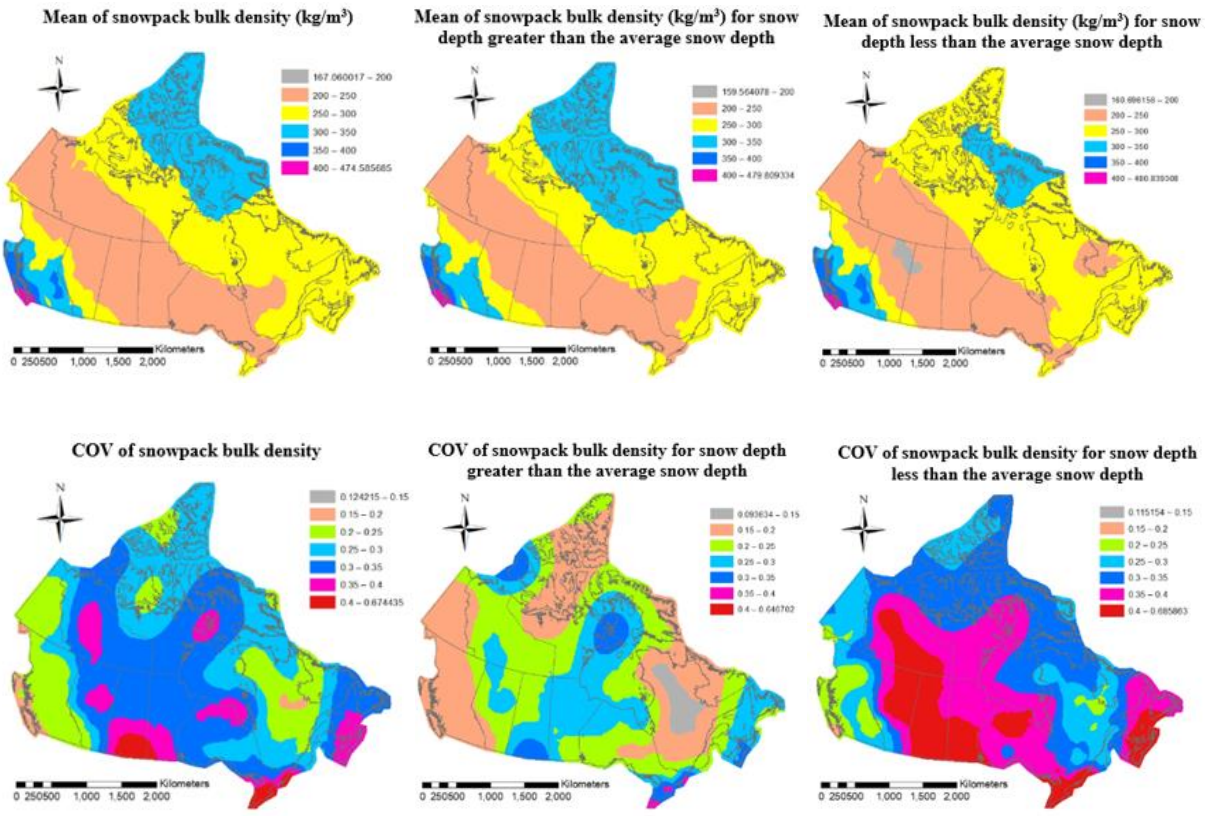

Figure 3.14. Spatial variation of the mean and COV of ρ_b.

3.4. Analysis and discussion on the rain load component

The evaluation of S_R was well explained in Newark et al. (1989) and mentioned in the introduction. Newark et al. (1989) suggested using the 30-year return period value of annual maximum 1-day "winter" rain amount as the rain component for the roof snow load. The 50-

year return period values of S_R and of S_L were used as the basis for the calculation of the roof snow load implemented in the 2015 edition of NBCC (see Eq. (3.5)). This implies the simultaneous occurrence of the T-year return period value of S_R and the T-year return period value of S_L. However, a statistical assessment of correlation or dependency between S_L and S_R was never presented. An attempt to validate the adequacy of using the same return period for S_L and S_R and their linear combination in defining the roof snow load in the NBCC was carried out in the following.

First, by using the data from DLY04, the maximum ground snow depth for the i-th year, $s_{\text{max-}i,}$ was identified, and its corresponding ground snow load, $s_{\text{Gmax},i}$, was calculated by using $s_{\text{max-}i}$ and applicable the snowpack bulk density, as shown in Figure 3.7. Also, a fraction of the ground snow load, $\xi s_{\text{Gmax},i}$, was calculated for $\xi = 0.7$. For each of the days within the i-th year, where the ground snow load is greater than $\xi s_{\text{Gmax},i}$, denoted as $s_{\text{Gmax}\xi,i}$, the 1-day winter rain load for the i-th year, $s_{\text{Rmax-}i}$, that is less than or equal to $s_{\text{Gmax}\xi,i}$ was extracted, where $s_{\text{Rmax-}i}$ is obtained by converting the 1-day winter rain amount. The samples of $s_{\text{Gmax}\xi,i}$ and $s_{\text{Rmax-}i}$ were then used to assess their correlation coefficient. Example plots of these two quantities for 14 capital cities were presented in Figure 3.15.

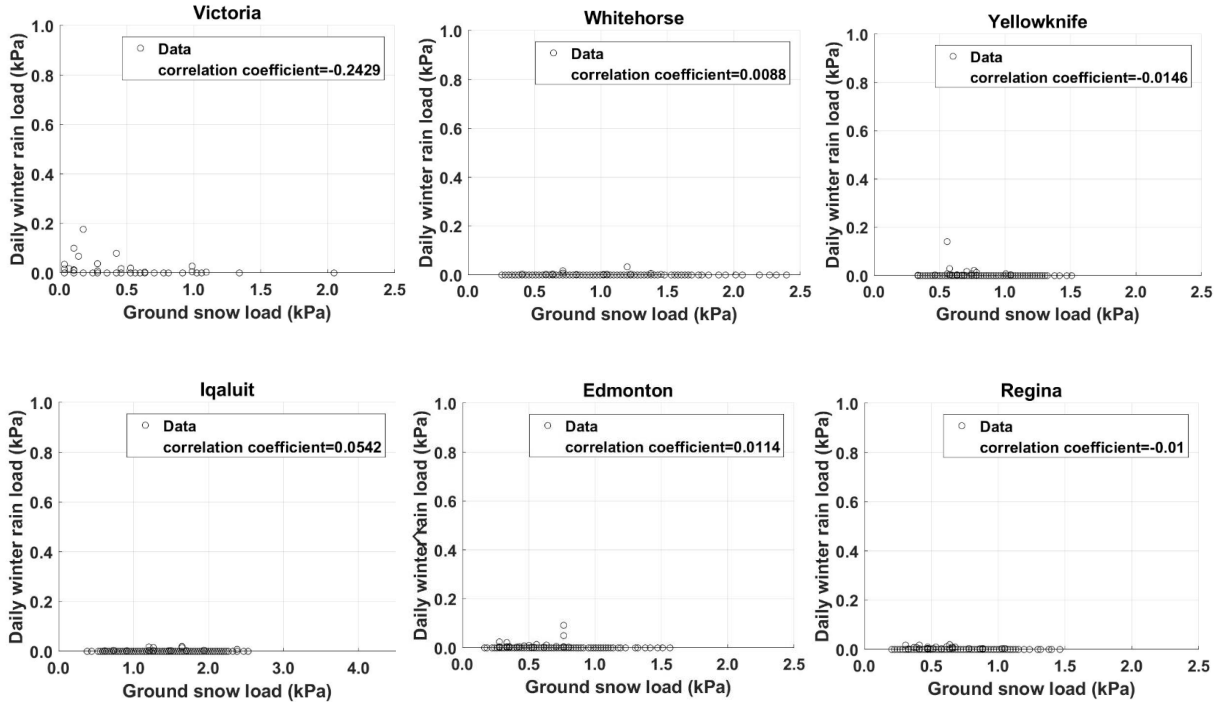

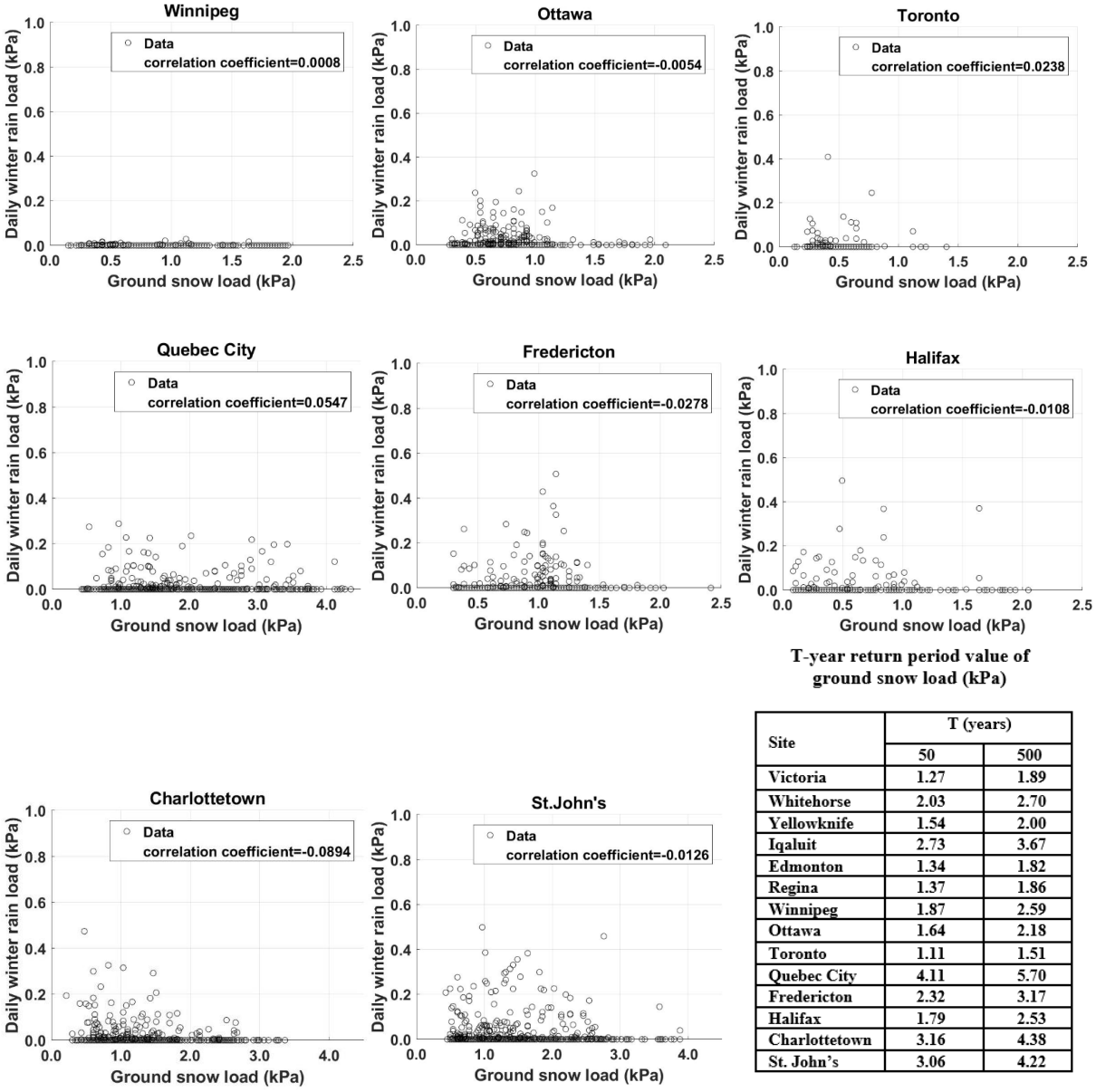

T-year return period value of ground snow load (kPa)

Site	T (years)	
	50	500
Victoria	1.27	1.89
Whitehorse	2.03	2.70
Yellowknife	1.54	2.00
Iqaluit	2.73	3.67
Edmonton	1.34	1.82
Regina	1.37	1.86
Winnipeg	1.87	2.59
Ottawa	1.64	2.18
Toronto	1.11	1.51
Quebec City	4.11	5.70
Fredericton	2.32	3.17
Halifax	1.79	2.53
Charlottetown	3.16	4.38
St. John's	3.06	4.22

Figure 3.15. Daily winter rain load $s_{\mathrm{Rmax}\text{-}i}$ versus ground snow load $s_{\mathrm{Gmax}\xi,i}$. For reference purposes. the *T*-year return period value of the ground snow load (kPa), that was calculated by using Eq. (3.7) and based on the information given in DLY04 by adopting the Gumbel distribution fitted using GLM, was also included.

The figure showed that the absolute value of the linear correlation coefficient between $s_{\mathrm{Gmax}\xi,i}$ and $s_{\mathrm{Rmax}\text{-}i}$, is less than 0.25 for all considered sites. Also, $s_{\mathrm{Rmax}\text{-}i}$ is significantly smaller than the 50-year return period value of ground snow load. The analysis carried out for the results

presented in Figure 3.15 was repeated for all the stations identified in Figure 3.9. In all cases, the correlation coefficient is very small. This indicated that the simultaneous occurrence of *T*-year return values of the annual maximum snow component of roof snow load and the annual maximum 1-day winter rain load is unlikely; hence, the use of the direct sum of the return period values of S_L and S_R to define the roof snow load (see Eq. (3.5)) could be too conservative. To reduce this conservatism, one could apply the well-known square-root-of-the-sum-of-squares (SRSS) rule instead of Eq. (3.5). In such a case, the *T*-year roof snow load could be calculated using,

$$(S)_T = \sqrt{\left(C_{gr} S_L\right)_T^2 + \left(S_R\right)_T^2} \tag{3.8}$$

where $(g)_T$ denotes the *T*-year return period value of its argument.

For consistency with the previous versions of NBCC and due to lack of a better ground snow model because of insufficient high-quality ground snow load data, it was suggested that the rain component S_R of the roof snow load is to be assigned based on the same return period that is used to calculate the snow component of roof snow load but combined using Eq. (3.8). This was further justified, considering that a systematic full-scale experimental investigation of the amount of the winter rain that could be retained by the roof snow was not reported in the literature.

It must be emphasized that S_R differs from the annual maximum 1-day rain amount, R_A. To quantify their differences, the *T*-year return period value of R_A, $r_{A\text{-}T}$, and the *T*-year return period value of S_R, $s_{R\text{-}T}$, were calculated and shown in Figure 3.16 for *T* equal to 50 and 500 years. For the calculation, it was assumed that R_A, as well as S_R, could be modelled using the Gumbel distribution. For the distribution fitting, the method of maximum likelihood was employed since the sample size was very large. The plots shown in the figure indicated that the spatial trends for $r_{A\text{-}T}$ differ from that of $s_{R\text{-}T}$. The ratio of $s_{R\text{-}T}$ to $r_{A\text{-}T}$ was shown in Figure 3.17. The ratio depends only slightly on the return period *T*. The ratio varies spatially, indicating that $s_{R\text{-}T}$ cannot be obtained by scaling the value of $r_{A\text{-}T}$ by a single constant for all the sites. The ratio

decreases from east to west, except for the coastal region in British Columbia, where the ratio is similar to that observed in the eastern coastal region.

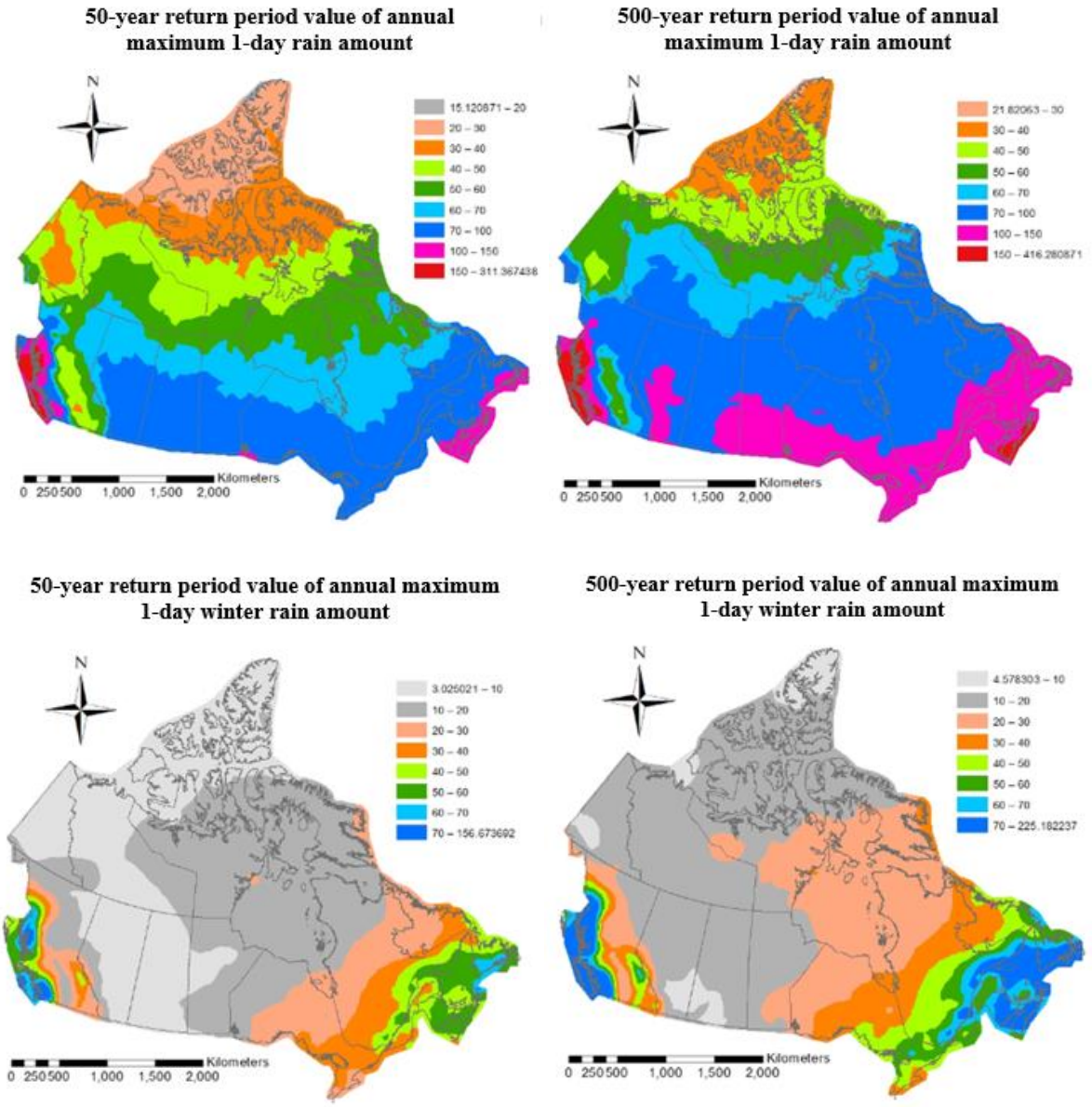

Figure 3.16. *T*-year return period value of annual maximum 1-day rain amount and annual maximum 1-day winter rain amount.

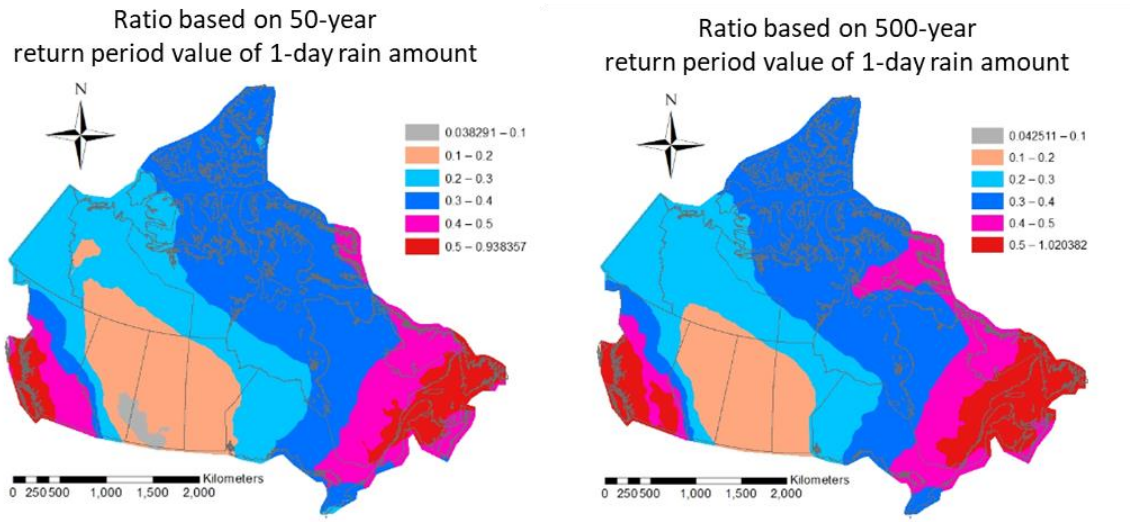

Figure 3.17. Ratio of $s_{R\text{-}T}$ to $r_{A\text{-}T}$ for T = 50 and 500 years.

3.5. Conclusions

Probabilistic analysis for the annual maximum ground snow depth, annual maximum ground snow load, snowpack bulk density, and the annual maximum 24-hour winter rainfall was carried out using the data from the DLY04 digital archive from ECCC and Canadian Snow Data CD-ROM. The analysis ranges from statistical evaluation, probability distribution fitting, and snow hazard mapping. For the distribution fitting, the commonly used distributions, such as the lognormal, Gumbel, and generalized extreme value distributions, were considered.

The use of the Akaike information criterion (*AICc*) indicated that the use of the lognormal, Gumbel, and GEV distributions for the annual maximum ground snow depth are preferred for 46%, 35%, and 19% of the cases, where each case represents fitting the samples of annual maximum ground snow depth, S_A, data from a meteorological station. A similar observation was made for the case of fitting the annual maximum ground snow load. The locations for the preference models are intermingled, and there are no clear spatial trends.

If only a single distribution model is to be used to map S_A, the lognormal distribution is preferred based on *AICc* alone. However, the Gumbel distribution could be adopted in practice since the use of the Gumbel distribution could be justified based on the extreme value theory, and the Gumbel distribution was traditionally used to map S_A and to develop the codified snow load for

structural design in Canada. It was observed that the coefficient of variation (COV) of S_A ranges from 0.2 to 0.8, with a typical value of about 0.5.

The obtained statistics of S_A based on the mentioned two data sources differ. The reason for the discrepancy was unknown. In general, the mean of the snowpack bulk density obtained in the present study differs from an earlier study. The COV of the snowpack bulk density varies spatially and ranges from about 0.1 to 0.3. Therefore, collecting quality data to investigate further the statistics of the snowpack bulk density and the ground snow load is an extremely valuable exercise.

It was suggested that the developed site-dependent S_A based on DLY04 digital archive from ECCC could be used as the basis to map the ground snow load (i.e., snow component of roof snow load) for Canada. Since the roof snow load also contains the rain load component, S_R, that is defined based on the 24-hour winter rain amount. The analysis of S_R was carried out, indicating that the correlation between S_R and the annual maximum ground snow load, S_L, is negligible. This suggested that the use of the sum of the ground snow load and rain load to evaluate the roof snow load that is implemented in the National Building Code of Canada could be conservative and the use of the well-known square-root-of-the-sum-of-squares (SRSS) rule to evaluate the roof snow load based on the snow component and rain component is recommended.

3.6. Reference

Akaike, H. (1974). A new look at the statistical model identification. IEEE Transactions on Automatic Control, 19 (6), 716–723.

Bartlett, F.M., Hong, H.P. and Zhou, W. (2003a). Load factor calibration for the proposed 2005 edition of the National Building Code of Canada: Statistics of loads and load effects, Canadian Journal of Civil Engineering, 30 (2) 429-439.

Bartlett, F.M., Hong, H.P. and Zhou, W. (2003b). Load factor calibration for the proposed 2005 edition of the National Building Code of Canada: Companion-action load combinations, Canadian Journal of Civil Engineering, 30 (2) 440-448.

Blanchet, J. and Davison, A.C. (2011). Spatial modeling of extreme snow depth. The Annals of

Applied Statistics, 5(3): 1699-2264.

Boyd, D.W. (1961) Maximum snow depths and snow loads on roofs in Canada. Division of Building Research, Research Paper No. 142, National Research Council, Ottawa, Ont. In: Proceedings of the Western Snow Conference, pp. 6–16, April

Cavanaugh, J.E. (1997). Unifying the derivations for the Akaike and corrected Akaike information criteria. Statistics & Probability Letters, 33(2), 201-208.

Coles, S. (2001). An introduction to statistical modeling of extreme values. Springer, London

Ellingwood, B. and Redfield, R.K. (1983). Ground snow loads for structural design. J. Struct. Eng. ASCE, 109(4): 950-964.

ESRI (2011). ArcGIS Desktop: Release 10. Redlands, CA: Environmental Systems Research Institute.

Hong, H.P. and Ye, W. (2014). Analysis of extreme ground snow loads for Canada using snow depth records. Natural hazards, 73(2), 355-371.

Hong, H.P., Li, S.H. and Mara, T. (2013) Performance of the generalized least-squares method for the extreme value distribution in estimating quantiles of wind speeds, Journal of Wind Engineering & Industrial Aerodynamics, 119: 121–132.

Hosking, J. R. M., Wallis, J. R., & Wood, E. F. (1985). Estimation of the generalized extreme-value distribution by the method of probability-weighted moments. Technometrics, 27(3), 251-261.

Hosking, J.R.M. and Wallis, J.R. (1997). Regional frequency analysis: an approach based on L-moments. Cambridge University Press, Cambridge, UK.

Johnston, K., Ver Hoef, J.M., Krivoruchko, K., and Lucas, N. (2003). ArcGIS9, Using ArcGIS geostatistical analyst, Redlands, CA: Environmental Systems Research Institute.

MSC. (2000). Canadian Snow Data CD-ROM. CRYSYS Project, Climate Processes and Earth Observation Division, Meteorological Service of Canada, Downsview, Ontario, January 2000. (online order form available at www.crysys.ca)

Newark, M.J. (1984). A new look at ground snow loads in Canada. Proceedings, Eastern Snow Conference, Vol. 29, 41st Annual Meeting, Washington, DC, pp. 37-48.

Newark, M.J., Welsh, L.E., Morris, R.J. and Dnes, W.V. (1989). Revised ground snow loads for the 1990 National Building Code of Canada. Canadian Journal of Civil Engineering,

16(3): 267-278.

NRC (2010) National Building Code of Canada. Institute for Research in Construction, National Research Council of Canada, Ottawa.

Taylor, D.A. and Allen, D.E. (2000). Statistical variation and duration of snow load on flat roofs in Canada. Institute for Research in Construction, National Research Council of Canada, Ottawa, Ont. Unpublished study.

Ye, W., Hong, H.P., and Mo, H.M. (2016) A comparison of ground snow load estimated using at-site analysis, regional frequency analysis, and region of influence approach, Report BLWT-2-2016, Boundary Layer Wind Tunnel Laboratory, the University of Western Ontario

Chapter 4

4. Calibration of the Design Wind load and Snow load Considering the Historical Climate Statistics and Climate Change Effects

4.1. Introduction

The National Building Code of Canada (NBCC) (NRC 2015) prescribes the design loads for design buildings in Canada. Similar to other structural design codes in the world, the load factors in the NBCC were calibrated based on the limit state design format. The nominal values of the resistance and load, as well as the load and resistance factors, were assigned and calibrated for selected target reliability indices. The use of calibrated structural design loads for structural design ensures that the desired target reliability index, on average, is achieved.

A key issue for the reliability-based design code calibration is the selection and assignment of the probabilistic models of the random variables involved in the limit state functions. The selected probabilistic models impact the calibrated design loads; the justification of the selected models is essential. The probabilistic models of extreme wind velocity and ground snow load can be developed based on their historical records alone if the effects of climate change can be neglected. In such a case, the extreme of the climatological elements could be assumed to be stationary. An influential study focused on the calibration of structural design codes in the U.S. was presented in Ellingwood et al. (1980). Some of the earlier studies on the reliability-based design code calibration focused on Canadian structural design practice were presented in Allen (1975), Nowak and Lind (1979), Kennedy (1984), MacGregor et al. (1983), and Foschi et al. (1993). An update to the probabilistic models used to calibrate load and companion load factors for wind and snow loads in the current NBCC was given in Bartlett et al. (2003a,b).

In general, the dead load is modelled as a normally distributed random variable. The extreme live load, annual maximum wind speed (which is related to the wind pressure), and annual maximum ground snow depth (which is associated with the ground snow load) are all modelled by using Gumbel distribution. The point-in-time live, wind, and snow loads are modelled as

Poisson pulse processes with the magnitude of the pulses represented by the Weibull distribution. These models are commonly used in civil engineering applications (Ang and Tang 2007; Madsen et al. 2006; Melchers and Beck 2018).

The modelling of the wind load essentially follows the wind load chain advanced by Davenport (1983, 2002). A review and development of new wind hazard maps for Canada were presented in Hong et al. (2014) and Hong and Ye (2014a). They emphasized the importance of the spatially-varying coefficient of variation (COV) of the annual maximum wind speed in wind hazard mapping. An additional wind hazard investigation was presented in Chapter 2 by treating the synoptic and thunderstorm winds separately, as the assessment of the extreme winds according to their types in mixed wind climates can be important for wind hazard mapping (Gomes and Vickery 1978; Lombardo et al. 2009). The probabilistic modelling of the ground snow load for Canada was given in Newark (1984), Newark et al. (1989), and Hong and Ye (2014b). The use of more up to date snow records in mapping the snow load, which consists of the snow component and rain component, was presented in Chapter 3. All these studies emphasized the spatially-varying uncertainty in the ground snow depth and ground snow load.

Besides the stationary extremes, the climate is changing, and the temporal temperature increasing trend affects the extreme environmental parameters, which need to be considered for structural design. Climate modelling and projections are computationally intensive processes. The spatially-varying statistics of extreme wind and snow were investigated in Jeong and Sushama (2018) by considering climate change. An extensive study was presented by Environment and Climate Change Canada (ECCC) (Cannon et al. 2019). An illustration of the temporal increase in the temperature was presented in Figures 4.1 based on the historical record and for selected Representative Concentration Pathways (RCPs). Most importantly, the study provided the percent changes in the extremes of climatological elements for a given temperature increment, which can be related to RCPs.

The design wind and snow loads in the past and current editions of the NBCC were calibrated using probabilistic models of extreme wind and snow loads that were developed based on the historical meteorological data. The possible effect of climate change on structural code making

was not considered. Climate change may have implications in structural design code making since climate change leads to nonstationary statistics of the extreme wind speed, ground snow depth, and precipitation (Cannon et al. 2019).

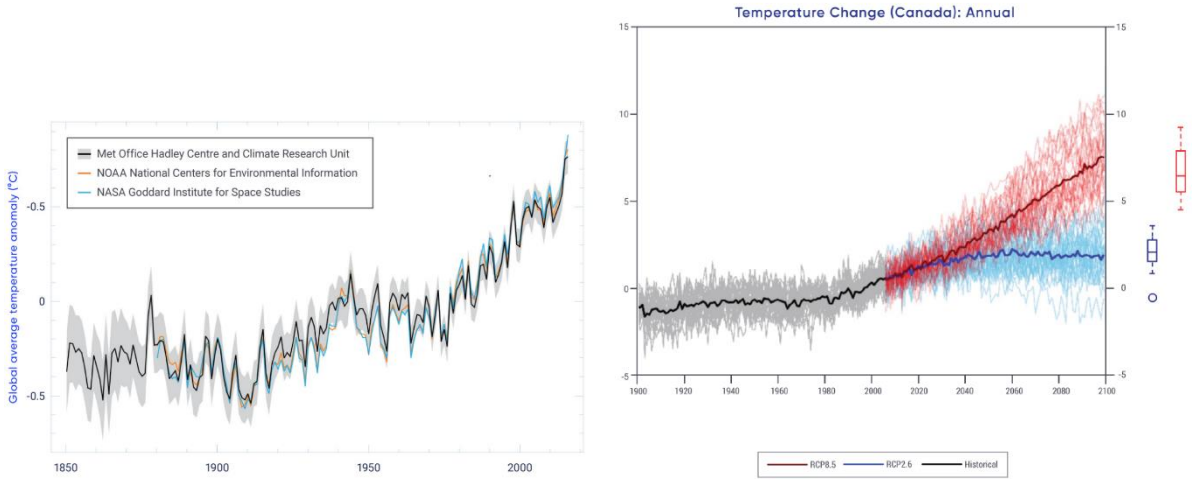

Figure 4.1. Change in global surface temperature: The left plot shows the observed temperature change, and the right plot shows the projected annual temperature changes (Canada) (after Cannon et al. (2019)).

It is noteworthy that the 2015 edition of the NBCC recommended a wind load factor of 1.4 and a snow load factor of 1.5 with the nominal wind pressure and snow load specified based on a relatively short return period, T_{Short}, (i.e., 50 years). A simple calculation shows that the factored design wind load and snow load correspond to a longer return period, T_{long} of about 500 and 1000 years, respectively, for typical applicable COV of annual maximum wind speed and the ground snow depth. The factored design loads were calibrated for a target reliability index of 3.0 or a tolerable failure probability of 1.35×10^{-3} for a design working life of 50 years (Bartlett et al. 2003a, b). This target reliability index is supported by the standard practice inferred from earlier editions of NBCC and the guideline for developing the limit state design codes (CAN/CSA S408 1981). It was suggested that the use of the 50-year return period value of the wind velocity pressure and the wind load factor of 1.4 is to be replaced by the 500-year return period value of the wind velocity pressure and a wind load factor of 1.0 for an improved reliability-consistency by considering site-dependent uncertainty in extreme wind speed (Tang

2016).

The present study was focused on the calibration of design wind and snow loads by including climate change (i.e., nonstationarity) effect on the extreme winds and snow loads. It also investigated the potential benefit of using a longer return period to assign the design wind load and snow load with the load factor equal to unity for spatially-varying COV of extreme environmental parameters. The results are to be used as the basis to recommend a new set of design loads and companion load factors.

4.2. Background and statistics of extreme wind and ground snow depth

The 2015 editions of NBCC (NRC 2015) recommended the use of the 50-year return period value of the annual maximum hourly-mean wind speed to calculate the reference wind velocity pressure (i.e., nominal wind load) and a wind load factor that is given in Table 4.1. These values are used for buildings in the normal importance category. The code also recommended an importance factor of 0.8, 1.15, and 1.25 for buildings in the low, high, and post-disaster importance categories, respectively. The importance factors were suggested for snow load. The nominal roof snow load, which consists of snow component and rain component, was based on a return period of 50 years. The load factors and companion load factors involving snow load were shown in Table 4.1, as well.

Table 4.1. Load combinations for ultimate limit state involving the wind load and snow load according to the 2015 edition of NBCC (D_n, L_n, W_n, and S_n are the nominal dead, live wind and snow loads).

Case according to NBCC	Load combination	
	Principal Loads	Companion loads
2	$1.25D_n + 1.5L_n$	$1.0S_n$ or $0.4W_n$
3	$1.25D_n + 1.5S_n$	$1.0L_n$ or $0.4W_n$
4	$1.25D_n + 1.4W_n$	$0.5L_n$ or $0.5S_n$

The suggested load factors for buildings in the normal importance category was calibrated for a target reliability index of 3.0 for a design working life of 50 years (Bartlett et al. 2003a, b). The calibration was carried out using the probabilistic models summarized in Table 4.2, except for

the annual maximum wind speed and ground snow depth, which were based on those suggested in Chapters 2 and 3. Each of the random variables for evaluating the environmental loads will be discussed shortly. To facilitate the reader and for easy reference, the spatially-varying models of the extreme wind and snow hazard models suggested in Chapters 2 and 3 were summarized below.

Based on the observed meteorological data, wind hazard mapping was carried out in Chapter 2. The analysis treated the thunderstorm and synoptic winds separately. It was concluded that the Gumbel distribution could be adopted for the modelling of annual maximum wind speed, V_{AH}, if only a single probabilistic model is to be considered for all sites in Canada. This is justified since it is the preferred probability distribution for wind records from about 70% of the considered meteorological stations. The model is adequate for the synoptic winds as well as for the thunderstorm winds. It was argued that the results from hourly data from ECCC (i.e., HLY01 digital archive from ECCC) with the mapped mean and COV of V_{AH} shown in Figure 4.2 could be used as a proxy for the synoptic winds. The wind speed was given in terms of the hourly-mean wind speed throughout this chapter. The COV ranges approximately from 0.05 to 0.2 with a mean of 0.132. It was suggested that a typical value of 0.138 is to be adopted by considering previous studies on the Canadian wind hazard mapping. The statistics of V_{AH} for 14 major capital cities (for the provinces and the country) were presented in Table 4.3.

The analysis of thunderstorm winds was carried out using the daily data from ECCC DLY04 digital archive. The statistics of V_{AH} for the annual maximum thunderstorm winds (based on winds from the years with thunderstorm events) were presented in Figure 4.3; it was shown that V_{AH} could be assumed to be Gumbel distributed. Also shown in the figure was the probability of no (reported) thunderstorm occurrence per year, p_{NT}. The statistics of V_{AH} and p_{NT} for 14 major capital cities were included in Table 4.3 for comparison purposes. The COV of V_{AH} for regions with the average number of thunderstorm events per year greater than ten is less than 0.2. The wind hazard at a site within southern Ontario and the southern part of the Prairies could be dominated by the thunderstorm winds, especially as the return period increases.

Table 4.2. Statistics considered for the calibration (N, LN, G, and W denote the normal, lognormal, Gumbel, and Weibull distributions).

Parameter	Mean	COV	Dist. type	Note
Normalized resistance, X_R	1.17	0.108	LN	This is typical for structural steel.
Normalized dead load, X_D	1.05	0.1	N	
Transformation factor for wind load, Z_W	0.68	0.22	LN	
Annual maximum wind speed, V_{AH}		0.05 to 0.2	G	The statistics are spatially-varying with a typical COV of 0.138 for synoptic winds. The considered range is based on Hong et al. (2014) and Chapter 2.
"Point-in-time" wind speed (pulse of 3 hours)			W	The parameters of the distribution are to be calculated based on the annual maximum distribution (Jordaan 2005).
Transformation factor for live load, Z_L	1.0	0.206	N	
50-year extreme live load, X_L	0.9	0.170	G	
"Point-in-time" live load represented by the pulse of a duration of 6 month	0.273	0.674	W	
Transformation factor for snow load, Z_S	0.6	0.42	LN	
Annual maximum snow depth, X_S		0.2 to 0.8	G	It is considered that the bias (i.e., mean of 50 years to 50-yr return period) equals 1.1. This is aimed at considering the rain load S_r associated with snow load. Also, see Chapter 3.
"Point-in-time" snow load represented by the pulses of a duration of 14 days within 3 months (i.e., about 6 pulses).			W	The parameters of the distribution can be calculated based on the annual maximum distribution (Jordaan 2005).
Snowpack bulk density normalized with respect to its mean value	1.0	0.17	N	

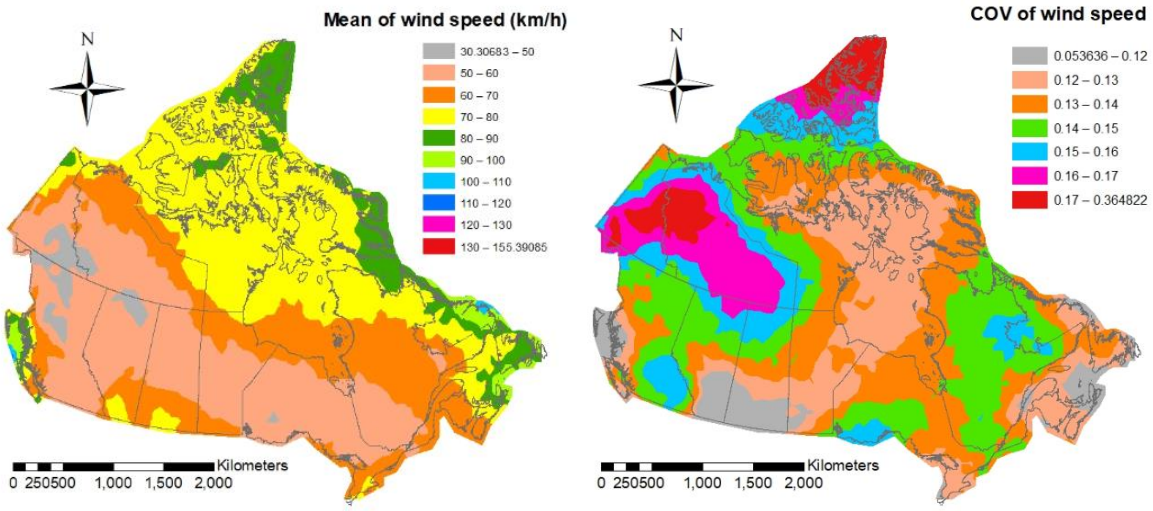

Figure 4.2. Spatial variation of the mean and coefficient of variation of V_{AH} considering the wind records from HLY01. Data from 439 stations, each with at least 20 years of useable data, were considered (from Chapter 2).

Table 4.3. Mean and COV of annual maximum wind (P_{NT} = probability of non-thunderstorm per year) (from Chapter 2).

	Annual maximum from HLY01 (treated as synoptic wind speed)		Annual maximum thunderstorm wind speed from DLY04		
City	Mean (km/hr)	COV	Mean (km/hr)	COV	P_{NT}
Victoria	61.4	0.126	34.5	0.257	0.280
Whitehorse	56.8	0.134	33.5	0.250	0.043
Yellowknife	51.7	0.119	32.7	0.166	0.044
Iqaluit	78.4	0.167			1.000
Edmonton	72.7	0.083	57.0	0.176	0.025
Regina	75.5	0.107	63.1	0.178	0.024
Winnipeg	67.7	0.114	61.6	0.167	0.000
Ottawa	66.7	0.114	55.4	0.150	0.000
Toronto	64.3	0.119	53.3	0.203	0.000
Quebec	69.3	0.113	53.7	0.165	0.051
Fredericton	60.0	0.115	54.0	0.231	0.021
Halifax	66.0	0.144	44.6	0.227	0.000
Charlottetowm	71.2	0.117	42.8	0.223	0.017
St.John's	91.9	0.122	52.1	0.306	0.017

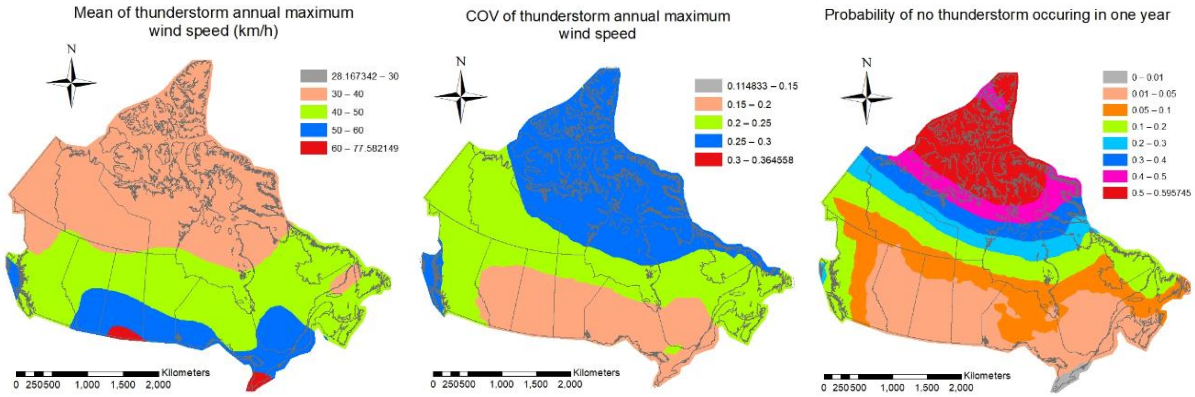

Figure 4.3. Spatial variation of the mean and COV of annual maximum thunderstorm wind speed and the probability of no thunderstorm occurrence per year based on DLY04 digital archive. Data from 195 stations, each with at least 10 years of useable data, were used. (from Chapter 2).

The above indicated that the reliability-based calibration needs to be carried out by considering the mixed wind climates, where the cumulative probability distribution of the annual maximum wind speed in the mixed wind climates, $F_{MC}(v_{AH})$, can be written as,

$$F_{MC}(v_{AH}) = P(\max(V_{TW}, V_{SW}) < v_{AH}) = P(V_{TW} < v_{AH})P(V_{SW} < v_{AH}), \tag{4.1}$$

where v_{AH} is the value of the annual maximum wind speed considering both the synoptic and thunderstorm winds, V_{TW} and V_{SW} denote the annual maximum wind speed for the thunderstorm winds and for the synoptic winds, respectively, and $P(\cdot)$ denotes the probability of its argument. Most importantly, if a long return period (e.g., 500 years) is used as the basis to recommend the tabulated wind velocity pressure in the design code, the T-year return period value of V_{AH} must be estimated based on Eq. (4.1). Since V_{SW} and V_{TW} (assuming the occurrence of the thunderstorm in a year) were assumed to be Gumbel distributed, Eq. (4.1) can be written as

$$F_{MC}(v_{AH}) = \left[p_{NT} + (1 - p_{NT}) \exp\left(-e^{-\alpha_{TW}(v_{AH} - u_{TW})}\right)\right] \exp\left(-e^{-\alpha_{SW}(v_{AH} - u_{SW})}\right), \tag{4.2}$$

where α_{TW} and u_{TW} are model parameters for V_{TW}, and α_{SW} and u_{SW} are model parameters for

V_{SW}. These parameters can be calculated using their mean and COV that were shown in Figures 4.2 and 4.3. By solving Eq. (4.2) with $F_{MC}(v_{AH}) = 1 - 1/T$, the obtained v_{AH} is the T-year return period value of V_{AH}, $v_{AH\text{-}T}$, for the mixed wind climates.

Based on the meteorological records in DLY04, the statistical analysis of the snow component and rain component of the roof snow load was carried out in Chapter 3. It was indicated that the Gumbel model could be adopted for the annual maximum ground snow depth, S_A. This was based on the distribution fitting results and, most importantly, the consideration that the Gumbel distribution was traditionally used to map S_A and to recommend the snow load in NBCC. The spatial trends of the mean and COV of S_A were illustrated in Figure 4.4. The COV of S_A ranges from 0.2 to 0.8, with a typical value of 0.5, which is almost identical to that used in Bartlett et al. (2003 a, b).

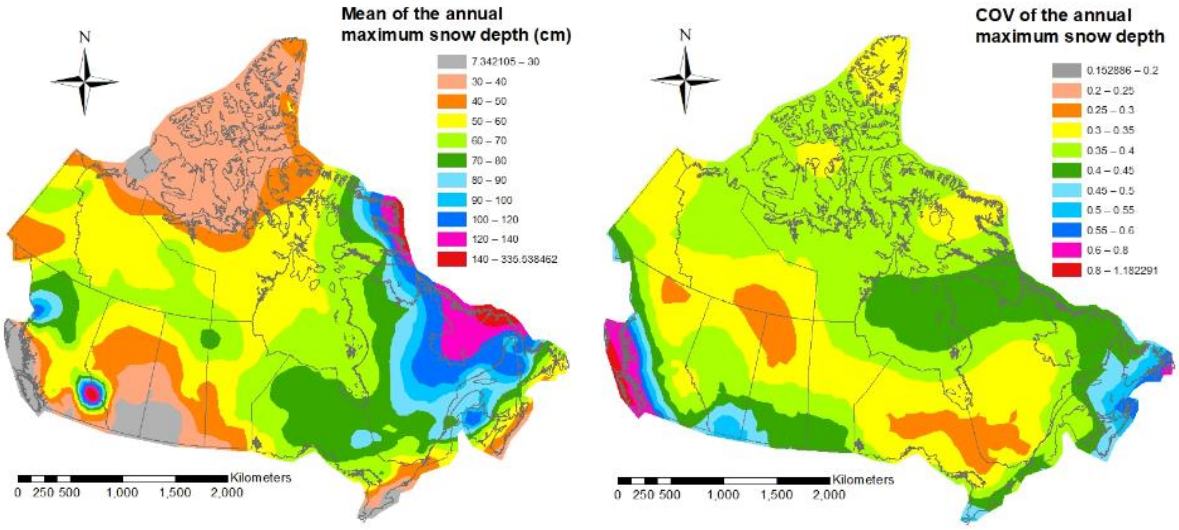

Figure 4.4. Contour maps of the mean and COV of S_A.

Note that for cases where zero value of S_A at a station with mild climates (e.g., coastal British Columbia) was observed, the probability of zero annual maximum S_A, p_0, for the station was calculated, and the cumulative probability distribution of the annual maximum ground snow depth, $F_{SA}(s_A)$, is given by,

$$F_{SA}(s_A) = p_0 + (1 - p_0) F_S(s_A), \tag{4.3}$$

where $F_S(s_A)$ is the distribution of S_A for the non-zero annual maximum ground snow depth. The T-year return period of S_A, $s_{A\text{-}T}$, is obtained by solving Eq. (4.3) for $F_{SA}(s_A) = 1 - 1/T$.

An attempt to update the snowpack bulk density was carried out using the Canadian Snow Data CD-ROM (MSC, 2000). Unfortunately, there were significant discrepancies between the obtained results and those reported by Newark et al. (1989). Since the details on the data quality control of the information reported in the Canadian Snow Data CD-ROM were unavailable to this project, the typical value used in Bartlett et al. (2003 a,b) (see Table 4.2) was to be used.

The rain component for a site represents the annual maximum 1-day "*winter*" rain load (or amount), S_R, which is defined as the observed rain amount in 1-day but limited to be less than the snowpack water equivalent amount (Newark et al. 1989). The analysis of S_R was presented in Chapter 3, indicating that S_R could be assumed to be independent of the annual maximum ground snow load. This implies that the use of the sum of the ground snow load and rain load to evaluate the roof snow load could be conservative. It was suggested that the sum could be replaced by the square-root-of-the-sum-of-squares (SRSS) rule. This will be elaborated further.

4.3. Wind load and calibration results

4.3.1. Wind load and limit state function

The wind velocity pressure, p, is used to evaluate the design wind pressure in NBCC according to,

$$p = qC_eC_gC_p \tag{4.4}$$

where q is the wind velocity pressure that equals $\rho_{air} V_{AH}^2 / 2$, in which ρ_{air} is the air density; C_e is the exposure factor; C_g is the gust effect factor, and C_p is the pressure coefficient averaged over the area of the surface considered. The topography factor, which was implemented in the newest NBCC (NRC 2015), is not considered in Eq. (4.4). By ignoring the uncertainty in the

air density, the *T*-year return period value of q, q_T, equals $\rho_{air} v_{AH-T}^2 / 2$.

Reliability-based structural design code calibration involves in selecting the target reliability index (as an objective) and calibrating the needed load and resistance factors for a set of assigned nominal design loads and resistances such that structures that satisfy,

$$\textit{Factored loads} \leq \textit{Factored Resistance} \tag{4.5}$$

will achieve, on average, the target reliability index with a relatively small scatter. If the design of a structural member involves only the resistance R, dead load D, and wind load W, the failure probability of structural member is the probability that the limit state function $g = R - D - W$ is less than or equal to zero. Consider that the ratio of R to its nominal value R_n denoted by X_R is a lognormally distributed random variable; that the ratio of D to its nominal dead load D_n, denoted by X_D, is a normally distributed random variable; and that the wind load effect, W, is represented by,

$$W = Z_W W_n \left(V_{AH} / v_{AH-T} \right)^2 \tag{4.6}$$

where Z_W is an uncertain transformation factor relating the (square of) wind speed to the wind load, Z_W is considered as a lognormally distributed, and W_n is the reference (or nominal) wind load effect calculated according to Canadian design code (for low buildings). The selected distribution models and the statistics of X_R, X_D, and Z_W were given in Table 4.2, which were consistent with those employed in Bartlett et al. (2013a, b) and Ellingwood et al. (1980).

By considering the above models, and the design requirement stated in Eq. (4.5) is just satisfied, the limit state function for designs governed by the dead load in combination with wind load, g, can be written as,

$$g = \frac{1}{\gamma_R} X_R - \frac{1}{1 + I_W R_{W/D}} \left(\frac{X_D}{\alpha_D} + R_{W/D} \frac{Z_W \left(V / v_{AH-T} \right)^2}{\alpha_W} \right) \tag{4.7}$$

where $\gamma_R = 0.9$ is the resistance factor (CAN/CSA S16 2014), $\alpha_D = 1.25$ is the dead load factor

(NRC 2015), $\alpha_W = 1.4$ is the wind load factor, and $R_{W/D}$ is the ratio of the factored design wind load effect to the factored design dead load effect. V in Eq. (4.7) represents the maximum wind speed for a design working life of 50 years; it is represented by a sequence of independent and identically distributed V_{AH}. The importance factor I_W for the wind load equals 1.0 for buildings in the normal importance category.

The most popular methods to evaluate the failure probability $P_f = P\left(g \le 0\right)$ are the first-order reliability method and simulation techniques (Madsen et al. 2006; Melchers and Beck 2018). The relation between the reliability index for a design working life of 50 years, β_{50}, equals $-\Phi^{-1}(P_f)$, where $\Phi^{-1}(g)$ is the inverse normal distribution function.

4.3.2. Calibration without considering the probabilistic model for mixed wind climates

For the moment, consider that V_{AH} could be modeled as a Gumbel distributed random variable (as opposed of using Eq. (4.1) or Eq. (4.2)), the estimated β_{50} by applying simulation technique was shown in Figure 4.5 for a range of γ values and several selected COV of V_{AH}. As expected, for the typical COV of 0.138, β_{50} is close to the target reliability index of 3.0. The figure showed that the difference between the failure probabilities is about one order of magnitude for the COV of V_{AH} varying from 0.1 to 0.2. The difference becomes about two orders of magnitude if V_{AH} varies from 0.05 to 0.3. This is partly due to that the wind load is proportional to the square of V_{AH}, resulting in that the COV of the wind load equals twice the COV of V_{AH} if all other variables involved in evaluating the wind force were treated deterministically.

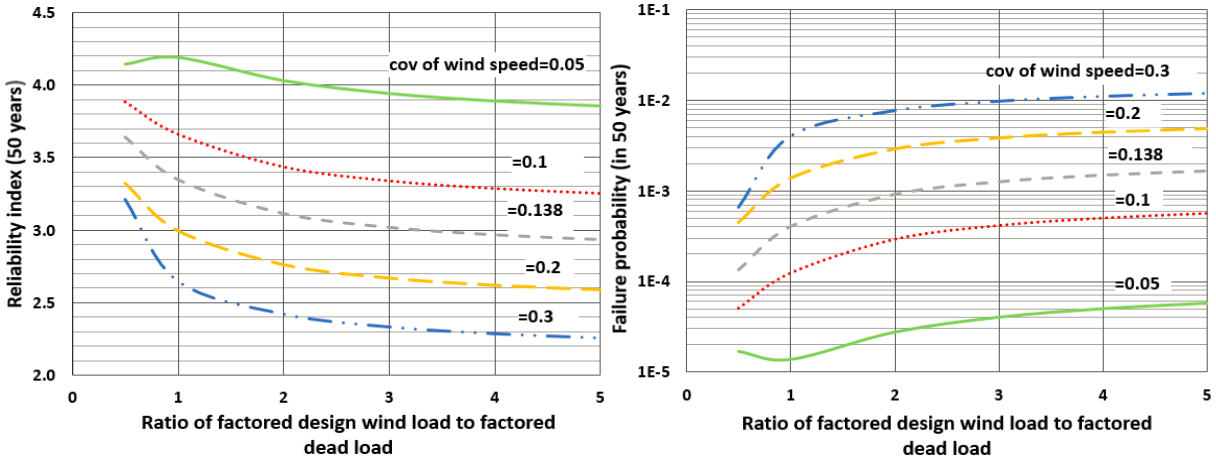

Figure 4.5. Estimated reliability index and corresponding failure probability for a design working life of 50 years by using the 50-year return period value and a wind load factor of 1.4.

Rather than using a wind load factor higher than one, it is noted that the ASCE-7-10 adopts a wind load factor of 1.0 with the design wind speed estimated using a return period, T, of 700 years for the strength design of Category II structures (Vickery et al. 2010; Cook et al. 2011). Also, Holmes et al. (2012) indicated that "Specification of high return period design wind speed (i.e., 1000 years) for ultimate limit state" was considered in AS 1170.2-1989. Different return period values are allowed in AS/NZS 1170.0 and 1170.2 (2002) for different regions (e.g., non-cyclonic and cyclonic regions).

Because the factored design wind load in the NBCC equals $1.4W_n$, where W_n denotes the nominal wind load and is directly proportional to $(v_{AH\text{-}50})^2$ (see Eq. (4.6)), the factored wind load is directly proportional to the square of wind speed $(1.4)^{1/2}\ v_{AH}\text{-}50$ if a wind load factor of 1.0 is employed. That is, one could assign a wind load factor of 1.0 and using the reference wind velocity pressure calculated for wind speed equal to $(1.4)^{1/2}\ v_{AH\text{-}50}$ to achieve the same design wind load. To see the required return period such that $v_{AH\text{-}T}$ equals $(1.4)^{1/2}v_{AH\text{-}50}$ for a range of values of COV of V_{AH}, a plot of the ratio of $v_{AH\text{-}T}$ to $v_{AH\text{-}50}$ versus T is presented in Figure 4.6 for a few values of the COV of V_{AH}. The figure showed that for the ratio of $v_{AH\text{-}T}$ to $v_{AH\text{-}50}$ to be equal to $(1.4)^{1/2}$, T is about 500 years if the value of the COV of V_{AH} equals 0.138. For the COV of V_{AH} varying from 0.2 to 0.1, the required T ranges from about 300 to 1000 years.

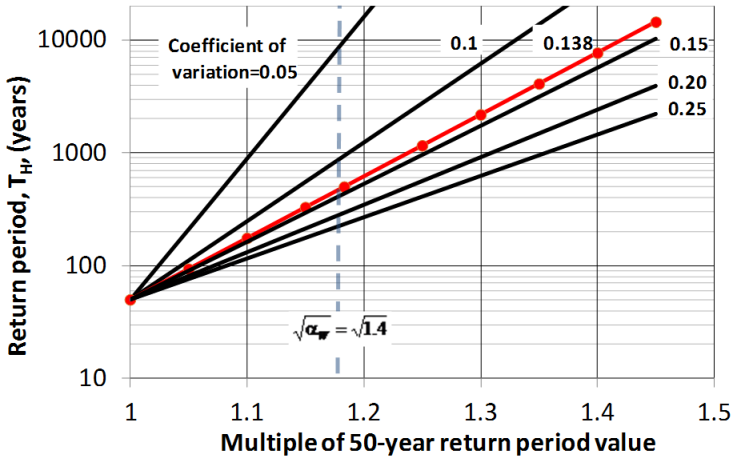

Figure 4.6. Ratio of $v_{AH\text{-}T}$ to $v_{AH\text{-}50}$ for T greater than 50 and a few COV values of V_{AH}.

By using the wind load factor of 1.0 and the reference wind velocity pressure corresponding to a return period of 500 years, and repeating the analysis carried out for the results shown in Figure 4.5, the obtained reliability index and the corresponding failure probability were shown in Figure 4.7. The results presented in the figure indicated that the difference between the failure probabilities is about one-half order of magnitude for the COV of V_{AH} varying from 0.1 to 0.2. The difference is less than one order of magnitude if V_{AH} varies from 0.05 to 0.3. This difference is much less than that shown in Figure 4.5.

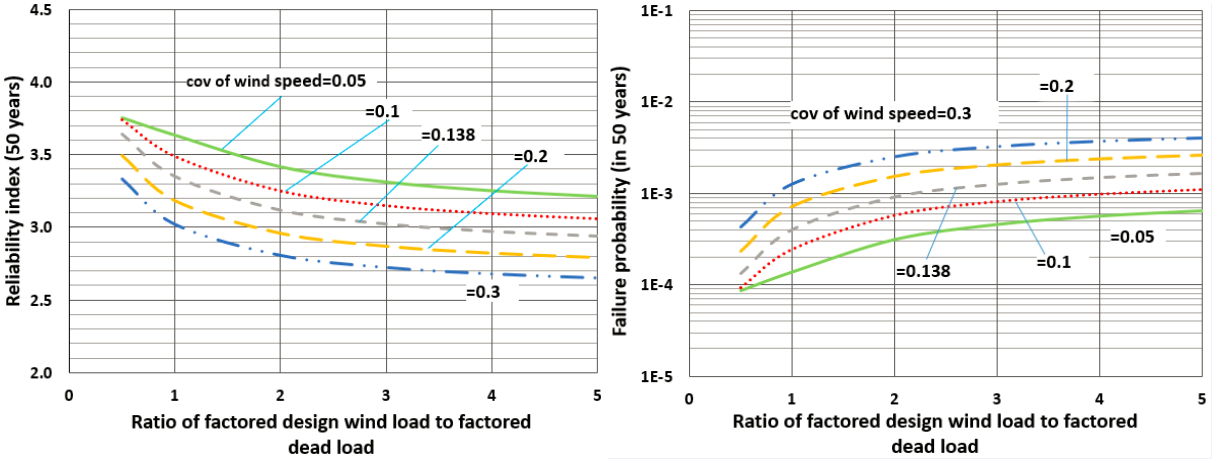

Figure 4.7. Estimated reliability index and corresponding failure probability for a design working life of 50 years by using the 500-year return period value and a wind load factor of 1.0.

This suggested that, from a reliability consistency point of view and considering the spatially-varying wind statistics, the use of a wind load factor of 1.0 and a reference wind velocity pressure calculated based on $v_{AH\text{-}500}$ is preferable to the use of a wind load factor of 1.4 and a reference wind velocity pressure based on $v_{AH\text{-}50}$. To better understand the impact of the return period on the estimated return period value of V_{AH}, the ratio $v_{AH\text{-}T}$ /$v_{AH\text{-}500}$ was calculated and presented in Table 4.4 for T near 500 years. The table showed that the ratio only deviates from 1.0 about less than 2% for T ranging from 400 to 600 (indicating a wind load difference up to about 4% as compared to that by using v_{AH}-500). If $v_{AH\text{-}700}$ was employed to specify the ultimate wind load for design, the design wind load is up to about 5% greater than that obtained by using $v_{AH\text{-}500}$ to specify the ultimate wind load.

In addition to the above, it must be noted that the calibrated wind load factor in Bartlett at al. (2003a, b) was 1.35, which is subsequently rounded to 1.4 and implemented in the NBCC. This rounding was a conservative measure. This conservatism was reflected in the calculated reliability index depicted in Figures 4.5 and 4.7, which is greater than 3.0 for COV of V_{AH} equal to 0.138 and $R_{W/D}$ less than about 3.0. For consistency, this slight conservatism was kept in the following.

Table 4.4. Ratio of $v_{AH\text{-}T}$ /$v_{AH\text{-}500}$, where V_{AH} is Gumbel distributed.

	T (years)				
COV	250	400	500	600	700
0.050	0.979	0.993	1	1.006	1.010
0.075	0.971	0.991	1	1.008	1.014
0.100	0.965	0.989	1	1.009	1.017
0.125	0.959	0.987	1	1.011	1.020
0.150	0.955	0.985	1	1.012	1.022
0.175	0.951	0.984	1	1.013	1.024
0.200	0.947	0.983	1	1.014	1.026

The impact by using the newly suggested design wind load as compared to the current implementation can be appreciated from Table 4.5, assuming that the same probabilistic model and method are employed to calculate the 50- and 500-year return period value of the annual maximum wind speed. As can be observed that the change of the factored design wind load depends on the COV of V_{AH}, the factored design wind load according to the new format was decreased for sites with a COV value less than 0.138 and was increased for sites with a COV value greater than 0.138.

Table 4.5. Comparison of the factored design wind load based on currently implemented format and suggested format.

COV of V_{AH}	Ratio of currently implemented factored design wind load to suggested factored design wind load
0.10	1.07
0.11	1.05
0.12	1.03
0.13	1.01
0.14	1.00
0.15	0.98
0.16	0.97
0.17	0.95
0.18	0.94
0.19	0.93
0.20	0.91

Based on a parametric investigation, it was suggested in Tang (2016) and Hong et al. (2017) that if a site-dependent (i.e., COV-value-dependent) return period value is used to specify wind load to improve reliability consistency, the following equation could be used,

$$T = 4300 \times \xi_V - 90, \text{ for } \xi_V \in [0.05, 0.30] \tag{4.8}$$

where ξ_V denotes the COV of V_{AH}. At least, this equation could be used as a guide in selecting a return period for different ξ_V.

The calibration results presented in the above were for the case where the design is governed by the wind load in combination with the dead load. The suggested new design wind load format should be verified by considering the wind load in combination with another time-varying load, such as the live load. The 2015 edition of the NBCC suggested that the design load for the wind load in combination with the dead and live loads can be calculated using ($1.25D_n + 1.5L_n + 0.4W_n$, $1.25D_n + 0.5L_n + 1.4W_n$), where L_n denotes the nominal live load (see Table 4.1).

In such a case, the limit state function can be written as,

$$g = \frac{1}{\gamma_R} X_R - \frac{1}{\max\left(1 + \alpha_{CL} R_{L/D} / \alpha_L + I_W R_{W/D}, 1 + R_{L/D} + I_W \alpha_{CW} R_{W/D} / \alpha_W\right)} \times \left(\frac{X_D}{\alpha_D} + \max \begin{bmatrix} R_{L/D} \dfrac{Z_L}{\alpha_L} \times \left(\text{EXT}(\text{Normalized Live load})\right) + R_{W/D} \dfrac{Z_W}{\alpha_W} \times \left(\text{PIT}\left((\text{Wind speed}) / v_{AH-T}\right)^2\right), \\ R_{L/D} \dfrac{Z_L}{\alpha_L} \times \left(\text{PIT}(\text{Normalized Live load})\right) + R_{W/D} \dfrac{Z_W}{\alpha_W} \times \left(\text{EXT}\left((\text{Wind speed}) / v_{AH-T}\right)^2\right) \end{bmatrix} \right) \tag{4.9}$$

where α with an additional subscript C represents the companion load factor, $R_{L/D}$ is the ratio of (factored) live load effect to (factored) dead load effect, Z_L is a transformation factor, and the normalized live load parameter is denoted by X_L with its characteristics given in Table 4.2, EXT( ) and PIT() denote the extreme and point-in-time variables of their corresponding arguments. Probabilistic models for Z_L and X_L were presented in Table 4.2. (Bartlett et al. 2003a,b). The reliability analysis for such a limit state function, which involves the consideration of pulses of extreme loads and pulses of point-in-time load effects, was discussed extensively in Wen

(1990). The pulses can be easily simulated based on the probabilistic models listed in Table 4.2 and used to evaluate P_f for the limit state function shown in Eq. (4.9).

By considering that α_L = 1.5, α_{CL} = 0.5, $v_{AH\text{-}T} = v_{AH\text{-}500}$, α_W = 1.0, α_{CW} = 0.3, reliability analysis was carried out using simulation technique for combinations of values of $R_{L/D}$ and $R_{W/D}$. The consideration of α_{CW} = 0.3 is justified since it is approximately equal to and greater than the ratio of the companion wind load factor to the wind load factor implemented in the current NBCC (i.e., 0.4/1.4 = 0.286). The obtained β_{50} were shown in Figure 4.8.

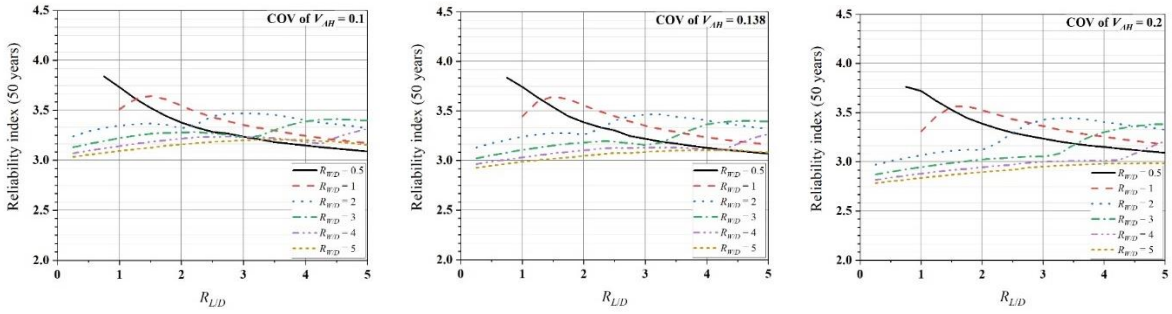

Figure 4.8. Estimated reliability index by considering dead, live and wind loads (α_L = 1.5, α_{CL} = 0.5, $V_{AH\text{-}T} = v_{AH\text{-}500}$, α_W = 1.0, α_{CW} = 0.3)

The results shown in the figure indicated that β_{50} ranges from about 2.8 to 3.7 if the COV value of V_{AH} ranges from 0.1 to 0.2. For a decreased and increased COV value of V_{AH}, the range of β_{50} values is shifted upwards and downwards, respectively. This shift is consistent with the trends shown in Figure 4.7 where only the dead load and wind load is considered. Most importantly, the results suggested that the use of α_{CW} = 0.3 is slightly conservative but adequate to achieve target reliability of 3.0.

Additional analyses were also carried out by varying α_{CW}. It is concluded that if a two decimal points factor α_{CW} would be accepted and implemented in the future edition of NBCC, α_{CW} = 0.28 could be adopted for economic efficiency.

4.3.3. Effect of mixed wind climates on the reliability

In this section, the reliability analysis was carried out by considering the mixed wind climates. For the analysis, statistics of the annual extreme wind speed for synoptic winds and for thunderstorm winds shown in Table 4.3 were considered. In this case, the cumulative probability distribution function was given in Eq. (4.2), and $v_{AH\text{-}T}$ can be obtained by solving Eq. (4.2) as explained earlier. Based on these considerations, by repeating the analysis that was carried out for Figures 4.7 and 4.8, the calculated β_{50} was shown in Figure 4.9. The results indicated that the estimated reliability index for the 14 considered sites with the consideration of the mixed wind climates, is near the target reliability index of 3.0, confirming the adequacy of the suggested new factored design wind load format (i.e., using a wind load factor of 1.0 with the reference wind velocity pressure specified based on $v_{AH\text{-}500}$).

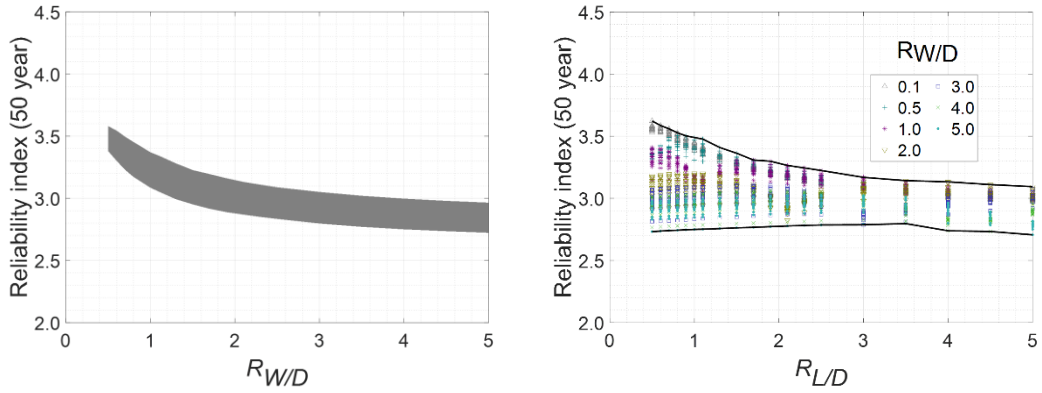

Figure 4.9. Estimated reliability index considering mixed wind climates for a design working life of 50 years by using $v_{AH\text{-}500}$ and a wind load factor of 1.0. The shaded area or the values within the band are for the 14 considered cities.

4.3.4. Implied reliability index by using the importance factor and consideration of serviceability

Since no detailed document on the rationale for the implemented values of the importance factor was available for wind load in NBCC, it was considered that such a factor is selected based on consensus at the time. In order to investigate the implication of using the importance factor suggested in NBCC on the reliability index, the analysis that was carried out for the results presented in Figures 4.5, 4.7 and 4.8 was repeated by considering the importance factor I_W equal

to 0.8, 1.15 and 1.25 for structures classified as buildings of low, high, and post-disaster importance categories. The obtained results were presented in Figures 4.10 and 4.11.

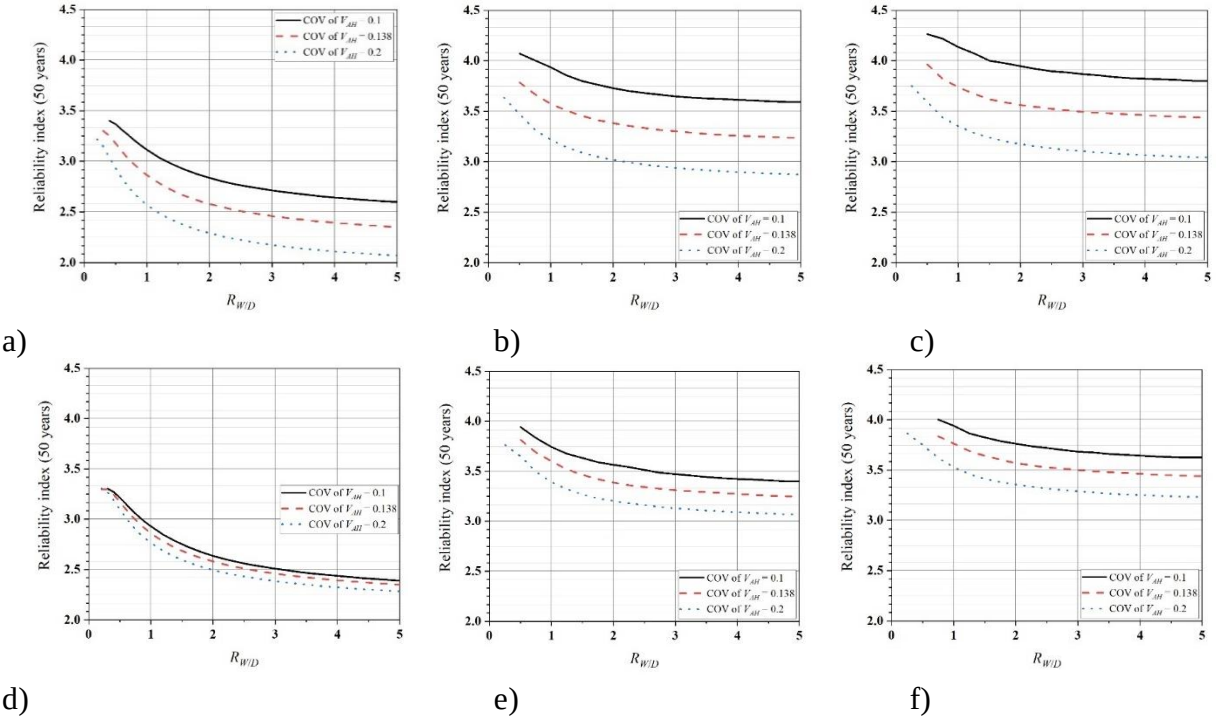

Figure 4.10. Estimated β_{50} considering the dead and wind loads and importance factor. $v_{AH\text{-}50}$ and α_W = 1.4 were used for a), b) and c); $v_{AH\text{-}500}$ and α_W = 1.0 were used for d), e) and f); I_W = 0.8 for a) and d); I_W = 1.15 for b) and e); and I_W = 1.25 for c) and f).

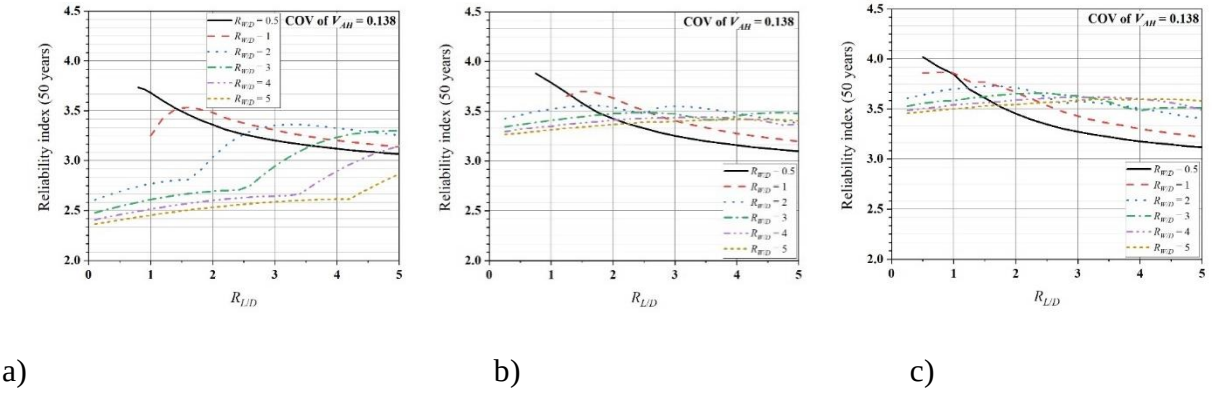

Figure 4.11. Estimated reliability index by considering dead, live and wind loads (α_L = 1.5, α_{CL} = 0.5, $v_{AH\text{-}500}$, α_W = 1.0, α_{CW} = 0.3). a) I_W = 0.8, b) I_W = 1.15, and c) I_W = 1.25. No reduction to live load is considered for consistency.

A comparison of the results shown in Figures 4.5, 4.7, and 4.10 indicated that by decreasing or increasing I_W, the reliability indices are consistently decreased and increased, respectively. In particular, for the COV of V_{AH} equal to 0.138, the increase in the failure probability is about five times by decreasing I_W from 1.0 to 0.8. The decrease in the failure probability is about four times by increasing I_W from 1.0 to 1.15 and about six times by increasing I_W from 1.0 to 1.25. The increase is comparable to the results obtained by using the current NBCC wind load and by using the newly suggested design wind load.

From the results presented in Figures 4.8 and 4.11, it can be observed that the decrease in failure probability is less pronounced if both the live and wind loads in combination are considered, especially if the live load is the dominant load (i.e., $R_{L/D}$ is large, and $R_{W/L}$ is small). This was expected since the importance factor only applies to the wind load component rather than the combined design live and wind loads.

The use of the importance factor of 0.8, 1.15, and 1.25 to calculate the factored design wind load defined based on $v_{AH\text{-}500}$ is equivalent to use the wind speed $\sqrt{0.8}v_{AH-500}$, $\sqrt{1.15}v_{AH-500}$, and $\sqrt{1.15}v_{AH-500}$ to calculate the factored design wind load with the importance factor of 1.0. These wind speeds $\sqrt{0.8}v_{AH-500}$, $\sqrt{1.15}v_{AH-500}$, and $\sqrt{1.15}v_{AH-500}$ correspond to $v_{AH\text{-}103}$, $v_{AH\text{-}1472}$, and $v_{AH\text{-}2910}$ if the COV of V_{AH} equal to the typical COV of 0.138 was considered. In other words, an alternative implementation of the importance factor is to use an importance factor of 1.0 but use the 100-year, 1500-year, and 3000-year return period values of annual maximum wind speed to evaluate the design wind loads for buildings of low, high, and post-disaster importance categories, respectively. The reliability analysis was carried out by using the return periods as well. As the obtained results are very similar to those shown in Figures 4.10 and 4.11, they were not plotted. However, because of potential statistical uncertainty caused by a small sample size in estimating $v_{AH\text{-}T}$ for very high return periods, it was suggested that the use of I_W = 0.8, 1.15, and 1.25 could be preferred considering their simplicity and familiarity to the designers.

Based on the findings in the previous sections and this section, the recommended design wind load was summarized in Table 4.6. In all cases, the same load combination factor α_{CW} of 0.3 is to be used when the dead, live, and wind load acting in combination was considered.

Table 4.6. Suggested factors and $v_{AH\text{-}T}$ for evaluating the wind velocity pressure.

	Low importance category	Normal importance category	High importance category	Post-disaster importance category
Ultimate	($v_{AH\text{-}500}$ and $I_W = 0.8$) or ($v_{AH\text{-}100}$ and $I_W = 1.0$)	($v_{AH\text{-}500}$ and $I_W = 1.0$)	($v_{AH\text{-}500}$ and $I_W = 1.15$) or ($v_{AH\text{-}1500}$ and $I_W = 1.0$)	($v_{AH\text{-}500}$ and $I_W = 1.25$) or ($v_{AH\text{-}3000}$ and $I_W = 1.0$)
Serviceability	$v_{AH\text{-}10}$	$v_{AH\text{-}10}$	$v_{AH\text{-}10}$	$v_{AH\text{-}10}$
Load combination with dead, live and wind loads	For principal load: Design wind load = I_W×Specified wind load; For wind acted as companion load: $\alpha_{CW} \times I_W \times$ Specified wind load, where $\alpha_{CW} = 0.3$			

It should be noted that I_W for serviceability requirements in the current NBCC is set equal to 0.75 for all structure categories. According to the commentary to the code, such a value is set less than 1.0 "because of less serious consequences of failure and because design criteria for serviceability are more subjective than for strength and stability." Therefore, the same $I_W = 0.75$ is considered to be applied according to the newly suggested format. Since for serviceability limit state, according to the current NBCC, the load factor of 1.4 should not be applied to the wind load defined based on $v_{AH\text{-}50}$, it can be shown that the use of $I_W = 0.75$ with the wind load specified based on $v_{AH\text{-}50}$ implies the use of a wind load based on $v_{AH\text{-}T}$ with T equal to 6.2, 9.6, and 13.9 years for the COV of V_{AH} equal to 0.1, 0.138 and 0.2, respectively. Therefore, it was suggested that I_W equals 1.0 and the wind load (i.e., wind velocity pressure) to be specified directly based on $v_{AH\text{-}10}$ for the serviceability.

4.4. Climate change effects on structural reliability focused on wind load

4.4.1. Impact on extreme wind speed

A very extensive study on climate change was presented by Cannon et al. (2019). Their study indicated that the time required to reach a specified temperature increase depends on the considered RCPs, as shown in Table 4.7. By plotting the results for RCP8.5 shown in the table in Figure 4.12, a nonlinear trend can be observed.

Table 4.7. Year at which the indicated global mean temperature increase (ΔT) relative to 1986-2016 reference period by the specified multi-model statistics. Ensemble mean ΔT, smoothed using a 31-year moving window (Cannon et al. (2019)).

Year of exceedance: Multi-model mean (upper, CMIP5one; lower, CMIP5all)									
Scenario	N_{runs}	ΔT=0.5°C	1	1.5	2	2.5	3	3.5	4
RCP 2.6	32	2023							
	65	2023							
RCP 4.5	42	2022	2043	2071					
	108	2022	2043	2071					
RCP 6.0	25	2025	2049	2069	2087				
	47	2025	2049	2069	2088				
RCP 8.5	39	2020	2035	2047	2059	2069	2080	2090	2100
	81	2020	2035	2048	2059	2069	2080	2091	2100
CanESM20LE	50	2012	2025	2036	2047	2057	2066	2076	2084

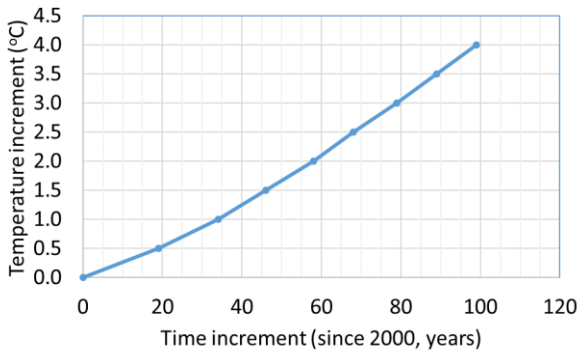

Figure 4.12. Relation between the (mean) temperature increment versus time increment for RCP8.5.

A simple regression analysis showed that the curve could be approximated well by

$$\Delta T = 1.5\times10^{-4}\times Y^2 + 2.546\times10^{-2}\times Y - 0.0253 \qquad (4.10)$$

where ΔT (°C) denotes the global warming level, and Y (year) denotes the time increment since 2000. For specified temperature increments, Cannon et al. (2019) also reported the percentage change in the mean and COV values of the annual maximum (hourly-mean) wind speed, snow load, and rain load. The percentage change for the annual maximum wind speed was shown in Table 4.8 with the definition of the regions, as shown in Figure 4.13.

Table 4.8. Percentage change in the mean and COV of the annual maximum hourly mean wind speed for specified temperature increments (From Cannon et al. (2019)).

	Global warming level ΔT (°C)							Global warming level ΔT (°C)						
	0.5	1	1.5	2	2.5	3	3.5	0.5	1	1.5	2	2.5	3	3.5
	Change in the mean of annual max. wind speed (%)							Change in COV annual max. wind speed (%)						
British Columbia	0.1	0.2	0.9	1.8	2.1	2.3	2.1	0.2	0.6	1.6	2.3	5.5	6.5	7.9
Prairies	-0.3	-0.6	-0.8	-1.1	-1.2	-1.6	-1.9	1.8	1.4	2.7	4.2	7	7.6	9.9
Ontario	0.4	0.6	0.8	1.1	1.6	1.9	2.1	0.9	2.3	3.5	5.3	8.4	10.2	13.2
Quebec	0.5	0.7	0.9	1.3	1.4	1.4	1.4	-1.5	0	0.7	0.7	0.2	1.5	1.1
Atlantic	0.7	1.1	1.6	2	2.4	2.4	2.8	0.2	1.6	2.5	3	2.9	3.1	4.7
North	0	0	0.1	0.5	0.9	1	1.2	-0.2	-1.6	-1.2	0.3	0.6	1.4	1.6
Canada	0.4	0.5	0.8	1	1.4	1.5	1.6	0.3	1.3	1.8	3	4.1	5.1	6.2

Figure 4.13. Definition of the regions used in Table 4.8 (after Cannon et al. (2019)).

To better visualize the temporal trends of the changes in V_{AH} due to climate change, the results presented in Table 4.8 were plotted in Figure 4.14. The mean of V_{AH} increases for all considered regions except for the Prairies. Moreover, the COV of V_{AH} increases as the global warming level increases for most regions. The increase in the mean and COV can lead to the increased quantile of V_{AH} in the upper tail region of the distribution. Such an increase may result in an increased failure probability.

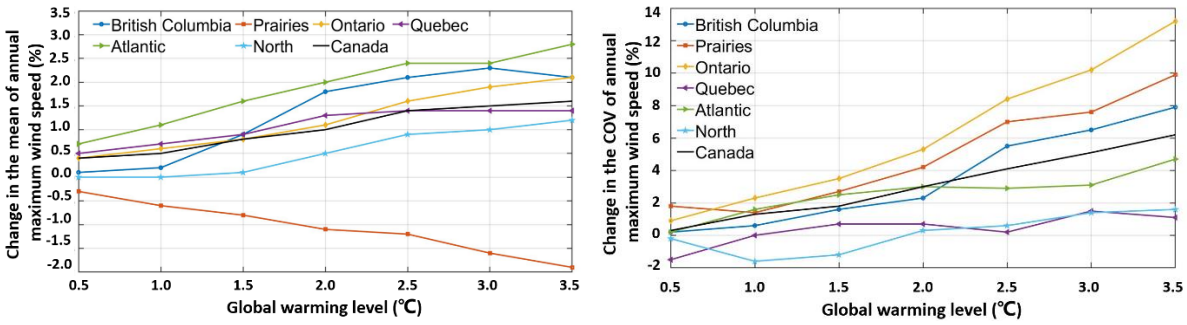

Figure 4.14. Variation of the changes in the mean and COV of the annual maximum hourly-mean wind speed as functions of the global warming level.

4.4.2. Effect on the structural reliability and calibrating the scaling factor for wind load due to the impact of climate change

To assess the potential increase in the failure probability, let $h_m(\Delta T)$ and $h_{COV}(\Delta T)$ denote the change in the mean and COV of V_{AH}, as shown in Figure 4.14. Therefore, by adopting the RCP8.5, for a given year Y (since 2000), the global warming level ΔT can be evaluated using Eq. (4.10). By using the calculated ΔT, the mean and COV of V_A, at Y year, can be calculated using,

$$(\text{Mean, COV})_{\text{At } Y \text{ year}} = \left(m_{VAH} + h_m(\Delta T), v_{VAH} + h_{COV}(\Delta T)\right) \tag{4.11}$$

where m_{VAH} and v_{VAH} represent the mean and COV of V_{AH} estimated based on historical wind records that can be considered to be representative of the year 2000. By using the calculated $(\text{Mean, COV})_{\text{At } Y \text{ year}}$ from 2025 to 2074, and considering that V_{AH} is Gumbel distributed, the reliability indices can be calculated for each year and for a design working life of 50 years by applying simulation technique.

Let the reliability index shown in Figure 4.7 for the COV of V_{AH} equal to 0.138 be the target reliability index β_{T50}. By considering v_{VAH} = 0.138 and a wind load scaling factor accounting for climate change, η_{CW}, (applied to the design wind load defined based on $v_{\text{AH-500}}$), one could iteratively adjust the value of η_{CW} such that the calculated β_{50} from 2025 to 2074 is approximately equal to β_{T50}. The obtained η_{CW} for each of the regions listed in Table 4.8 was shown in Figure 4.15. This calculation was repeated, but considering the initial year for the design working life period was shifted upwards by one year (i.e., 2027, 2028, 2029 and 2030). The obtained results were also included in Figure 4.15 as well. The figure indicated that sets of scaling factors to the wind load due to the consideration of climate change could be suggested for the development of the 2025 edition of NBCC.

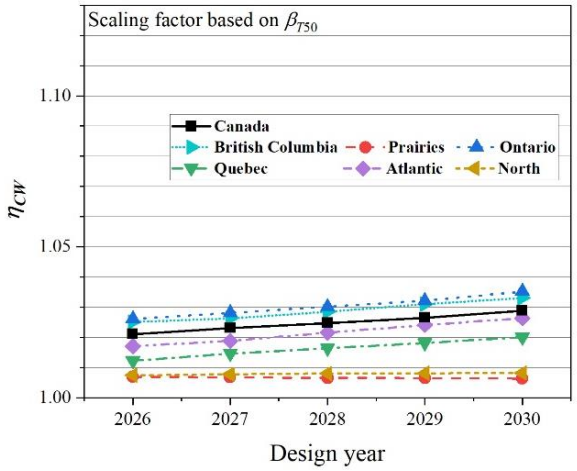

Figure 4.15. Calibrated scaling factor for the design wind load by considering the impact of climate change and using β_{T50} as the target.

Rather than calibrating η_{CW} for the calculated β_{50} to meet β_{T50} as was done for the results presented in Figure 4.15, one could calibrate η_{CW} such that the minimum annual reliability index β_{minA} within a specified design working life equal to a target β_{TminA}. For example, consider that the β_{TminA}, $\beta_{TminA} = -\Phi^{-1}\left(1-\left(1-\Phi(-\beta_{T50})\right)^{1/50}\right)$. By carrying out the reliability-based calibration that was carried out for all the considered cases shown in 4.15, the obtained η_{CW} values, in this case, were presented in Figure 4.16. A comparison of the results presented in Figures 4.15 and 4.16 indicated that the calibrated η_{CW} based on β_{TminA} is greater than that based on β_{T50}. This can be explained since the wind hazard and risk due to climate change effect in an individual year is captured by calculating the annual probability of failure while such an effect is smeared by evaluating β_{50}. In all cases, the increase in the design wind load was very modest.

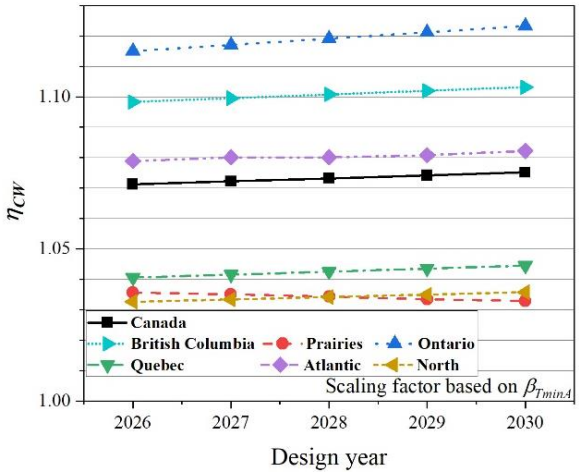

Figure 4.16. Calibrated scaling factor for the design wind load by considering the impact of climate change and β_{TminA}.

For those η_{CW} values calculated based on β_{T50}, the maximum increase was about 3%, which is for sites in Ontario, and the minimum increase was about 1%, which is for sites in North or in Prairies. The increase ranges from about 2% to 3% if the statistics for Canada shown in Figure 4.15 were used. By considering the range of changes obtained by adopting β_{T50} as the target, it was suggested that a constant increase of 2% to the calibrated design wind load obtained without considering climate change could be considered in the future edition of NBCC (i.e., the 2025 edition of NBCC). However, by considering β_{TminA} as the target, Figure 4.16 showed that η_{CW} ranges from 1.03 to 1.13, which is much wider than the range shown in Figure 4.15. If a single value of η_{CW} is to be applied to the country, a value of 1.07 could be adopted, otherwise different values need to be considered for different regions. The use of η_{CW} = 1.07 is conservative as compared to the required increase in design wind load calculated based on β_{T50}. An illustration of using η_{CW} =1.02 and 1.07 in the structural reliability by considering the impact of climate change was illustrated in Figure 4.17.

Note that no increase of the design wind load within a code cycle (i.e., from 2025 to 2030) is suggested since the results indicate that the increase within a code cycle is very small, and such an implementation is likely to cause unnecessary burden to designers.

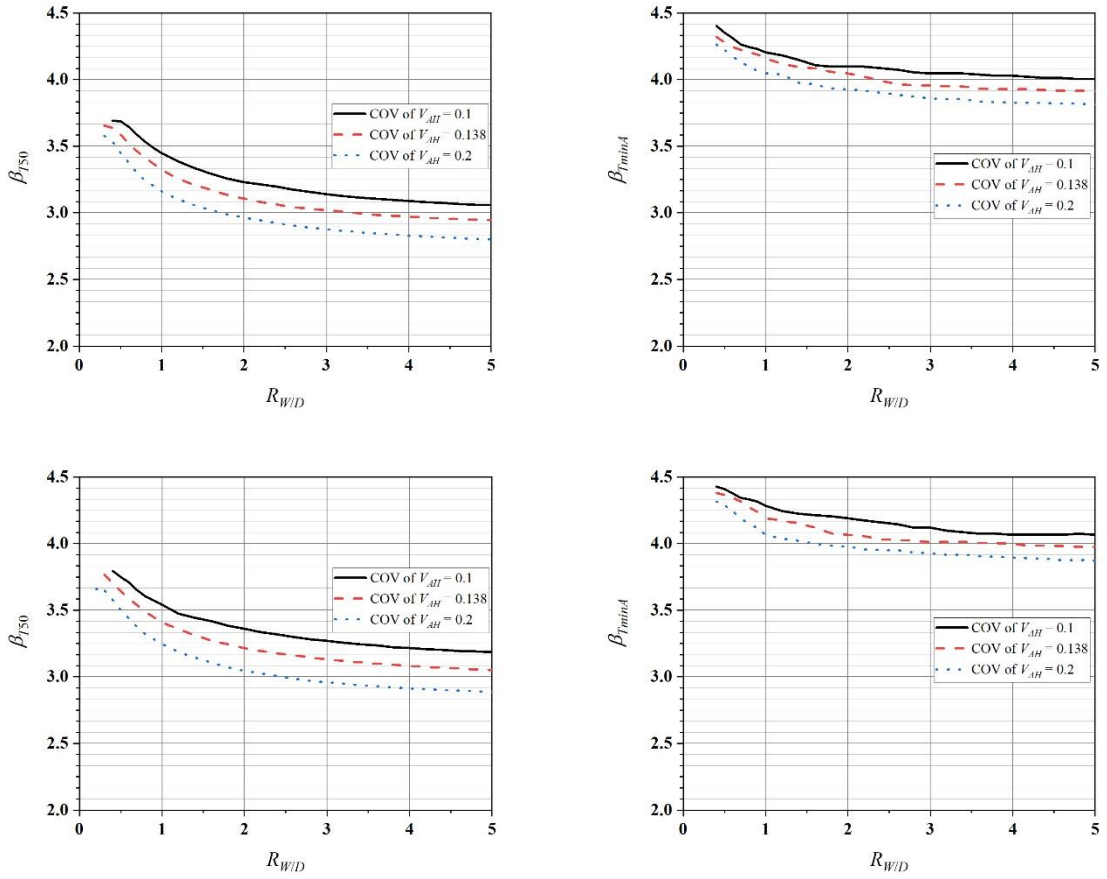

Figure 4.17 Calculated reliability index for a structure with a design working life of 50 years starting from 2028. The first row is calculated by considering η_{CW} = 1.02. The second row is calculated by considering η_{CW} = 1.07. It is considered the design working life is from 2028 to 2077.

4.5. Snow load and calibration results

4.5.1. Snow load and limit state function

According to the NBCC, the roof snow load, *S* can be expressed as,

$$S = (C_b C_w C_s C_a) S_S + S_R \tag{4.12}$$

where S_S is the ground snow load, S_R is the associated rain load, C_b is the basic roof snow load

factor and equals 0.8, C_w is the wind exposure factor; C_s is the slope factor, and C_a is the accumulation factor. The ground snow load equals $0.01\rho_b g S_A$, where g = 9.81 (m/s^2) is gravitational acceleration, ρ_b (kg/m^3) is the snowpack bulk density, and S_A (cm) is the ground snow depth. The transformation factor, C_{gr}, that converts the ground snow load at a given site to an appropriate roof snow load is,

$$C_{gr} = C_b C_w C_s C_a \tag{4.13}$$

The mean to the nominal value of this transformation factor denoted as Z_S can be considered to be a lognormal random variable with the statistics listed in Table 4.2. According to NBCC, S_R need not be taken greater than $C_{gr} S_S$. Arguments were made in Bartlett et al. (2003a,b) to carry out reliability-based design code calibration by considering $C_{gr} S_S$ only when the snow load is involved. This assumption was adopted below. A discussion of including S_R will be given after the presentation of the calibration results.

Similar to the case of dead and wind load considered earlier, the limit state function by considering the dead and snow loads, g, can be written as,

$$g = \frac{1}{\gamma_R} X_R - \frac{1}{1 + I_S R_{S/D}} \left(\frac{X_D}{\alpha_D} + R_{S/D} \frac{Z_S Z_\rho X_S}{\alpha_S} \right) \tag{4.14}$$

where α_S = 1.5 is the snow load factor, and $R_{S/D}$ is the ratio of the factored design snow load effect to the factored design dead load effect, Z_S is the normalized transformation factor, Z_ρ is the normalized snowpack bulk density, X_S represents the extreme snow depth S_A normalized with $s_{A\text{-}T}$, and I_S represents the importance factor for the snow load, which equals 1.0 for buildings in the normal importance category. The probabilistic models for X_D, Z_S, Z_ρ and S_A were already discussed previously (see Table 4.2). Note that for the current NBCC implementation, the nominal snow load was defined based on the mean of snowpack bulk density and $s_{A\text{-}T}$ with T = 50 years.

The implication of using α_S = 1.5 in terms of multiple of the 50-year return period value of S_A, $s_{A\text{-}50}$, is illustrated in Figure 4.18. From this figure, it can be observed that the use of α_S = 1.5 with $s_{A\text{-}50}$ implies an equivalent factored design snow load with α_S = 1.0 and $s_{A\text{-}T}$ for T = 6443, 1297, 941, 760 and 582 years for COV of S_A equal to 0.2, 0.4, 0.5, 0.6 and 0.8, respectively. It is instructive to note that the calibration results presented in Bartlett et al. (2003a,b) indicate that a snow load factor of 1.7 was needed to achieve a target reliability index of 3.0 for a design working life of 50 years for the ratio of the snow to dead load equal to about 1.0. The implemented snow load factor of 1.5 was based on the mentioned study and the consensus of the code committee. The use of a snow load factor of 1.7 with $s_{A\text{-}50}$ implies an equivalent factored design snow load with α_S = 1.0 and $s_{A\text{-}T}$ for T = 45170, 4787, 3056, 2266 and 1559 years for COV of S_A equal to 0.2, 0.4, 0.5, 0.6 and 0.8, respectively.

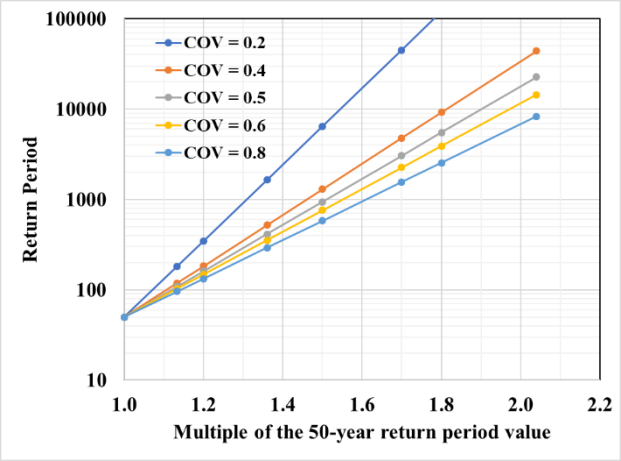

Figure 4.18. Relation of multiple of 50-year return period value versus return period (the COV in the figure represents the COV of annual maximum ground snow depth).

Based on the above, for the typical COV of S_A equal to 0.5, one could suggest the use of α_S = 1.0 and $s_{A\text{-}T}$ for T = 1225 years (i.e., 4% in 50 years), resulting in the factored snow load that is consistent with the current NBCC. The suggested return period is slightly greater than 941 years shown in Figure 4.18 for COV of S_A equal to 0.5. The adequacy of this suggested factored design snow load was assessed below.

In order to investigate the implication of using the currently implemented factored design snow

load format (i.e., α_S = 1.5 and $s_{A\text{-}50}$) and the newly suggested format (i.e., α_S = 1.0 and $s_{A\text{-}1225}$), reliability analysis was carried out by considering the limit state function presented in Eq. (4.14), and the probabilistic models summarized in Table 4.2. The obtained β_{50} was shown in Figure 4.19 for (α_S = 1.5 and $s_{A\text{-}50}$) and Figure 4.20 for (α_S = 1.0 and $s_{A\text{-}1225}$). A comparison of the results presented in these figures indicated that the use of the newly suggested format leads to a slightly enhanced reliability-consistent design for a range of COV values of S_A that are applicable for different sites in Canada. Moreover, this newly suggested snow load format lead to β_{50} near 3.0 for $R_{S/D}$ around 1.0, which is consistent with that obtained by considering the currently implemented factored design snow load. The consideration of the value of β_{50} for $R_{S/D}$ around 1.0 rather than for greater $R_{S/D}$ values was justified since, in most realistic design scenarios, $R_{S/D}$ is not much greater than the dead load. Therefore, from a reliability consistency point of view and considering the spatially-varying snow statistics, the use of (α_S = 1.0 and $s_{A\text{-}1225}$) is preferable to the use of (α_S = 1.5 and $s_{A\text{-}50}$).

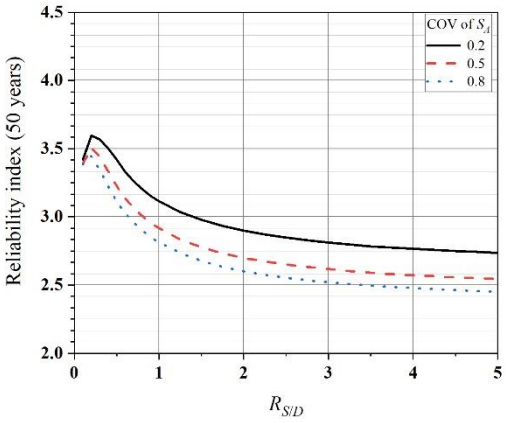

Figure 4.19. Estimated reliability index for a design working life of 50 years by using the 50-year return period value and a snow load factor of 1.5.

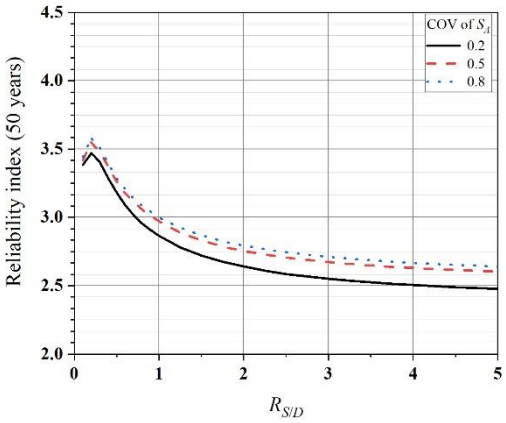

Figure 4.20. Estimated reliability index and corresponding failure probability for a design working life of 50 years by using the 1225-year return period value and snow load factor of 1.0.

One additional observation is that the reliability-consistency achieved by using the newly suggested format is not as significant as that for the wind load. This can be explained by noting that the uncertainty in the ground to roof transformation is very large (see Table 4.2). An alternative implementation would be to increase the nominal value of C_{gr} and lower the return period T to evaluate the ground snow load. Also, an improvement in the codified design with improved reliability-consistency could be achieved by collecting additional full-scale information on the ground snow load and roof snow load so to develop better relations between them. These were beyond the scope of this study.

Note the reversal of the trend in β_{50} for different COV values depicted in Figure 4.19 as compared to that in Figure 4.18. This was attributed to the combined effect of a large COV value of Z_S and the use of high return period value. The high COV value of Z_S also explains the reason why the range of β_{50} values for a range of $R_{S/D}$ was not as narrow as that observed for a range of $R_{W/D}$.

The impact of using the newly suggested design snow load as compared to the current implementation can be appreciated from Table 4.9, assuming that the same probabilistic model

and method were employed to calculate the 50- and 1225-year return period values of the annual maximum ground snow depth. It can be observed that the change depends on the COV of the annual maximum ground snow depth. The factored design snow load, according to the new format, will be decreased for sites with a COV value less than about 0.45 and will be increased for sites with a COV value greater than 0.45. The decrease in the factored design snow load by using the newly suggested format was not very important for regions with COV of S_A less than 0.3 since the number of sites with COV of S_A less than 0.25 is almost negligible and the regions with COV of S_A within 0.25 to 0.3 are associated with much less populated area (see Figure 4.4). As most populated areas are associated with COV of S_A within 0.35 to 0.6, the decrease and increase in the factored design snow load by using the new format as compared to that implemented in the current NBCC are about 3% and 6%, respectively.

Table 4.9. Comparison of the factored deisgn snow load based on currently implemented format and newly suggested format.

COV of annual maximum ground snow depth	Ratio of currently implemented factored design snow load to suggested factored design snow load
0.20	1.13
0.25	1.09
0.30	1.05
0.35	1.03
0.40	1.01
0.45	0.99
0.50	0.97
0.55	0.96
0.60	0.94
0.65	0.93
0.70	0.92
0.75	0.92
0.80	0.91

4.5.2. Companion load factors for snow load

The reliability analysis and calibrated snow load in the previous section were for the case where the design was governed by the snow load in combination with the dead load. The companion load factor must be developed by considering the snow load in combination with another time-varying load, such as the live load. The 2010 edition of NBCC suggested that the design load

for the snow load in combination with the dead and live loads can be calculated using ($1.25D_n + 1.5L_n + 0.5S_n$, $1.25D_n + 0.5L_n + 1.5S_n$). The 2015 edition of the NBCC suggests a different set of load combination factors ($1.25D_n + 1.5L_n + 1.0S_n$, $1.25D_n + 1.0L_n + 1.5S_n$). In both cases, the limit state function can be written as,

$$g(v_T) = \frac{1}{\gamma_R} X_R - \frac{1}{\max\left(1+\alpha_{CL} R_{L/D}/\alpha_L + I_S R_{S/D}, 1+R_{L/D} + I_S \alpha_{CS} R_{S/D}/\alpha_S\right)} \times \left(\frac{X_D}{\alpha_D} + \max \left[\begin{array}{l} R_{L/D} \dfrac{Z_L}{\alpha_L} \times \mathrm{EXT}\left(\text{Normalized Live load}\right) + R_{S/D} \dfrac{Z_S Z_\rho}{\alpha_S} \times \mathrm{PIT}\left(\text{Normalized snow load}\right), \\ R_{L/D} \dfrac{Z_L}{\alpha_L} \times \mathrm{PIT}(\text{Normalized Live load}) + R_{S/D} \dfrac{Z_S Z_\rho}{\alpha_S} \times EXT\left(\text{Normalized snow load}\right) \end{array} \right] \right) \tag{4.15}$$

where α_{CS} represents the companion load factor if the snow load act as companion load. The normalized snow load represents the ground snow load normalized with respect to the nominal ground nominal snow load. Other variables were already defined previously (see Table 4.2).

For comparison purposes, reliability analysis was carried out by considering α_{CS} implemented in the 2010 edition and the 2015 edition of NBCC, the obtained reliability indices for the typical value of COV of S_A equal to 0.5 were shown in Figure 4.21. As expected, the use of α_{CS} = 1.0 results in a significant increase in the reliability index.

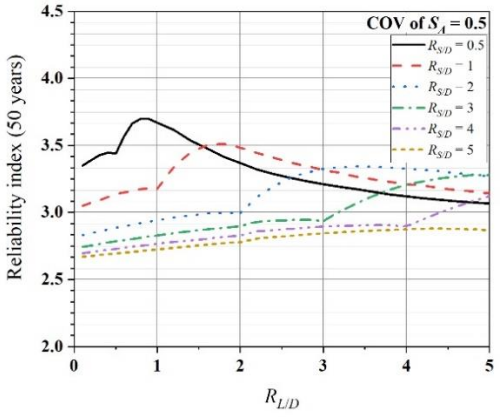

(2010-edition of NBCC, α_{CS} = 0.5)

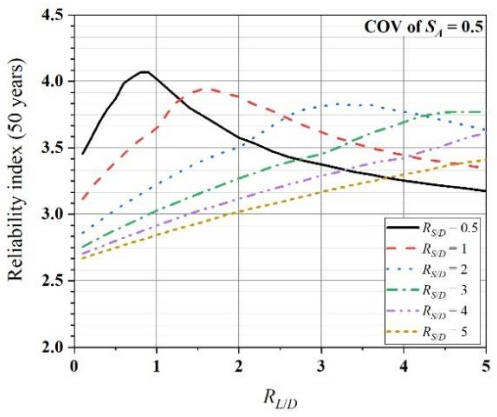

(2015-edition of NBCC, α_{CS} = 1.0)

Figure 4.21. Estimated reliability index by considering dead, live, and snow loads (for $s_{A\text{-}T} = s_{A\text{-}50}$).

Now consider the case where α_L = 1.5, α_{CL} = 0.5, $s_{A\text{-}T} = s_{A\text{-}1225}$, α_S = 1.0, and α_{CS} = 0.3. The consideration of 0.3 was based on the ratio of the snow load factors implemented in the 2010 edition of NBCC (0.5/1.5 = 0.33). Its use also resulted in the companion load factors for both snow and wind loads to be consistent. For this considered case, the reliability analysis was carried out for combinations of values of $R_{L/D}$ and $R_{S/D}$. The obtained results were shown in Figure 4.22 for COV of S_A equal to 0.2 0.5 and 0.8. A comparison of the results shown in Figures 4.21 and 4.22 for the COV of S_A equal to 0.5 indicated that the adoption of the newly suggested design snow load and α_{CS} = 0.3 leads to consistent β_{50}. In other words, for this particular case, the use of the suggested design snow loads (i.e., $s_{A\text{-}1225}$, α_S = 1.0, and α_{CS} = 0.3) maintained the same reliability consistency as that can be obtained based on the 2010 edition of NBCC. Also, the use of the suggested design snow loads resulted in a narrow range of reliability indices for COV of S_A varying from 0.2 to 0.8, as shown in Figure 4.22.

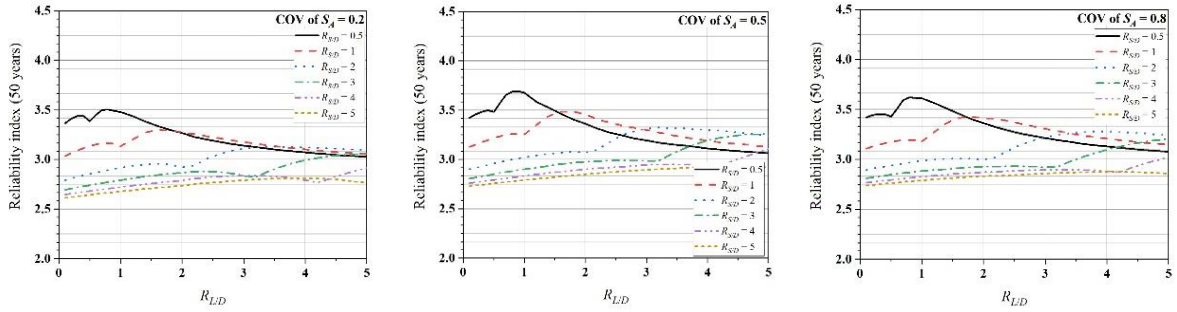

Figure 4.22. Estimated reliability index by considering dead, live and snow loads (for α_L = 1.5, α_{CL} = 0.5, $s_{A\text{-}T} = s_{A\text{-}1225}$, α_S = 1.0, α_{CS} = 0.3).

As the companion snow load factor in the 2015 edition of the NBCC differs from that in the 2010-edition of the NBCC, the analysis that was carried out for the results presented in Figure 4.22 was repeated but replacing α_{CL} = 0.5 and α_{CS} = 0.3 with α_{CL} = 0.7 and α_{CS} = 0.7 (i.e., 1/1.5). The consideration of 0.7 is based on the load combination ($1.25D_n + 1.5L_n + 1.0S_n$, $1.25D_n + 1.0L_n + 1.5S_n$) suggested in the 2015 edition of the NBCC. In this case, the obtained results were presented in Figure 4.23. As expected, the results presented in this figure for the

COV of S_A equal to 0.5 agreed well with those shown in the right plot in Figure 4.21; they are much too conservative as compared to those shown in Figure 4.22.

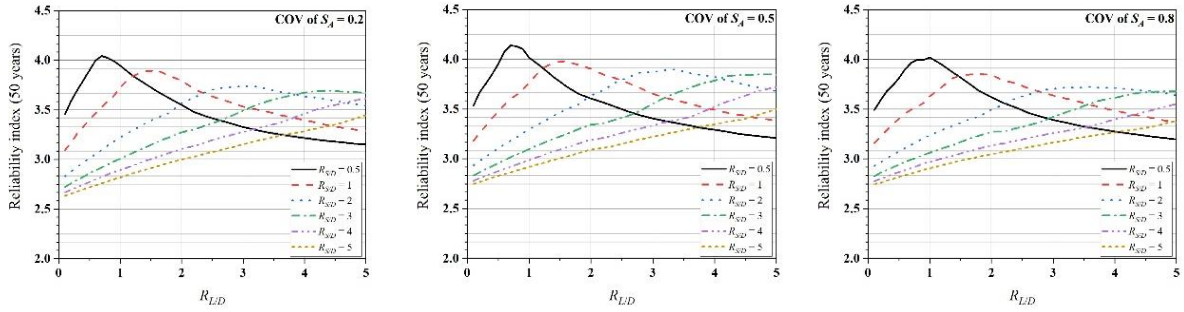

Figure 4.23. Estimated reliability index by considering dead, live and snow loads (for α_L = 1.5, α_{CL} = 0.7, $s_{A\text{-}T}$ = $s_{A\text{-}1225}$, α_S = 1.0, α_{CS} = 0.7).

Additional reliability analysis was carried out by varying α_{CL} and α_{CS}. The results indicated that the use of ($1.25D_n + 1.5L_n + 0.5S_{n\text{-}1225}$, $1.25D_n + 0.5L_n + 1.0S_{n\text{-}1225}$) could be adequate but slightly conservative, where $S_{n\text{-}1225}$ in here represents that obtained based on 1225-year return period value of the ground snow load. The use of $1.25D_n + 1.5L_n + 0.5S_{n\text{-}1225}$ resulted in the companion load factors of 0.5 for both live and snow loads.

4.5.3. Implied reliability by using the importance factor and consideration of serviceability

As detailed documentation on the values of importance factor for snow load implemented in NBCC was unavailable, it was considered that such a factor was selected based on consensus. In order to study the implication of the importance factor suggested in NBCC on the reliability index, the analysis carried out for the results presented in Figures 4.19 to 4.20 was repeated by considering I_S equal to 0.8, 1.15, and 1.25 which were suggested in the current NBCC. The obtained results were shown in Figure 4.24.

A comparison of the results shown in Figures 4.19, 4.20 and 4.24 indicated that for the typical COV of S_A, the decrease in the failure probability for a design working life of 50 years and $R_{S/D}$ = 1.0 is about 2.5 times by increasing I_S from 1.0 to 1.15 and about 4.5 times by increasing I_S from 1.0 to 1.25. These observed decreases are less than those by considering the importance

factor for the wind load. This reflected the magnitude of uncertainty in different climatological elements and their transformation to the load effects.

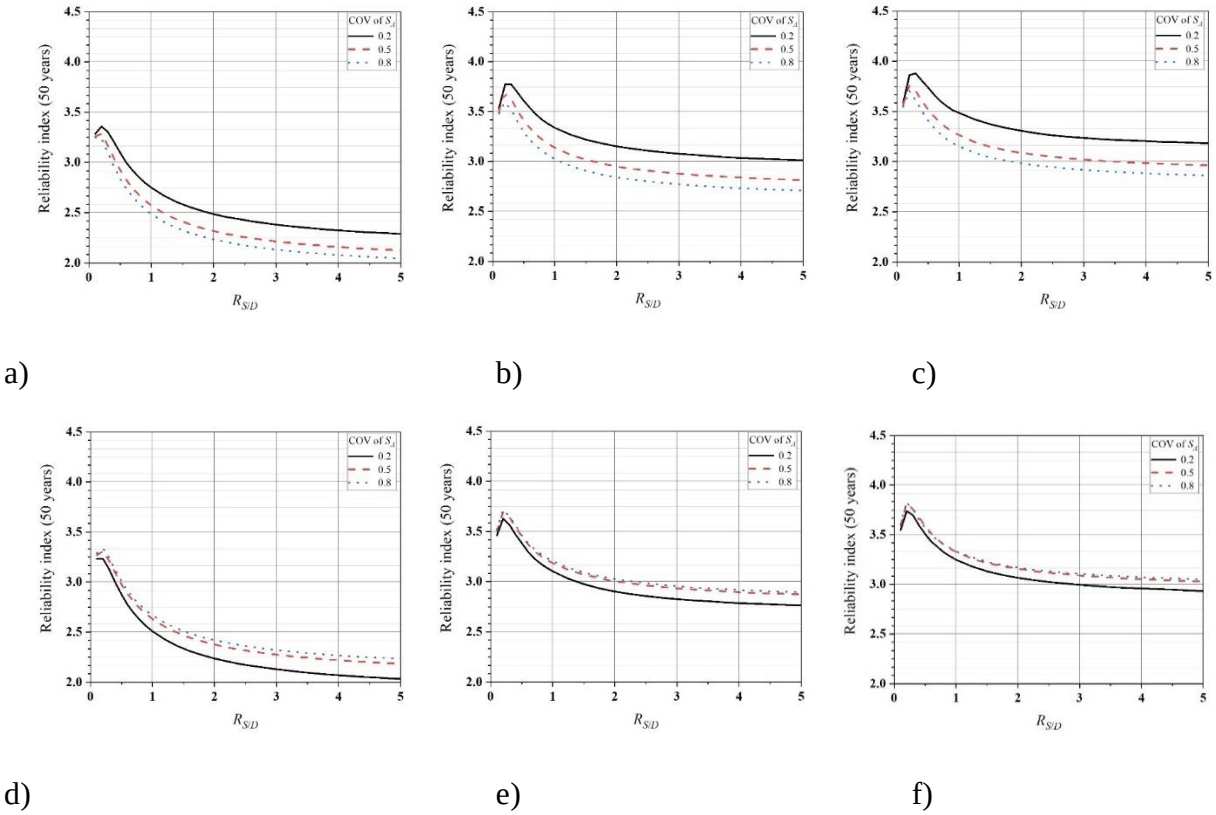

Figure 4.24. Estimated reliability index for a design working life of 50 years by considering the importance factor. a), b) and c) were based on $s_{A\text{-}50}$, α_S = 1.5 suggested in the 2015 edition of NBCC, and were for I_S = 0.8, 1.15, and 1.25, respectively. d), e) and f) were based on $s_{A\text{-}1225}$, α_S = 1.0, and were for I_S = 0.8, 1.15, and 1.25, respectively.

Now, for the typical COV value of S_A equal to 0.5 and based on the suggested load combination ($1.25D_n + 1.5L_n + \alpha_{CS}S_{n\text{-}1225}$, $1.25D_n + 0.5L_n + 1.0S_{n\text{-}1225}$), the reliability was carried out and the obtained results were presented in Figure 4.25 for I_S = 0.8, 1.15, and 1.25, and for α_{CS} = 0.3 and 0.7. In all cases, the obtained reliability index was relatively consistent. The use of α_{CS} = 0.7 resulted in the reliability index much greater than that for α_{CS} = 0.3. The results for α_{CS} = 0.5 were also obtained. Since they were between those for α_{CS} = 0.3 and 0.7, they were not plotted.

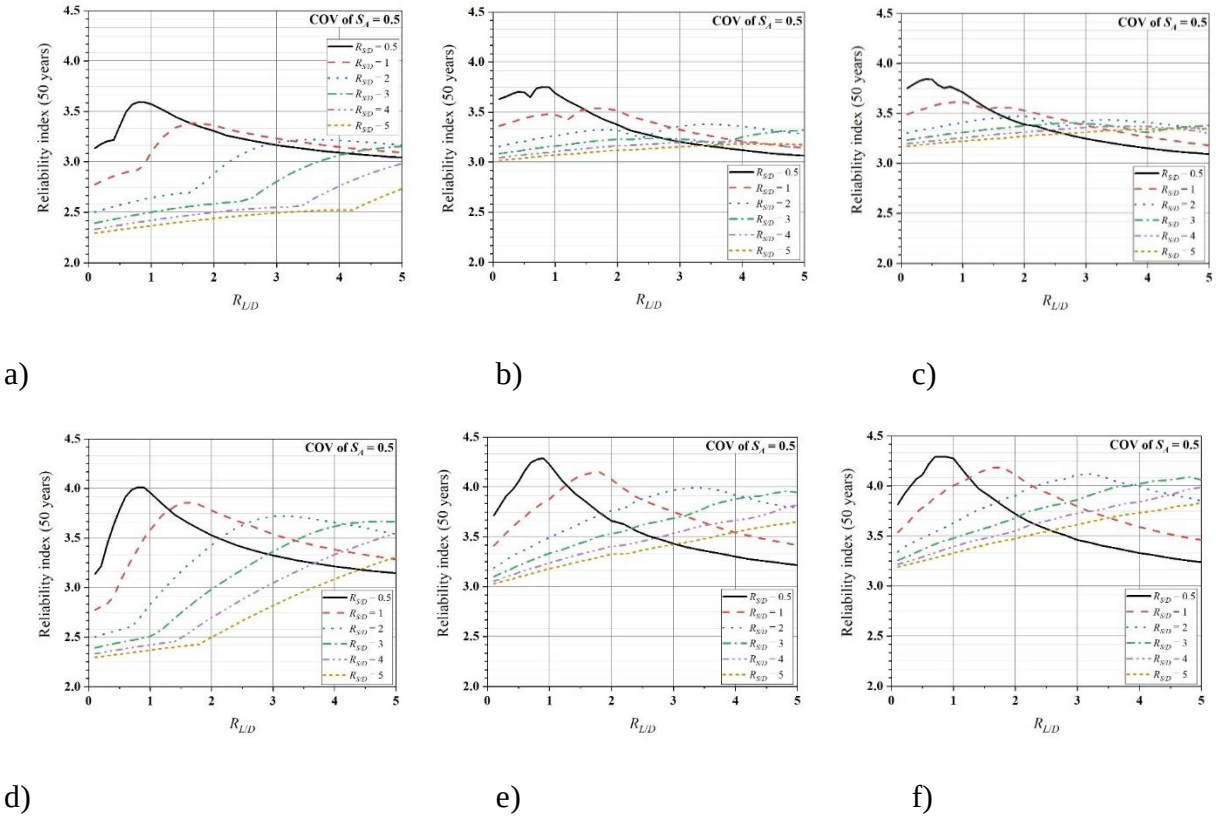

Figure 4.25. Estimated reliability index by considering dead, live and snow loads (α_L = 1.5, α_{CL} = 0.5, $s_{A\text{-}1225}$, α_S = 1.0). The first and the second rows were for α_{CS} = 0.3 and 0.7. From left to right, the plots were for I_S = 0.8, 1.15, and 1.25. No reduction for the live load is considered for consistency.

Note that the use of the importance factor of 0.8, 1.15, and 1.25 in calculating the snow load is equivalent to calculate the snow load with the importance factor 1.0 and the ground snow load corresponding to $s_{A\text{-}T}$ with T = 200, 4793, and 11906 years if the COV of S_A equal to the typical COV of 0.5 is considered. Due to the large T value, such a suggested implementation may not be very popular. Therefore, it was suggested that I_S = 0.8, 1.15, and 1.25 to be retained in the next edition of NBCC with the design snow load corresponding to $s_{A\text{-}1225}$.

Based on the findings in the previous section and this section, the recommended design snow loads were summarized in Table 4.10. In all cases, the preferred load combination factors were α_{CL} = 0.5 and α_{CS} = 0.3 when the dead, live, and snow load acting in combination is considered.

The use of α_{CS} = 0.3 resulted in companion load that is consistent with that suggested in the 2010 edition of NBCC. The use of α_{CL} = 0.5 for the combination of the dead, live, and snow loads resulted in companion load that is consistent with that suggested in the 2015 edition of NBCC.

Table 4.10. Suggested factors and $s_{A\text{-}T}$ for evaluating the ground snow pressure.

	Low importance category	Normal importance category	High importance category	Post-disaster importance category
Ultimate	($s_{A\text{-}1225}$ and I_S = 0.8) or ($s_{A\text{-}200}$ and I_S = 1.0)	($s_{A\text{-}1225}$ and I_S = 1.0)	($s_{A\text{-}1225}$ and I_S = 1.15) or ($s_{A\text{-}5000}$ and I_S = 1.0)	($s_{A\text{-}1225}$ and I_S = 1.25) or ($s_{A\text{-}12000}$ and I_S = 1.0)
Serviceability	Using the snow load corresponding to $s_{A\text{-}10}$ and a load factor of 1.2; or use the load corresponds to $s_{A\text{-}30}$	Using the snow load corresponding to $s_{A\text{-}10}$ and a load factor of 1.2; or use the load corresponds to $s_{A\text{-}30}$	Using the snow load corresponding to $s_{A\text{-}10}$ and a load factor of 1.2; or use the load corresponds to $s_{A\text{-}30}$	Using the snow load corresponding to $s_{A\text{-}10}$ and a load factor of 1.2; or use the load corresponds to $s_{A\text{-}30}$
Load combination with dead, Live and snow loads	For principal load: Design snow load = I_S × Specified snow load; For snow acted as companion load: α_{CS} × I_S × Specified snow load, where α_{CS} = 0.3 (is preferred, or alternatively use 0.5 for consistency in implementation). The companion load factor for live load + snow loads, α_{CL} = 0.5.			

It should be noted that I_S for the serviceability requirements in the current NBCC was set equal to 0.9 for all structure categories. The value was set less than 1.0 "because of less serious consequences of failure and because design criteria for serviceability are more subjective than for strength and stability." Therefore, the same I_S = 0.9 was considered to be applied according to the newly suggested format. Since for the serviceability limit state, according to the current NBCC, the snow load factor of 1.5 should not be applied to the snow load defined based on $s_{A\text{-}50}$, it could be shown that the use of I_S = 0.9 with the ground snow load specified based on $s_{A\text{-}50}$ implies the use of a snow load based on $s_{A\text{-}T}$ with T equal to 19, 28, and 30 years for the COV

of S_A equal to 0.2, 0.5 and 0.8, respectively. Also, a simple analysis showed that the ratio of $0.9s_{A\text{-}50}$ to $s_{A\text{-}10}$ is about 1.2. One could tabulate the snow load correspond to $s_{A\text{-}30}$ and using it for the serviceability analysis. Alternatively, one may apply a load factor of 1.2 for serviceability checking using the snow load corresponding to $s_{A\text{-}10}$. This suggested implementation was included in Table 4.10 as well.

4.5.4. Discussion on the rain component of roof snow load

The calculation procedure of the rain component of roof snow load, S_R, as part of the ground snow load, was explained in the previous sections. The use of a 50-year rather than 30-year return period value of the annual maximum 1-day winter rain amount was recommended in the 2015 edition of the NBCC. Statistical analysis carried out in Chapter 3 indicated that S_R could be assumed to be independent of the annual maximum ground snow load, indicating that the use of the sum of the ground snow load and rain load to evaluate the roof snow load could be conservative. To reduce this conservatism, one could apply the well-known square-root-of-the-sum-of-squares (SRSS) rule. In such a case, the T-year roof snow load is to be calculated using,

$$(S)_T = \sqrt{\left(C_{gr} S_L\right)_T^2 + \left(S_R\right)_T^2} \tag{4.16}$$

where $(\mathrm{g})_T$ denotes the T-year return period value of its argument.

For consistency with the current and previous version of NBCC and due to lack of a better roof snow model that takes into account the winter rain, it is suggested that the rain component of the design snow load is to be assigned based on the same return period that is used to calculate the snow component of ground snow load.

4.6. Climate change effects on structural reliability focused on snow load

4.6.1. Impact on extreme snow depth

Similar to the case for the wind load, the impact of climate change described in Cannon et al. (2019) for snow load is expressed in terms of the percent change in annual maximum snow load

and annual maximum rain load statistics. These changes are shown in Table 4.11. Plots of the results shown in the table are presented in Figure 4.26.

Table 4.11. Percent change in the annual maximum mean and COV of snow load and rain load. (From Cannon et al. (2019)).

	Global warming level ΔT (ºC)							Global warming level ΔT (ºC)						
	0.5	1	1.5	2	2.5	3	3.5	0.5	1	1.5	2	2.5	3	3.5
	Change in the mean of annual max. snow load (%)							Change in COV of annual max. snow load (%)						
British Columbia	-20.2	-34.3	-46.3	-56.9	-64.8	-71.7	-77	6.3	13.6	23.4	30.3	45.8	61.3	84.4
Prairies	-2.2	-3.8	-7.3	-11.7	-16.4	-21.4	-26.4	2.2	4.5	7.7	11.3	14.6	20.2	27.3
Ontario	-12.4	-22.4	-33.5	-41.4	-49.9	-56.5	-63.1	6	8.3	15.5	24.8	35.9	48.7	59.4
Quebec	-11.9	-21	-31.3	-38.5	-47	-53.1	-60.2	8.5	12.9	21.5	30.1	37.9	46.8	53
Atlantic	-20.1	-34	-46.8	-58	-67.6	-75.2	-80.8	10.1	20	35	53.5	69.2	88.5	111.2
North	1.7	2.5	3.2	3.4	3.1	3.2	1.4	1.4	3	3.2	4.9	5.5	7.6	10.8
Canada	-11.7	-21.3	-31.8	-40	-48.5	-55	-61.3	6.3	9.4	17.1	26.7	35.6	46.3	54.1
	Change in the mean of annual max. rain load (%)							Change in COV of annual max. rain load (%)						
British Columbia	0.5	-1.6	-5.9	-13.6	-24.3	-35.2	-46.6	2.3	4.5	16.3	31.3	59.8	81.1	110.6
Prairies	4	8	11.7	14.9	18.1	19.4	21.4	-4.1	-7.7	-10.6	-13.6	-15.7	-17.8	-18.4
Ontario	-6.3	-13.3	-22.1	-31.3	-39.4	-46.5	-53.3	5.6	10.1	17.4	27.9	40.4	52.9	63
Quebec	-2.3	-7.3	-13.5	-20.1	-26.8	-33.8	-41	3.3	5.7	12.2	23	34.8	41.9	53.8
Atlantic	-12.9	-23.1	-34.2	-46.1	-57.8	-66.7	-73.5	12.5	26.4	43.4	61.8	85.1	103.4	133.7
North	3.2	6.3	8.4	13.2	17	20.4	25.5	-0.6	-2.2	-3.7	-4.8	-6.3	-9.6	-11.7
Canada	-2.7	-7.3	-13.6	-20.7	-28.4	-35.8	-42.8	3.1	5.8	12.2	21.5	30.6	41.3	49.7

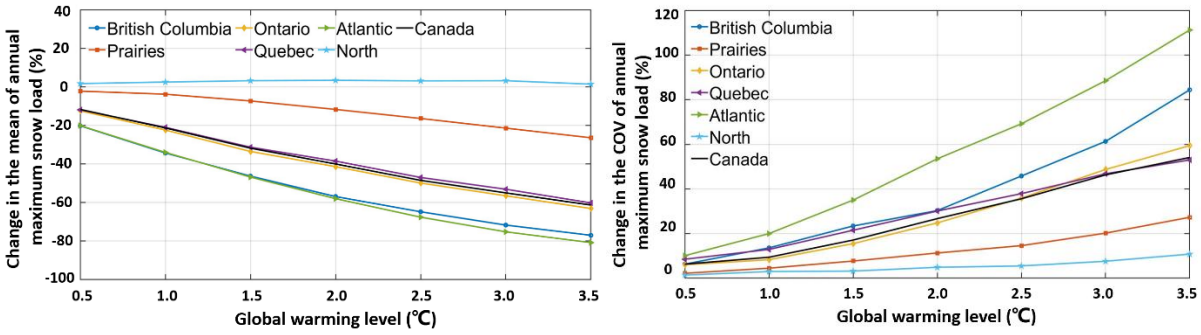

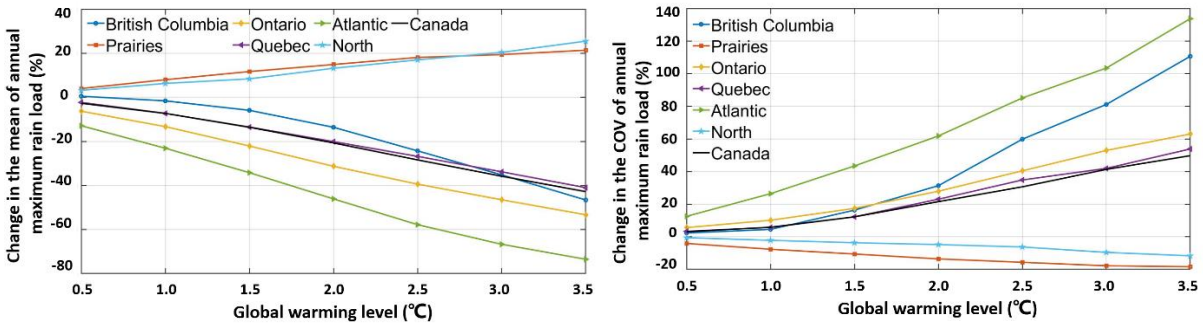

Figure 4.26. Variation of the changes in annual maximum mean and COV of snow load and rain load as functions of the global warming level.

Since there is significant uncertainty in the snowpack bulk density and the ground to roof snow transformation, the percent change of the annual maximum snow load was interpreted as the percent change of the annual maximum snow depth S_A. A few major observations could be made from the results presented in Table 4.11 and Figure 4.26. The mean of S_A decreases for all considered regions except for the region labelled North. This alone would lead to a decreased snow load and increased structural reliability if the structure was designed according to the current NBCC. However, there is a significant increase in the COV of S_A. This increase can be as high as 40% for Canada, and 120% for the region labelled Atlantic. Such large increases in the COV of S_A alone could cause decreased structural reliability. The combined effects (i.e., decreased mean and increased COV of S_A) on the required design snow load for specified target reliability was evaluated in the next section.

4.6.2. Effect on the structural reliability and calibrating the scaling factor for snow load due to the impact of climate change

To assess the effect of climate change on the failure probability, let $h_m(\Delta T)$ and $h_{COV}(\Delta T)$ denote the change in the mean and COV of S_A in the following. By adopting the RCP8.5, for a given year Y since 2000, and the global warming level ΔT can be evaluated using Eq. (4.10). By using the calculated ΔT, the mean and COV of S_A, at Y year, can be evaluated using,

$$(\text{Mean, COV})_{\text{At } Y \text{ year}} = \left(m_{SA} + h_m(\Delta T), v_{SA} + h_{COV}(\Delta T)\right) \tag{4.17}$$

where m_{SA} and v_{SA} represent the mean and COV of S_A estimated based on historical snow records that can be considered to be representative of the year 2000.

Following the analysis procedure used for the reliability analysis subjected to wind load with climate change effect, the reliability analysis subjected to snow load was carried out for a typical COV of S_A = 0.5 and the target reliability index β_{T50} equal to the value shown in Figure 4.20 for COV of S_A = 0.5. The calculated scaling factor due to climate change for snow load, η_{CS}, for β_{50} to be approximately equal to β_{T50} was shown in Figure 4.27. The results indicated that the combined effect of decreased mean and increased COV of S_A resulted in an increased reliability index; hence, η_{CS} less than unity. η_{CS} is similar and equals about 0.95 for all regions, except for "North", where η_{CS} equals about less than 1.02. In other words, one could reduce the snow load by 5% for all regions except for "North", where a increase of 2% can be considered.

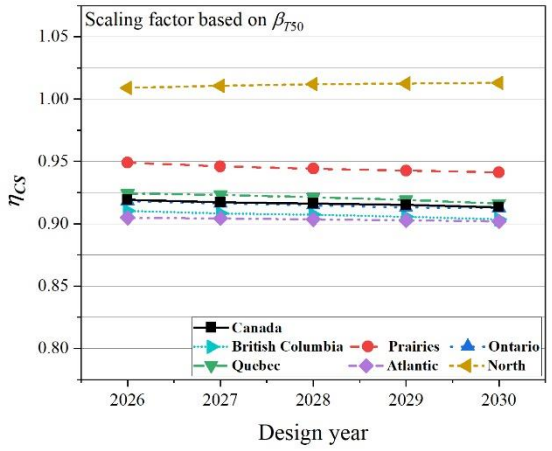

Figure 4.27. Calibrated scaling factor for the design snow load by considering the impact of climate change and using β_{T50} as the target.

Similar to the calibration of η_{CW} for the wind load, the calibration of η_{CS} was also carried out for the minimum annual reliability index β_{minA} within a specified design working life equal to the target β_{TminA}. The obtained values of η_{CS} were presented in Figure 4.28. A comparison of the results shown in Figures 4.27 and 4.28 indicated that the obtained η_{CS} based on β_{TminA} differs

from that obtained by using β_{T50} as the target. This large discrepancy was attributed to the smearing effect by using β_{T50} as the target. The results shown in Figure 4.28 suggested that an increased design snow load was required for "North" and a reduction could be allowed for other regions. Since the reduction of the snow load may be perceived as unnecessary and perhaps dangerous by the practitioner, as a conservative measure, no reduction was suggested for all regions. Furthermore, an increase in the design snow load of 5% (i.e., η_{CS} = 1.05) was suggested for "North".

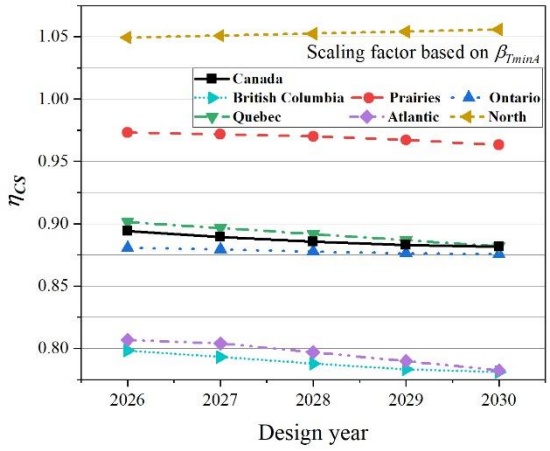

Figure 4.28. Calibrated scaling factor for the design snow load by considering the impact of climate change and β_{TminA} as the objective criterion.

An illustration of using η_{CS} =0.87 and 0.91 (obtained for Canada) in the structural reliability by considering the impact of climate change on the snow load is illustrated in Figure 4.29.

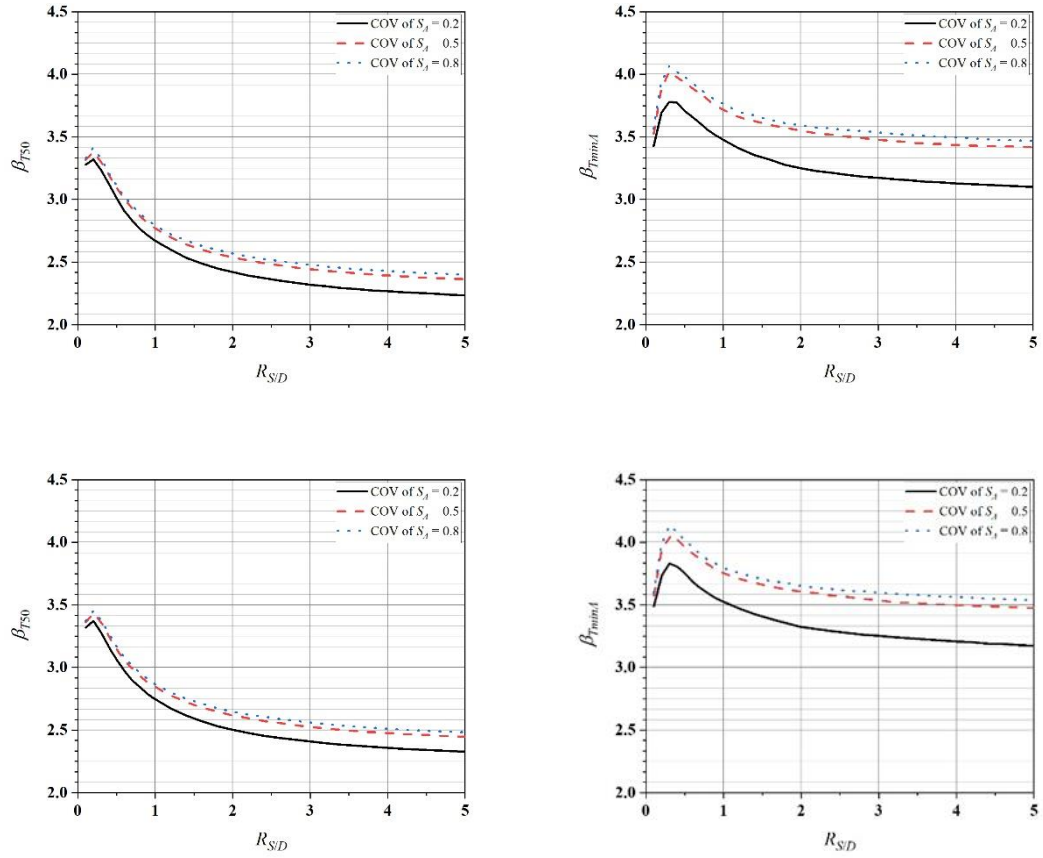

Figure 4.29. Calculated reliability index for a structure with a design working life of 50 years starting from 2028. The first row was calculated by considering η_{CS} = 0.87. The second row was calculated by considering η_{CS} = 0.91.

As no reliability analysis for the rain component of snow load was carried out, following the current practice, it is suggested that the use of the same return period value of 1225-year should be considered to estimate the annual maximum 1-day winter rain amount. For the estimation, the percent change in the mean and COV of the annual maximum rain component of snow load could be used to calculate the mean and COV of those obtained from the historical records.

4.7. Summary and recommendations

A reliability-based design code calibration for the National Building Code of Canada was carried out. The analysis was focused on the design wind load, design snow load, and

companion load factors. The analysis considered the stationary extremes derived from observed meteorological data and included the nonstationary climate change effects. For the wind load, the thunderstorm winds and synoptic winds were considered separately. It showed that the use of return periods longer than that currently used in NBCC to define the design wind load and design snow load but with a load factor equal to one was preferred. This preference is based on an improved reliability consistency as compared to use short return periods and load factor greater than one, as implemented in the current NBCC. The specific recommendations were listed in Table 4.12.

Table 4.12. Recommended design load for the ultimate limit state and serviceability limit state by considering wind load and snow load.

Limit State	Principal load	Factored load combination
Ultimate	Dead + Live	Preferred: $1.25D_n + 1.5L_n + (0.3\eta_{CW}W_n$ or $0.3\eta_{CS}S_n)$, Alternative: $1.25D_n + 1.5L_n + (0.3\eta_{CW}W_n$ or $0.5\eta_{CS}S_n)$,
	Dead +Wind	$1.25D_n + \eta_{CW}W_n + 0.5L_n$
	Dead +Snow	$1.25D_n + \eta_{CS}S_n + 0.5L_n$
	Preferred W_n is to be specified based on a return period of 500 years. S_n is to be specified based on a return period of 1225 years; I_W and I_S of 0.8, 1.15, and 1.25 are to be used for buildings classified as the low, high, and post-disaster importance categories, respectively. Using a single η_{CW} value of 1.07 otherwise using the values shown in Figure 4.16; and η_{CS} equal to 1.0 except for North $\eta_{CS} = 1.05$.	
	Alternatively to use the importance factors (i.e., use $I_W = 1$ and $I_S = 1$), • W_n calculated for the return period T = 100, 1500, and 3000 years may be considered for the buildings classified as the low, normal, high, and post-disaster importance categories, respectively; • S_n calculated for the return period T = 200, 5000, and 12000 years may be considered for the buildings classified as the low, normal, high, and post-disaster importance categories, respectively.	
Serviceability	Using 10-year return period value of wind load for serviceability checking.	
	Using 10-year return period value of snow load and a factor 1.2 for serviceability checking (or 30-year return period value of snow load and a factor 1.0 for serviceability checking, which is preferred).	

The consideration of climate change effect on the extreme wind load and snow load resulted in suggesting a wind load scaling factor of 1.07, and a snow load scaling factor of 1.0, except that this scaling factor becomes 1.05 for North.

4.8. Reference

Allen, D.E. (1975). Limit states design - a probabilistic study. Canadian Journal of Civil Engineering, 2(1), 36-49.

Ang, A.H.S. and Tang, W.H. (2007). Probability concepts in engineering planning and design: Emphasis on application to civil and environmental engineering. Wiley.

AS/NZS 1170.0 and 1170.2 (2002) Standards Australia/ Standards New Zealand, Structural design actions. Part 2: Wind actions.

Bartlett, F.M., Hong, H.P. and Zhou, W. (2003). Load factor calibration for the proposed 2005 edition of the National Building Code of Canada: Statistics of loads and load effects, Canadian Journal of Civil Engineering, 30 (2) 429-439.

Bartlett, F.M., Hong, H.P. and Zhou, W. (2003b). Load factor calibration for the proposed 2005 edition of the National Building Code of Canada: Companion-action load combinations, Canadian Journal of Civil Engineering, 30 (2) 440-448.

CAN/CSA S16 (2014) Limit States Design of Steel Structures, Rexdale, Ontario, Canada.

CAN/CSA S408 (1981). Canadian Standards Association, guideline for the development of limit states design. CSA Special publication S408, Rexdale, Ontario, Canada.

Cannon A. (2019). Climate-Resilient Buildings & Core Public Infrastructure Guidance on Updating Climate Design Values for Enhanced Resilience to Future Climate Conditions, ECCC, Draft report.

Cook, R., Griffis, L., Vickery, P. and Stafford, E. (2011). ASCE 7-10 wind loads. In Proceedings of the 2011 Structures Congress, ASCE, Las Vegas, NV.

Davenport, A.G. (1983). The relationship of reliability to wind loading. Journal of Wind Engineering and Industrial Aerodynamics, 13(1-3), 3-27.

Davenport, A.G. (2002). Past, present and future of wind engineering. Journal of Wind Engineering and Industrial Aerodynamics, 90(12-15), 1371-1380.

Ellingwood, B., Galambos T.V., MacGregor J.G. and Cornell C.A. (1980). Development of a probability based load criterion for American national standard A58. Nat. Bureau of Standards Special Pub. No. 577.

Foschi, R.O., Folz, B. and Yao, F. (1993). Reliability-based design of wood structures: background to CSA-086.1-M89. Canadian Journal of Civil Engineering, 20(3), 349-357.

Gomes, L., & Vickery, B. J. (1978). Extreme wind speeds in mixed wind climates. Journal of Wind Engineering and Industrial Aerodynamics, 2(4), 331-344.

Holmes, J.D., Kwok, K.C., and Ginger, J.D. (2012). Wind Loading Handbook for Australia and New Zealand.

Hong, H.P. and Ye, W. (2014a). Estimating extreme wind speed based on regional frequency analysis. Structural Safety, 47, 67-77.

Hong, H.P. and Ye, W. (2014b). Analysis of extreme ground snow loads for Canada using snow depth records. Natural hazards, 73(2), 355-371.

Hong, H.P., Mara, T.G., Morris, R., Li, S.H. and Ye, W. (2014). Basis for recommending an update of wind velocity pressures in Canadian design codes. Canadian Journal of Civil Engineering, 41(3), 206-221.

Hong, P., Tang, Q. and Hong H.P. (2017) Calibrating wind load and importance factor for codified design considering spatially varying statistics of extreme wind speed, Submitted for publication.

Jeong, D.I. and Sushama, L. (2018). Projected changes to extreme wind and snow environmental loads for buildings and infrastructure across Canada. Sustainable Cities and Society, 36, 225-236.

Jordaan, I.J. (2005). Decisions under uncertainty: probabilistic analysis for engineering decisions. Cambridge University Press, New York.

Kennedy, D.L. (1984). Limit states design of steel structures in Canada. Journal of Structural Engineering, 110(2), 275-290.

Lombardo, F.T., Main, J.A. and Simiu, E. (2009). Automated extraction and classification of thunderstorm and non-thunderstorm wind data for extreme-value analysis. Journal of Wind Engineering and Industrial Aerodynamics, 97(3-4), 120-131.

MacGregor, J.G., Mirza, S.A. and Ellingwood, B. (1983). Statistical analysis of resistance of

reinforced and prestressed concrete members. In Journal Proceedings (Vol. 80, No. 3, pp. 167-176).

Madsen, H.O., Krenk, S. and Lind, N.C. (2006). Methods of structural safety. Courier Corporation.

Melchers, R.E. and Beck, A.T. (2018). Structural reliability analysis and prediction. John Wiley & Sons.

MSC. (2000). Canadian Snow Data CD-ROM. CRYSYS Project, Climate Processes and Earth Observation Division, Meteorological Service of Canada, Downsview, Ontario, January 2000. (online order form available at www.crysys.ca)

Newark, M.J. (1984). A new look at ground snow loads in Canada. Proceedings, Eastern Snow Conference, Vol. 29, 41st Annual Meeting, Washington, DC, pp. 37-48.

Newark, M.J., Welsh, L.E., Morris, R.J. and Dnes, W.V. (1989). Revised ground snow loads for the 1990 National Building Code of Canada. Canadian Journal of Civil Engineering, 16(3): 267-278.

Nowak, A.S. and Lind, N.C. (1979). Practical code calibration procedures. Canadian Journal of Civil Engineering, 6: 112–119

NRC (2015) National Building Code of Canada. Institute for Research in Construction, National Research Council of Canada, Ottawa

Tang, Q. (2016). Effects of small sample size on the wind hazard mapping over Canada, M.E.Sc. thesis University of Western Ontario.

Vickery P.J., Wadhera D. Galsworthy J., Peterka, J.A., Irwin, P.A. and Griffis, L.A. 2010. Ultimate wind load design gust wind speeds in the United States for use in ASCE-7. Journal of Structural Engineering, ASCE, 136(5), 613-625.

Wen, Y.K. (1990). Structural load modeling and combination for performance and safety evaluation. Developments in civil engineering, 31.

Chapter 5

5. Conclusions and future research

5.1. Summary and recommendations

A probabilistic assessment of wind hazard and snow hazard in the context of the structural design was carried out for Canada using the routinely recorded meteorological variables. The results of wind hazard modelling were presented in Chapter 2, while the results of snow hazard modeling were presented in Chapter 3. Moreover, the hazard assessment results were used to calibrate new design wind load and snow load for the National Building Code of Canada with and without including the climate change effects.

The statistical analysis and estimation of the spatially-varying wind hazard were carried out. The major conclusions were:

1. The Gumbel distribution could be adopted to model the annual maximum wind speed if only a single probabilistic model is to be considered over Canada. This is justified since it is the preferred probability distribution for wind records from about 70% of the considered meteorological stations. This distribution is not only adequate for the synoptic winds but also for the thunderstorm winds.

2. The statistics of wind records from the HLY01 digital archive indicated that the COV ranges approximately from 0.05 to 0.2 with a typical value of 0.138. The statistics of wind records from the DLY04 digital archive showed that for thunderstorm winds, the COV of V_{AH} ranges approximately from 0.1 to 0.35 with a mean value of 0.21. However, for sites with significant thunderstorm activities, and the wind hazard being dominated by the thunderstorm winds, the COV value is less than 0.2. It implies that if the return period values of the annual maximum wind speed for the synoptic winds and for the thunderstorm winds are properly estimated for a high return period (say 500 years), the distribution of the extreme winds in the upper tail could be approximated by using the Gumbel model with COV less than about 0.2 for most cases.

3. The wind hazard at a site within southern Ontario and the southern part of the Prairies could be dominated by the thunderstorm winds, especially as the return period increases. This indicated that for these regions, the return period values of the annual maximum wind speed should be estimated by considering both thunderstorm winds and synoptic winds separately. Such estimated values should be used as the basis to recommend the reference wind velocity pressure for codified design. This is especially the case if a high return period, such as T = 500 years, is considered to assign the design wind load.

4. For practical consideration, outside of the regions mentioned in item 4), the return period values of the annual maximum wind speed estimated based on synoptic winds are suggested.

The results of the probabilistic assessment of snow hazard indicated that

1. The use of the lognormal, Gumbel, and GEV distributions for the annual maximum ground snow depth are preferred for 46%, 35%, and 19% of the cases, where each case represents fitting the samples of annual maximum ground snow depth, S_A, data from a meteorological station. The locations for the preferred models are intermingled, and there are no clear spatial trends.

2. However, although the lognormal distribution is the most preferred, the Gumbel distribution could be adopted in practice since the use of the Gumbel distribution could be justified based on the extreme value theory, and the Gumbel distribution was traditionally used to map S_A and to develop the codified snow load for structural design in Canada.

3. It was observed that the coefficient of variation (COV) of S_A ranges from 0.2 to 0.8, with a typical value of about 0.5. The obtained statistics of S_A based on the two data sources (i.e., DLY04 and CSD-CD-ROM) differ. The reason for the discrepancy was unknown. In general, the mean of the snowpack bulk density obtained in the present study differs from an earlier study. The COV of the snowpack bulk density varies spatially and ranges from about 0.1 to 0.3.

4. The roof snow load in NBCC consists of snow component and rain component, S_R, which is defined based on the 24-hour winter rain amount. The estimated correlation between S_R and

the annual maximum ground snow load, S_L, is negligible, suggesting that the use of the sum of the ground snow load and rain load to evaluate the roof snow load that is implemented in the National Building Code of Canada could be conservative. The use of the well-known square-root-of-the-sum-of-squares (SRSS) rule to evaluate the roof snow load based on the snow component and rain component is recommended.

The calibration of the design wind and snow load and companion load factors were carried out. The results of the reliability-based design code calibration showed that the use of the return periods longer than the one currently used in NBCC to define the design wind and snow loads but with a load factor equal to one can result in an improved reliability consistency. Specific recommendations were summarized in Table 5.1. The consideration of climate change effect on the extreme wind load and snow load resulted in suggesting a wind load scaling factor of 1.07, and a snow load scaling factor of 1.0, except that this scaling factor becomes 1.05 for North.

Table 5.1 Recommended design load for the ultimate limit state and serviceability limit state by considering wind load and snow load.

Limit State	Principal load	Factored load combination
Ultimate	Dead + Live	Preferred: $1.25D_n+1.5L_n+(0.3\eta_{CW}W_n$ or $0.3\eta_{CS}S_n)$, Alternative: $1.25D_n+1.5L_n+(0.3\eta_{CW}W_n$ or $0.5\eta_{CS}S_n)$,
	Dead +Wind	$1.25D_n+\eta_{CW}W_n + 0.5L_n$
	Dead +Snow	$1.25D_n+\eta_{CS}S_n + 0.5L_n$
	Preferred W_n is to be specified based on a return period of 500 years. S_n is to be specified based on a return period of 1225 years; I_W and I_S of 0.8, 1.15, and 1.25 are to be used for buildings classified as the low, high, and post-disaster importance categories, respectively. Using a single η_{CW} value of 1.07 otherwise using the values shown in Figure 4.16; and η_{CS} equal to 1.0 except for North η_{CS} = 1.05.	
	Alternatively to use the importance factors (i.e., use $I_W = 1$ and $I_S = 1$), • W_n calculated for the return period T = 100, 1500, and 3000 years may be considered for the buildings classified as the low, normal, high, and post-disaster importance categories, respectively; • S_n calculated for the return period T = 200, 5000, and 12000 years may be considered for the buildings classified as the low, normal, high, and post-disaster importance categories, respectively.	
Serviceability	Using 10-year return period value of wind load for serviceability checking.	
	Using 10-year return period value of snow load and a factor 1.2 for	

	serviceability checking (or 30-year return period value of snow load and a factor 1.0 for serviceability checking, which is preferred).

5.2. Future research

There are several future research topics could be of value for the design code development. Although consistent return periods are implemented or suggested for the design codes, the use of a consistent return period may not be economically efficient. This aspect needs to be investigated in a future study for both wind and snow loads.

The investigation carried out in the present study should be extended to other environmental load parameters such as ice accretion and permafrost.

There are inconsistencies in the probabilistic characterization of non-synoptic winds based on the HLY01 and DLY04 archives. The source of this inconsistency needs to be scrutinized further.

The obtained snowpack bulk density in the present study differs from that reported in a previous study; this could have serious implications in design code making. It is suggested that quality data to be collected to investigate further the statistics of the snowpack bulk density and the ground snow load. This could be an extremely valuable exercise.

Curriculum Vitae

Name: Qian Tang

Post-secondary Education and Degrees:

East China Normal University
Shanghai, China
2009-2013 B.Sc.

The University of Western Ontario
London, Ontario, Canada
2014-2016 M.E.Sc.

The University of Western Ontario
London, Ontario, Canada
2016-2020 Ph.D.

Related Work Experience

Teaching Assistant
The University of Western Ontario
2014-2020

Research Assistant
The University of Western Ontario
2014-2020